

Understanding proteostasis dysregulation in phenylketonuria – a paradigm disease for inborn error of metabolism

Karina Skjervheim Prestegård

Thesis for the degree of Philosophiae Doctor (PhD)
University of Bergen, Norway
2022

UNIVERSITY OF BERGEN



Understanding proteostasis dysregulation in phenylketonuria – a paradigm disease for inborn error of metabolism

Karina Skjervheim Prestegård



Thesis for the degree of Philosophiae Doctor (PhD)
at the University of Bergen

Date of defense: 06.09.2022

© Copyright Karina Skjervheim Prestegård

The material in this publication is covered by the provisions of the Copyright Act.

Year: 2022

Title: Understanding proteostasis dysregulation in phenylketonuria – a paradigm disease for inborn error of metabolism

Name: Karina Skjervheim Prestegård

Print: Skipnes Kommunikasjon / University of Bergen

ABSTRACT

Phenylketonuria (PKU) is an inborn error of metabolism caused by mutations in the phenylalanine hydroxylase (*PAH*) gene, resulting in unstable and often misfolded enzyme with reduced ability to metabolize the amino acid phenylalanine (Phe). The subsequent buildup of blood Phe (hyperphenylalaninemia, HPA) can reach neurotoxic levels, and if left untreated it will result in severe intellectual disability, motor deficits, epilepsy, and behavioral problems. Patients are therefore treated with a strict low-Phe diet from birth and are advised to stay on the diet throughout their life. The phenotypic variability is high, as most patients are heterozygotes, and more than 1200 PKU mutations are registered. Several mouse models for PKU (*Enu1*, *Enu2* and *Enu3*) have been available for PKU investigations, and in this work we present a novel mouse model representing a mutation with high prevalence in patients, *Pah-R261Q*.

The complex proteostasis network, including the translational machinery, molecular chaperones and cochaperones, the ubiquitin-proteasome system (UPS), and the autophagy machinery manages and controls the folding and levels of native proteins, and it is especially involved in counteracting the accumulation of misfolded and aggregated proteins. Mutated PAH has previously been shown to form small aggregates that are presumed to be degraded by the UPS, but much is unknown about the proteostasis regulation and the degradation mechanisms of PAH and its mutants in patients. Recently, DNAJC12, a molecular cochaperone of the HSP40 family, has been identified as the specific cochaperone of the tetrahydrobiopterin (BH₄) dependent aromatic amino acid hydroxylases, the protein family to which PAH belongs, and is important for their correct folding and maintenance. We studied the role of DNAJC12 in the folding and degradation of wild-type (WT) and mutant PAH, both *in vitro* and *in vivo*. Our results showed lower levels of PAH and DNAJC12 in cells expressing PAH mutants, as well as in *Enu1* mice (homozygous for the *Pah* variant *V106A*) compared to *WT* mice. Most mutant PAH, but not WT-PAH, appeared mono-ubiquitinated in mouse liver lysates. Moreover, by co-immunoprecipitation experiments in liver lysates we probed the complex formation between DNAJC12 and PAH (both WT and ubiquitinated

mutant), and our results support that the cochaperone plays a role both in the folding of PAH and in the processing of its misfolded ubiquitinated conformations.

Further, we generated and characterized the *Pah-R261Q* mouse model, which presented BH₄ responsive HPA. The mutant PAH was misfolded and displayed amyloid aggregation in liver, associated with toxic gain-of-function. This type of aggregation has so far been unknown for HPA or PKU mutations, where it appears associated with proteostasis dysregulation, altered lipid metabolism, and oxidative stress. Compared with *Enu1* and *WT*, which show comparable mRNA expression of DNAJC12, *Pah-R261Q* presented an upregulation of the cochaperone, further confirming the oxidative stress in this mouse. Differently to the smaller PAH aggregates in *Enu1*, the ubiquitinated amyloid-like PAH aggregates appear too large for the UPS, and engagement of the autophagy system was indicated by colocalization of mutant PAH aggregates and autophagy markers. Whereas PKU has traditionally been considered a loss-of-function disorder, our work shows that some mutations may display a toxic gain-of-function due to large PAH aggregates, possibly leading to oxidative stress and additional comorbidities.

Aging has been shown to lead to a decline in proteostasis network efficiency, disturbance of the proteomic balance and increased oxidative stress, as well as a worsening of age-related diseases. We therefore expected that the *Pah-R261Q* mice, with their large PAH aggregates in liver and increased oxidative stress, would exhibit a reduced general health, increased comorbidities, and possibly early death when reaching old age. The aging *Pah-R261Q* mice did present an increased serum concentration of Phe compared to both old *WT* and young *Pah-R261Q* mice but did not show signs of neurological issues. Unexpectedly, several of the biomarker concentrations indicating oxidative stress in the young *Pah-R261Q* mice seemed to have normalized towards *WT* levels in the old mice. Although the biomarker concentrations were similar in old *Pah-R261Q* and *WT* mice, interrelation plots between pairs of biomarkers revealed distinct differences, suggesting that different underlying metabolic mechanisms may be at work in the mutant mice. The slightly improved motor function and prevention of premature

death and comorbidities may be explained by the strong activation of autophagy in the mutant mice from a young age.

To conclude, this work has revealed new knowledge about the aggregation and degradation of mutant PAH with the involvement of DNAJC12, visualization of small PAH aggregates in *Enul* mouse livers, large amyloid-like aggregates in *Pah-R261Q* mouse livers, and engagement of autophagy to degrade the large aggregates. In *Pah-R261Q* mice we found the unexpected toxic gain-of-function of PAH misfolding. As PKU has been a model disease for many inborn errors of metabolism, the present findings are expected to contribute to a better mechanistic understanding of the phenotypic variability in these genetic disorders.

ABSTRAKT

Fenylketonuria (PKU) er en medfødt stoffskiftesykdom forårsaket av mutasjoner i genet for fenylalanin hydroksylase (PAH), og fører til ustabile og ofte feilfoldete enzymer med nedsatt evne til å metabolisere aminosyren fenylalanin (Phe). Den påfølgende opphopningen av Phe i blodet (hyperfenylalaninemi, HPA) kan nå nevrotoksiske nivåer, og uten behandling vil dette føre til alvorlige fysiske og psykiske funksjonshemninger, epilepsi og adferdsproblemer. Pasienter behandles derfor med en streng lav-Phe diett fra fødsel og anbefales å forbli på dietten livet ut. Den fenotypiske variasjonen er høy, da de fleste pasientene er heterozygoter, og mer enn 1200 PKU mutasjoner er registrert. Flere musemodeller for PKU (*Enu1*, *Enu2* og *Enu3*) har vært tilgjengelige for PKU-forskning, og i dette arbeidet presenteres en ny musemodell som representerer en mutasjon med høy utbredelse i pasienter, *Pah-R261Q*.

Det komplekse proteostase-nettverket omfatter translasjonsmaskineriet, molekylære chaperoner og cochaperoner, ubiquitin-proteasom systemet (UPS) og autofagimaskineriet. Proteostase-nettverket bistår og kontrollerer dannelsen, foldingen og nivåene av native proteiner, og er spesielt involvert i å motvirke akkumuleringen av feilfoldete og aggregerte proteiner. Mutert PAH har tidligere vist seg å danne små aggregater som er antatt å bli nedbrutt av UPS, men mye er fortsatt uvisst når det kommer til proteostase-reguleringen og nedbrytningsmekanismene for PAH og dets mutanter i pasienter. DNAJC12, en molekylær cochaperon i HSP40 familien, har nylig blitt identifisert som en spesifikk cochaperon for de tetrahydrobiopterin (BH₄)-avhengige aromatiske aminosyre-hydroksylasene, proteinfamilien PAH tilhører, og er viktig for deres korrekte folding og vedlikehold. Vi studerte rollen DNAJC12 har i folding og nedbrytning av villtype (WT) og mutert PAH, både *in vitro* og *in vivo*. Våre resultater viste lavere nivåer av PAH og DNAJC12 i cellene som uttrykte PAH-mutanter, samt i *Enu1* mus (homozygote for Pah varianten V106A) sammenlignet med WT mus. Mesteparten av det muterte PAH, men ikke WT-PAH, viste seg å være mono-ubiquitinert i leverlysater fra mus. I tillegg viste eksperimenter med co-immunopresipitering i leverlysater komplekse formasjoner mellom DNAJC12 og PAH (både WT og ubiquitinert mutant), og våre resultater underbygger at cochaperonen

spiller en rolle både i folding av PAH og i prosesseringen av dens misfoldede ubiquitinerte former.

Vi genererte og karakteriserte *Pah-R261Q* musmodellen som viste BH₄-responderende HPA. Det muterte PAH var feilfoldet og presenterte amyloid aggregering i lever, assosiert med en toksisk "gain-of-function". Denne typen aggregering har ikke tidligere vært vist for HPA eller PKU mutasjoner, og ser ut til å assosieres med deregulering av proteostase, endret lipid metabolisme og oksidativt stress. Sammenlignet med *Enu1* og WT, som viser lignende mRNA-nivåer av DNAJC12, hadde *Pah-R261Q* en oppregulering av cochaperonen, som er en videre bekreftelse av oksidativt stress i denne musen. Til forskjell fra de mindre PAH aggregatene i *Enu1*, ser de ubiquitinerte amyloid-lignende PAH-aggregatene ut til å være for store for nedbrytning av UPS, og aktiveringen av autofagisystemet ble indikert ved kolokaliseringen av muterte PAH aggregater og markører for autofagi. Mens PKU tradisjonelt har vært ansett som en "loss-of-function" sykdom har vårt arbeid vist at noen mutasjoner kan vise en toksisk "gain-of-function" grunnet store PAH aggregater, som muligens fører til oksidativt stress og ytterligere tilleggssykdommer.

Aldring har blitt påvist å føre til nedgang i proteostasenettverkets effektivitet, forstyrrelser i den proteomiske balansen og økt oksidativt stress, i tillegg til forverring av alders-relaterte sykdommer. Vi forventet derfor at *Pah-R261Q* musene, med deres store PAH aggregater i lever og økt oksidativt stress, skulle ha en redusert generell helsestatus, økte tilleggssykdommer og muligens tidlig død når de ble gamle. Den aldrende *Pah-R261Q* musen hadde en økt serum-konsentrasjon av Phe sammenlignet med både WT og unge *Pah-R261Q*, men viste ingen tegn på nevrologiske problemer. Flere av biomarkør-konsentrasjonene som indikerte oksidativt stress i de unge *Pah-R261Q* musene viste en uventet normalisering mot WT nivåer i de gamle musene. Selv om biomarkør-konsentrasjonene var like i gamle *Pah-R261Q* og WT mus så viste interrelasjons-plot mellom par av biomarkører en distinkt forskjell, som kan indikere at en annen underliggende metabolsk mekanisme kan påvirke de muterte musene. Den lille forbedringen i motorfunksjon og forebyggingen av tidlig død og tilleggssykdommer kan

muligens forklares med den sterke aktiveringen av autofagi fra tidlig alder i den muterte musen.

For å konkludere har dette arbeidet avdekket ny kunnskap om aggregeringen og nedbrytningen av mutert PAH; involvering av DNAJC12, visualisering av små PAH aggregater i lever fra *Enu1* mus, store amyloid-lignende aggregater i lever fra *Pah-R261Q* mus og aktivering av autofagi for å bryte ned de store aggregatene. I *Pah-R261Q* musen fant vi en uventet toksisk "gain-of-function" grunnet feilfoldet PAH. PKU har vært en modellsykdom for mange medfødte stoffskiftesykdommer, og våre funn forventes å bidra til bedre mekanistisk forståelse av fenotypiske variasjon i flere av disse arvelige sykdommene.

SCIENTIFIC ENVIRONMENT

This dissertation is the result of an industrial PhD, a collaboration between the University of Bergen and Pluvia AS. The work has been carried out at the Department of Biomedicine under the supervision of Professor Aurora Martinez (Department of Biomedicine). Dr. Ann Kari Grindheim (Pluvia AS) and Dr. Maja Elgsaas Mujic (VIS) has served as cosupervisors. The animal experiments were conducted at the Animal Facilities at the Department of Clinical Medicine at the University of Bergen.

The project was financially supported by the Research council of Norway and Pluvia AS. Grants from Digital life Norway Research School, the Norwegian Biochemical Society and “Dr. Nils Henrichsen og hustru Anna Henrichsens legat” have funded participation in scientific conferences, relevant courses and new equipment needed.

ACKNOWLEDGEMENTS

After finishing my master thesis in 2013 I swore that I would never do a PhD, but here we are now, with my thesis all done! This all started when my main supervisor, Aurora Martinez, decided to hire me in 2016 to manage the mouse-colony and animal experiments. With her backing I took the path I had sworn never to take, and I am happy I did it in this group and with Aurora as my supervisor. The support and positive attitude in the Biorecognition group is amazing and gave me the confidence to start on this project. Pluvia and everybody in the team has been very supportive, especially in the last months when I have focused solely on my own work and been of little use to you. I appreciate the patience and understanding I have received in this stressful time.

Thank you, Aurora, for believing in me and giving me this opportunity. The amount of work and dedication you put into every member of this group is admirable, and I am incredibly grateful for all the late hours you have spent helping me with this thesis.

A big thank you to my co-supervisor Ann Kari Grindheim as well. You have been there when I needed advice on writing, planning, and prioritizing. But you have also been there when I needed to complain, drink tea, and knit for a bit. These small breaks have been essential when things have been tough.

My second co-supervisor, Maja Mujic Elgsaas, thank you for helping me structure the last year of my work. Our bi-weekly talks helped me prioritize and complete tasks as time went flying by, and that is important for a procrastinator like me.

Thank you to Chimge for being wonderfully dependable and supporting during extremely long experiments, I am very glad we have been two people during the late evenings (and nights). Having workdays that run for more than 18 hours is not ideal, but together we always had fun doing it.

Thank you to my science-idols; Marte and Helene. You know the answers to every silly question I have asked in the last years, and never made me feel stupid for asking them. Knowing you had my back gave me the courage to start on this journey, and your advice have helped me push my boundaries and evolve in so many ways. Thank you for all our chats at the lunch table, in the office, on messenger and on Snap.

Thank you to my wonderful husband Simen for always supporting me and never doubting that I can do whatever I put my mind to. I am also grateful that you saw my need for a distraction and agreed to let me adopt Max, the wonderful dog who has kept me balanced and sane for the last months.

My amazing boys, Baste and Theo, you have been very understanding when I have had to work late and my brain has been preoccupied when at home. It warms my heart to think of the interest you boys have shown in my work, especially around the time of “Forsker Grand Prix” when you were a patient audience during my repeated trial-runs.

Thank you to my parents and in-laws for picking up the kids, making dinners and helping us in the chaos that sometimes occurs in everyday life with two working parents and two active kids. You never say no when we ask for any kind of help, and this has made our life so much easier.

Lastly, I would like to send a thank you to the mice who have unknowingly helped aid us in our research. It is often easy to ignore their contribution, but none of this would have been possible without their sacrifice. I do not take lightly on the responsibility we as researchers have to do our job correctly, and I hope the results we have found will prove important enough to have demanded so many mice.

Karina Skjervheim Prestegård

Bergen, May 2022

Table of Contents

ABSTRACT	iii
SCIENTIFIC ENVIRONMENT	vii
ACKNOWLEDGEMENTS	xiii
ABBREVIATIONS.....	xvii
LIST OF PUBLICATIONS.....	xix
1 GENERAL INTRODUCTION	1
1.1 PHENYLKETONURIA AND PHENYLALANINE HYDROXYLASE	1
1.1.1 EARLY HISTORY	1
1.1.2 HEREDITY, CLASSIFICATION AND PREVALENCE	2
1.1.3 PHENYLALANINE HYDROXYLASE.....	3
1.1.4 PKU-ASSOCIATED <i>PAH</i> MUTATIONS.....	8
1.1.4.1 THE p.R261Q-PAH MUTATION	12
1.1.5 MUTATION-DEPENDENT INSTABILITY OF PAH.....	12
1.1.6 CURRENT TREATMENTS OF PKU.....	13
1.1.7 COMORBIDITIES IN PKU.....	16
1.1.8 PKU IS A PARADIGM DISEASE.....	17
1.2 PROTEOSTASIS NETWORK	18
1.2.1 PROTEIN FOLDING AND AGGREGATION	18
1.2.2 MOLECULAR CHAPERONES.....	20
1.2.3 UBIQUITIN-DEPENDENT PROTEASOME SYSTEM.....	22
1.2.4 AUTOPHAGY SYSTEM	22
1.2.5 PROTEOSTASIS REGULATION OF PAH MUTANTS IN PKU	24
1.3 ANIMAL MODELS.....	24
1.3.1 ANIMAL MODELS FOR HUMAN DISEASE	24
1.3.2 PKU MOUSE MODELS.....	26
1.3.3 PHENOTYPING ANIMAL MODELS.....	27
1.4 METABOLOMIC STUDIES.....	28
1.4.1 METABOLOMICS IN PKU.....	29
1.5 OXIDATIVE STRESS.....	30
1.5.1 OXIDATIVE STRESS IN PKU.....	31
2 AIMS.....	33
3 SUMMARY OF RESULTS	35
3.1 PAPER I	36
3.2 PAPER II.....	37

3.3	PAPER III.....	39
4	GENERAL DISCUSSION.....	41
4.1	MOUSE MODELS OF PKU – HOW TO MODEL A COMPLEX DISEASE	41
4.2	PAH INSTABILITY AND AGGREGATION.....	43
4.3	METABOLIC PROFILE AND OXIDATIVE STRESS.....	44
4.4	DNAJC12	46
4.5	A NEW UNDERSTANDING OF MOUSE MODELS OF PKU	47
5	CONCLUDING REMARKS AND FUTURE PERSPECTIVES	49
6	BIBLIOGRAPHY	53

ABBREVIATIONS

3Rs	replace, reduce, refine
AAAH	aromatic amino acids hydroxylase
ACT	Aspartate kinase-Chorismate mutase-TyrA
BH ₄	6 <i>R</i> -L-erythro-5,6,7,8-tetrahydrobiopterin
CLAMS	comprehensive lab animal monitoring system
DHPR	dihydropteridine reductase
DNA	deoxyribonucleic acid
Enu	N-ethyl-N-nitrosourea
HPA	hyperphenylalaninemia
Hsp	heat-shock protein
IEM	inborn error of metabolism
LC-MS	liquid chromatography mass spectroscopy
L-DOPA	3,4-dihydroxyphenylalanine
NMR	nuclear magnetic resonance
MS	mass spectroscopy
PAH	phenylalanine hydroxylase
PAL	phenylalanine ammonia lyase
PCD	carbinolamic-4a-dehydratase
PEG	polyethylene glycol
Phe	phenylalanine
PKU	phenylketonuria
RER	respiratory exchange ratio
RNA	ribonucleic acid
ROS	reactive oxygen species
THA	3-(2-thienyl)-L-alanine
Tyr	tyrosine
TH	tyrosine hydroxylase
TPH	tryptophan hydroxylase
UPS	ubiquitin proteasome system
WT	wild type

LIST OF PUBLICATIONS

I Kunwar Jung-KC, Nastassja Himmelreich, Karina S. Prestegård, Tie-Jun Sten Shi, Tanja Scherer, Ming Ying, Ana Jorge-Finnigan, Beat Thöny, Nenad Blau, and Aurora Martinez (2019). **Phenylalanine hydroxylase variants interact with the co-chaperone DNAJC12**. *Human Mutation* **40**(4): 483-494. doi: 10.1002/humu.23712

II Oscar Aubi*, Karina S. Prestegård*, Kunwar Jung-KC, Tie-Jun Sten Shi, Ming Ying, Ann Kari Grindheim, Tanja Scherer, Arve Ulvik, Adrian McCann, Endy Spriet, Beat Thöny, and Aurora Martinez. *These authors contributed equally (2021). **The *Pah-R261Q* mouse reveals oxidative stress associated with amyloid-like hepatic aggregation of mutant phenylalanine hydroxylase**. *Nature Communications* **12**(1):2073. doi: 10.1038/s41467-021-22107-1

III Karina S. Prestegård, Altanchimeg Altankhuyag, Arve Ulvik, Adrian McCann, Ann Kari Grindheim, and Aurora Martinez. **Aging *Pah-R261Q* mouse model of phenylketonuria suggests that unknown compensatory mechanisms may limit progression of metabolism related comorbidities**. *Manuscript in preparation*.

1 GENERAL INTRODUCTION

1.1 PHENYLKETONURIA AND PHENYLALANINE HYDROXYLASE

Phenylketonuria (PKU) is the most common inborn error of metabolism (IEM). It requires early treatment through diet to avoid severe irreversible physical and mental disabilities and is part of the neonatal screening in most countries. Appropriate diet avoids neurotoxic buildup of the amino acid phenylalanine (Phe), which is otherwise the consequence of untreated PKU. The high levels of Phe that accumulate in PKU (see details in section 1.1.3) will result in severe intellectual disability, motor deficits, epilepsy, and behavioral problems [1]. Today, PKU patients receive treatment from the time of diagnosis and are advised to continue for the rest of their life. At first glance, PKU may seem like a well-defined and treatable disease, but research shows that PKU is more complicated than it first appears [2-4].

1.1.1 EARLY HISTORY

The medical history of PKU started in 1934 when the Norwegian physician Asbjørn Følling examined two siblings suffering from physical and mental developmental abnormalities. He found that their urine had an abnormal musty odor and discovered that this was caused by an excess of phenylpyruvic acid, which is a metabolite of Phe [5]. For a long time, the disease was known as Følling's disease, especially in the Northern countries.

Følling's discovery was quickly picked up by Lionel Penrose in Britain, who identified the inheritance pattern of the disease, and that a buildup of Phe in blood and brain was the cause [6, 7]. He was the first to test out a dietary intervention, by removing all proteins and thereby Phe from the diet. As recounted by Daly et al. [8], Penrose's one patient was only allowed to eat fruit, sugar, olive oil, and vitamins, and the experiment was discontinued when the lack of all amino acids resulted in malnutrition. Twenty years after the description of PKU, Bickel, Gerrard, and Hickman worked together to develop a Phe-free protein substitute suitable for PKU patients [9]. It was first tested on a 2-year-old patient in Britain and required several months of adjustments to avoid malnutrition. Although the diet was extremely limited and the protein-supplements were distasteful,

the patient's improvement was clear [8]. The dietary treatment for PKU patients today is still based on this work by Bickel and Co. in the 1950s [9].

Despite the progress in treatment, patients were still diagnosed too late to avoid the destructive consequences of Phe build-up. By coincidence, the cancer researcher Robert Guthrie became personally interested in PKU late in the 1950s and discovered that he could adapt an already existing bacterial-inhibition-assay to react to high Phe concentrations. This test was easy, effective, and relatively inexpensive, and it only took a few years before most newborns in the US had their Phe-levels measured [10]. Today, most countries do routine neonatal screening to detect elevated levels of Phe in blood (heel prick test) and thus PKU [11]. Early diagnosis is therefore possible, and a low-Phe dietary treatment can start only weeks or even days after birth.

1.1.2 HEREDITY, CLASSIFICATION AND PREVALENCE

PKU is an autosomal recessive disease, meaning that a person must inherit a gene mutation from both parents to have the disease. A person who only inherits one mutated gene will not develop PKU but will be a carrier and can pass the gene on to their children.

Historically, patients with PKU were classified based on their untreated blood Phe levels; mild hyperphenylalaninemia (HPA) (120-600 $\mu\text{mol/L}$), mild PKU (600-1200 $\mu\text{mol/L}$), and classic, also called severe, PKU (>1200 $\mu\text{mol/L}$) [12]. However, according to the new European Guidelines from 2017 [13], PKU is now classified into mild HPA (120-360 $\mu\text{mol/L}$), which will not need treatment, and PKU (>360 $\mu\text{mol/L}$), where treatment is required. PKU patients are again divided into 6*R*-L-erythro-5,6,7,8-tetrahydrobiopterin (BH₄) responsive and non-BH₄-responsive [13], referring to the response to treatment with BH₄ supplementation (see sections 1.1.3 and 1.1.6). The new classification has been introduced since the highest untreated blood Phe levels are no longer reached with early diagnosis and treatment. The alternative Phe-tolerance testing has also been shown to be unreliable as several factors can interfere with the results [1]. The historical classification will be used in this work to correctly cite the data found in published sources.

Despite PKU being the most common of the IEMs it is still a rare disease with a prevalence that varies greatly between ethnicities and geographic regions worldwide.

PKU is most common in Caucasian and East Asian populations with a prevalence ranging from 1:10 000–15 000 live births, but even within Europe the prevalence ranges widely: Italy (1:2700 live births) and Ireland (1:4500 live births) have very high prevalence, while Finland is on the other side of the scale with <1:100 000 live births [14]. In some regions of Middle Eastern countries, such as Turkey and Iran, the prevalence is extremely high compared to the adjacent regions, possibly due to the more frequent occurrence of consanguineous marriages. In addition to geographic variations in prevalence, the severity of phenotype seems to follow a gradient across Europe, from classic PKU in the east to mild PKU in the southwest and mild HPA in the south. Also, the frequency of classic PKU relative to the total HPA/PKU cases increases from Europe (54%) via the Middle East (71%) to Australia (80%) [14].

In Norway, PKU occurs in around 1:11 500 live births with 52% showing a severe classic phenotype with blood Phe levels >1200 $\mu\text{mol/L}$ and 43% presenting with a mild to moderate PKU with Phe levels <1200 $\mu\text{mol/L}$ [14].

1.1.3 PHENYLALANINE HYDROXYLASE

PKU is caused by mutations in the gene coding for the enzyme phenylalanine hydroxylase (PAH), resulting in the production of unstable enzyme forms with impaired catalytic activity. PAH catalyzes the hydroxylation of the amino acid Phe to tyrosine (Tyr), using the cofactor BH_4 and non-heme ferrous iron, as well as molecular oxygen as additional substrate [1] (Figure 1). In the reaction, the cofactor is hydroxylated to 4a-hydroxy- BH_4 , which is regenerated back to BH_4 by the consecutive action of carbinolamine-4a-dehydratase (PCD), that produces quinoid dihydrobiopterin (q- BH_2), and NADH-dependent dihydropteridine reductase (DHPR). In addition, BH_4 is synthesized by the *de novo* pathway from guanosine triphosphate (GTP) by the enzymes GTP cyclohydrolase I, 6-pyruvoyltetrahydropterin synthase and sepiapterin reductase [15].

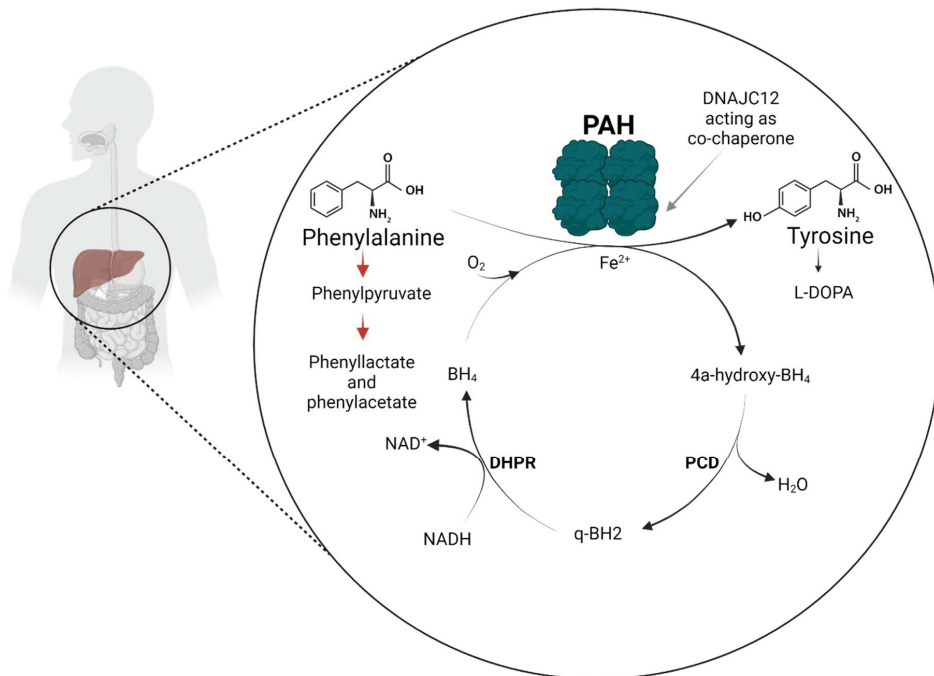


Figure 1: The phenylalanine hydroxylating system. The system includes the iron (Fe^{2+})-dependent enzyme phenylalanine hydroxylase (PAH), which converts phenylalanine (Phe) into tyrosine (Tyr) using tetrahydrobiopterin (BH_4) as cofactor and molecular oxygen (O_2) as additional substrate. It also includes the regeneration of BH_4 by the enzymes carbinolamine-4a-dehydratase (PCD) and the NADH-dependent dihydropteridine reductase (DHPR). In the case of PAH dysfunction, normally caused by *PAH* mutations, other reactions are favored for the degradation of Phe (indicated by the red arrows), with accumulation of phenylpyruvate and other phenylketones. The figure was created using Biorender.

Phe is an essential amino acid and can only be obtained from diet and degradation of endogenous proteins. It is estimated that ~80–90% of dietary Phe is converted to the non-essential amino acid Tyr by PAH. Among other important metabolic fates, Tyr is important in the production of the neurotransmitters dopamine, adrenaline, and noradrenaline. When the PAH enzymes are mutated and impaired, they are unable to metabolize Phe at an acceptable rate and the result is a toxic buildup of Phe in blood and brain, i.e., HPA.

1.1.3.1 THE BH₄-DEPENDENT AROMATIC AMINO ACID HYDROXYLASE FAMILY

PAH belongs to the aromatic amino acid hydroxylase (AAAH) protein family, which in addition to PAH, is comprised of tyrosine hydroxylase (TH), and the tryptophan hydroxylases (TPH1 and TPH2). All four enzymes catalyze crucial metabolic reactions in a BH₄ and non-heme Fe²⁺ dependent manner [16]. The hydroxylation of Phe to Tyr by PAH in the liver is the first and rate limiting step in the catabolism of excess Phe. TH in the central and peripheral nervous system, and in adrenal medulla, catalyzes the hydroxylation of Tyr to 3,4-dihydroxyphenylalanine (L-DOPA), the rate limiting step in the synthesis of catecholamine neurotransmitters and hormones dopamine, noradrenaline, and adrenalin. The TPHs in the brain and gastric system catalyze the first step in the biosynthesis of serotonin and melatonin.

The AAAHs are comparable in structure and domain organization (regulatory, catalytic, and oligomerization domains), but while their catalytic domains present high sequence identity, the regulatory ones are more diverging [17]. This is reflected in the similar catalytic reactions with their specific substrates, yet very different regulatory mechanisms of the different enzymes [18].

1.1.3.2 THE STRUCTURE AND CATALYTIC MECHANISM OF PAH

While the other AAAHs are homotetramers, the PAH molecule occurs in an equilibrium of dimeric and tetrameric forms, with tetramers that undergo allosteric conformational change upon activation by Phe [19, 20] (Figure 2A, B). Each PAH subunit is organized in three domains: An N-terminal regulatory domain, a catalytic domain, and a C-terminal oligomerization domain that mediates the dimerization and tetramerization of the subunits, the latter by a helix bundle [21, 22] (Figure 2C). Residues 30-100 in the regulatory domain constitute an Aspartate kinase-Chorismate mutase-TyrA (ACT) domain, which is a regulatory module that often dimerizes and binds to amino acids [23] and is necessary for the regulatory properties of PAH [19]. The catalytic domain includes the binding site for iron, the cofactor BH₄, and the amino acid substrate (Figure 2D).

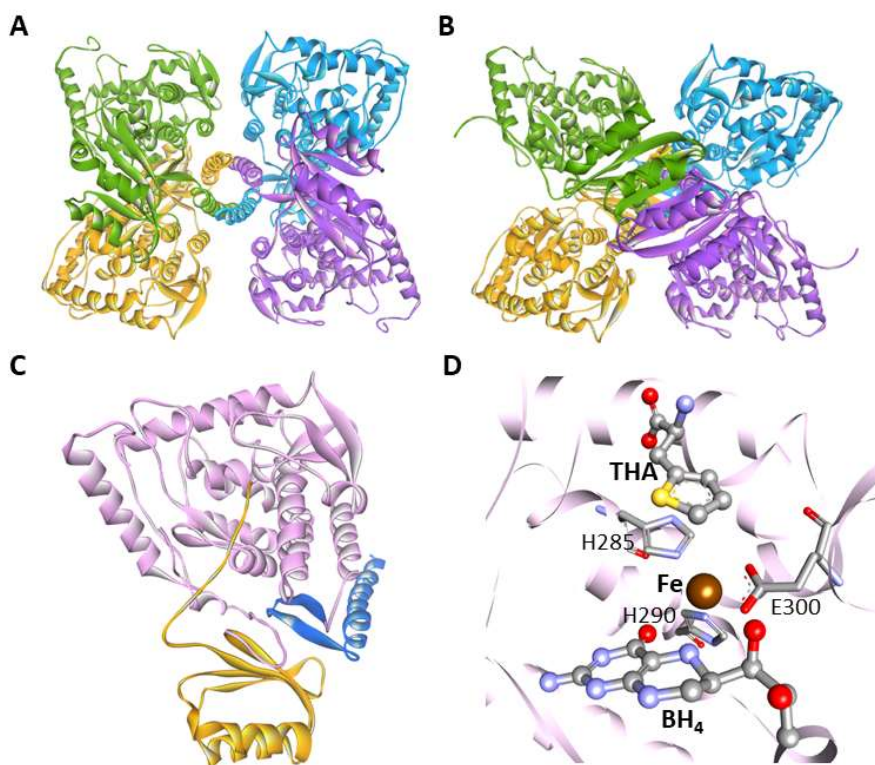


Figure 2. The structure of PAH. A) The crystal structure of inactivated, BH₄-bound PAH (PDB 6HYC), with each subunit shown in a different color. B) The modeled structure of tetrameric PAH activated by Phe [19]. C) The structure of PAH from PDB 6HYC, showing the regulatory domain (residues 1-110) in orange with an unstructured N-terminal (residues 1-29) and an ACT domain-fold (residues 30-110), the catalytic domain (residues 111-410) in pink, and the oligomerization domain (residues 411-452) in blue. D) The active site of PAH forming a ternary complex with the bound Phe analogue 3-(2-thienyl)-L-alanine (THA) and BH₄, with the catalytic iron (Fe) in brown. THA and BH₄ as well as the Fe-coordinating residues H285, H290 and E300 are highlighted (from PDB 1MMK) [24].

The catalytic mechanism is rather similar for all the enzymes in the AAHAH family and it has been elucidated partly by characterization of structures of stable ligand-enzyme complexes, such as the ternary complex of the Phe analogue 3-(2-thienyl)-L-alanine (THA) and BH₄ [24] (Figure 2D). The hydroxylation reaction starts with the binding of O₂ to the ternary PAH-Phe-BH₄ complex, forming an iron-and oxygen-mediated adduct Fe(II)-OO-BH₄ and a consecutive hydroxylating intermediate Fe(IV)=O [25, 26]. The reaction then continues with the incorporation of one oxygen atom into BH₄, forming

4a-hydroxy-BH₄ (Figure 1), and another oxygen atom into the aromatic ring of Phe, which reorganizes to Tyr [26].

1.1.3.3 REGULATION OF PAH

As Phe is an essential amino acid needed for protein synthesis it is important that it is not fully catabolized, however, it is also crucial to avoid the neurotoxic effects of HPA. To keep Phe at an optimal level, mammalian PAH is regulated by several mechanisms. PAH is activated by Phe in a positive cooperative manner, so that enzyme activity is low at low Phe levels (<150 μM), and it increases in a sigmoidal manner with rising levels of Phe [27, 28]. At the same time BH₄, despite its essential role for PAH activity as cofactor, it also acts as a negative effector of the enzyme. At low Phe concentrations, PAH exists mainly in stable and inactive complexes with BH₄ [29]. In this state, the BH₄ molecule is bound to the active site in a position not suitable for catalysis and when Phe binds to the active site, BH₄ moves to a more favorable catalytic position closer to the iron, compatible with the formation of the hydroxylating intermediate Fe(IV)=O [20].

Phosphorylation of PAH at Ser16 by cAMP-dependent protein kinase (PKA) is a posttranslational modification that can regulate PAH activity, both *in vivo* [30] and *in vitro* [31]. The concentration of Phe required to activate PAH is decreased by phosphorylation, presumably due to a subtle conformational change at the N-terminal tail that increases the accessibility to the active site [31, 32].

Recently, a new mechanism of regulation of PAH stability and activity was identified when a subgroup of patients diagnosed with HPA did not present mutations in PAH or in enzymes involved in the synthesis and regeneration of BH₄, but in the *DNAJC12* gene, coding for a cochaperone of the heat shock protein 40 (Hsp40) family [33]. In addition to HPA, patients with mutations in *DNAJC12* present dystonia and other motor disorders, as well as intellectual disability and a profile of neurotransmitter deficiencies indicative of dysfunction of PAH, TH and the TPHs [33-35]. In addition, specific immunoprecipitation-mass spectrometry and co-expression analyses of *DNAJC12* and the AAAHs demonstrated that *DNAJC12* is the specific Hsp40 cochaperone of the AAAH enzyme family [33, 36]. The members of the Hsp40/DNAJ protein family

belong to the proteostasis network, working as cochaperones of the Hsp70 molecular chaperones to assist in the quality control of their client proteins, assisting in their folding and degradation, but also protecting them from aggregation [37] (See 1.2.2).

Furthermore, more recently Li et. al [38] have investigated the functional role of long noncoding RNAs (lncRNAs) in the Phe metabolism. These authors have shown that the binding of a lncRNA modulator to the N-terminal regulatory domain of PAH stabilized the Phe-activated PAH conformation, making it more accessible to both Phe and BH₄ [39]. This could be the “unknown” allosteric factor that previously has been hypothesized to stabilize the interaction between PAH and Phe [40]. Furthermore, N-acetylgalactosamine (GalNAc)-tagged lncRNA-mimics appear to have therapeutic potential [38].

1.1.4 PKU-ASSOCIATED *PAH* MUTATIONS

More than 1200 different mutations in the *PAH* gene that can cause PKU have been reported and are recorded in the BIOPKU database [41]. Three of four PKU patients are heterozygotes, i.e., expressing two different *PAH* mutations at the same time [14]. The severity of the phenotype is linked to the inherited mutations and how much damage the mutation causes on the PAH enzyme stability and activity. The heterozygosity explains the great variety of phenotypes found in patients, as the co-expression of different *PAH* mutations can alter the stability and activity of the resulting tetrameric PAHs through interallelic positive and negative complementation compared to what is predicted for either mutation in homozygosity [42].

To understand the relationship between genotype and phenotype, and its inconsistencies, the molecular mechanisms of the disease must be taken into consideration. Gene variants resulting in PAH with mutations around the active site may reduce or totally obliterate the catalytic activity [43]. Moreover, splice-site and non-sense mutations often result in non-functional protein [44]. Thus, patients with both a catalytic and a splice-site mutation usually present with a severe, classic PKU phenotype [45]. Nevertheless, a large number of reported PKU variants are missense mutations that lead to impaired protein stability and misfolding, with concomitant reduced activity, causing mild to moderate phenotype [46-48], but several of the most frequent mutations are associated

with classic PKU (Table 1). The degree of decreased protein stability appears decisive for remaining activity and phenotypic outcome, which are also closely linked with BH₄ responsiveness [45, 47]. Nevertheless, there are some mutations that present inconsistent clinical phenotypes and varying BH₄ responsiveness, e.g., p.L48S-PAH, p.I65T-PAH and p.R261Q-PAH [49].

Table 1. Frequent HPA and PKU mutations. The most frequent HPA and PKU mutations with allele frequency, effect on protein activity and levels, as well as expected associated phenotype and location in the PAH structure, are summarized.

PAH variant	Allele ^a frequency (%)	PAH ^b activity (%)	PAH ^c protein (%)	Associated ^a phenotype	Location in PAH
p.R408W	19.2	2 (0)	12 (7)	Classic PKU	Catalytic domain
p.R261Q	5.5	23 (19)	41 (26)	Mild PKU ^d	Catalytic domain
p.I65T	4.0	33 (10)	19 (7)	Mild PKU	Regulatory domain
p.L48S	2.7	43 (5)	12	Mild PKU	Regulatory domain
p.R243Q	2.7	6 (1)	3 (2)	Classic PKU	Catalytic domain
p.A403V	2.4	33 (21)	113 (38)	Mild HPA	Catalytic domain
p.V388M	1.8	83 (46)	98 (17)	Mild PKU	Catalytic domain
p.A300S	1.5	65 (24)	77 (21)	Mild HPA	Catalytic domain
p.R252W	1.4	15 (9)	0 (0)	Classic PKU	Catalytic domain
p.E280K	1.3	11 (4)	1 (1)	Classic PKU	Catalytic domain
p.R241C	1.1	33 (21)	113 (38)	Mild HPA	Catalytic domain
p.L348V	0.9	25 (24)	4 (2)	Mild PKU	Catalytic domain
p.R413P	0.69	11 (7)	17 (7)	Classic PKU	Oligomerization domain
p.R408Q	0.63	41 (22)	80 (16)	Mild PKU	Catalytic domain
p.R68S	0.6	25 (21)	76 (32)	Mild PKU	Regulatory domain
p.I306V	0.6	25 (4)	123 (15)	Mild HPA	Catalytic domain
p.D415N	0.44	35 (32)	80 (26)	Mild HPA	Oligomerization domain

^a Allele frequency and associated phenotype for homozygous patients according to the BIOPKU database [41]

^b Residual *in vitro* PAH activity and ^c PAH total protein, both relative to WT-PAH (100%) in expression studies in COS cells [50] presented as mean (SD).

^d Phenotype varying from mild HPA to classic PKU, with most patients presenting mild PKU.

The frequent mutations presented in Table 1 are located in all three domains of PAH, but they are most abundant in the catalytic domain, which also contains the most common severe mutations associated with classic PKU (Figure 3). Mutations that concentrate in an area comprising residues 235–330, corresponding to exons 7–9 of *PAH*, which seems crucial for PAH stability and active site integrity, are associated with severe phenotype [47].

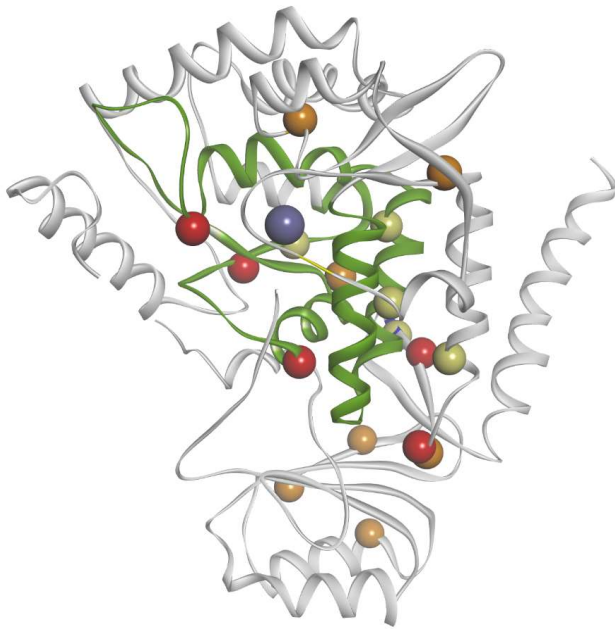


Figure 3. The location of frequent HPA and PKU associated mutations represented on the subunit structure of PAH. The mutations summarized in Table 1 have been represented in the subunit structure of PAH (PDB 6HYC) according to their associated phenotype; classic PKU (red), mild PKU (orange) and mild HPA (yellow). The area of the backbone colored in green (residues 235-330) corresponds to the hotspot region for destabilization of PAH identified in [47]. The active-site iron is shown in indigo.

While PKU always causes HPA, not all HPA is associated to PKU and PAH deficiency. Approximately 2% of all HPA cases are associated with BH₄ metabolism deficiency: Mutations in enzymes involved in the synthesis and recycling of BH₄ (Figure 1) lead to reduced cofactor levels and thereby an increase in Phe [51]. More rarely, HPA is caused by DNAJC12 deficiency [33] (see 1.1.3.3). BH₄ and DNAJC12 deficiencies are treatable if detected early, however, their treatment is not identical to that of PKU, as the other AAAs (TH and TPHs) are affected as well as PAH. BH₄ deficiency and severe cases of DNAJC12 deficiency requires treatment with L-DOPA/carbidopa, BH₄ and 5-hydroxytryptophan, in addition to the Phe-reduced diet [52]. Thus, a correct and early diagnosis on the origin of HPA is crucial.

1.1.4.1 THE p.R261Q-PAH MUTATION

The p.R261Q-PAH mutation is one of the most frequent mutations, with an average worldwide allele frequency of 5.5% (Table 1), and approximately 2% of PKU patients are homozygous for this mutation [49]. In Europe, it is the second most common mutation with an allele frequency of 11%, with a prevalence ranging between 10–30% in most countries (from 2.3% in Denmark and Czechia to 29.7% in Bulgaria and 23.5% in Portugal) [14]. When in homozygosity it is mostly associated with mild PKU, but an unexplained variability in the phenotype is encountered, and some patients present classic PKU [53]. This mutation has been shown to cause unstable and misfolded PAH [50, 54] that responds to BH₄ treatment, although with a highly variable effect [49, 54].

1.1.5 MUTATION-DEPENDENT INSTABILITY OF PAH

A number of studies have contributed to the understanding of the molecular pathogenic mechanism in PKU, where a loss-of-function caused by the decreased stability and/or folding efficiency in mutated PAH appears to be predominant and determinant of the phenotypic outcome of the disease [46, 55-57]. In general, the larger destabilizing effect the mutation has on the structure of PAH, as found for mutations in the hotspot destabilizing area (Figure 3), the lower the activity *in vitro* and the more severe the phenotype [47]. Nevertheless, a genotype-phenotype correlation is challenging as the patient's phenotype is affected by several genetic and non-genetic modifying factors that contribute to the metabolic and cognitive phenotypes [47]. This understanding led to an early characterization of PKU as a “complex trait” genetic disease [2, 3], an attribute that is being extended to IEMs in general [58].

When expressed *in vitro*, several missense mutations demonstrate folding and stability defects, and a propensity to aggregate [46, 56, 57, 59]. Misfolding and aggregation of PKU-associated PAH mutants *in vitro* was first studied in the 90s using *E. coli* to express different PKU mutations [59, 60]. A tendency to form high-molecular-mass PAH aggregates was found when overexpressed in *E. coli*, and the enzyme architecture was revealed to be very sensitive to single point mutations [59]. Moreover, Gersting et al. [48] found that not only the enzyme activity, but also allostery, was severely affected by mutations in all three domains, concluding that amino acid substitutions in the side-

chain could induce long-range, global conformational changes affecting PAH activity and regulation [48].

Several studies on aggregates in PKU have focused on the p.G46S-PAH mutation that results in a severe phenotype in patients. The p.G46S-PAH mutant is known to form soluble and insoluble aggregates when overexpressed in prokaryotic systems and undergo a rapid degradation when expressed in eukaryotic cells [60-62]. These aggregates have been shown to form linear fibrils that bundle together in branched networks much larger than amyloid/amyloid-like fibrils that form nonbranching structures [63].

Expression and characterization studies thus show that mutated PAH is predisposed for abnormal folding and aggregation. However, it must be pointed out that PAH is overexpressed in these experiments and may not aggregate permanently in patients the same way as in *E. coli*, as eukaryotic cells have a much more sensitive and specific systems for handling protein aggregates [55]. The studies indicated that it only takes a single amino acid substitution to disrupt domain interactions and stability, inducing protein misfolding, aggregation, and early degradation. All together, these factors can result in loss of functional PAH, impaired Phe metabolism and HPA/PKU [48, 64]. As mentioned above, the severity of HPA or PKU in a patient is dependent on the combination of mutations and how these mutations affect the structure of their PAH.

1.1.6 CURRENT TREATMENTS OF PKU

Today, due to newborn screening and the dietary treatment of the disease it is exceedingly rare to find cases of untreated PKU. Since the 1950s, PKU patients have been treated with strict Phe-reduced-diets. This is achieved by consuming food low in protein (both natural and specially made) and replacing all other amino acids in supplements also containing necessary micronutrients [65]. Both the European and US Guidelines for PKU recommend this as a life-long treatment since the consequences for an adult to live off diet has been found to span from clinical issues like tremors and visual abnormalities [66, 67] to adverse effects on attention and executive function [68, 69].

The dietary treatment has a profound effect in decreasing the neurocognitive consequences of PKU. But the strict diet negatively affects the patient's quality of life and more than 50% of patients stop adhering to the diet and monitoring their Phe levels when they reach adolescence and adulthood [70]. The need for new and improved therapies is high, and in the last decades two new treatments have reached the market.

Kuvan, also known as sapropterin, is a synthetic form of the PAH cofactor BH₄, that increases the PAH activity so that responding patients can metabolize more Phe and allow more protein in their diet [54, 71]. However, it is estimated that only 20% to 50% of PKU patients are responding to Kuvan with a Phe reduction in blood of 30% or more, which is the limit for clinical efficacy [72, 73]. Responsiveness to Kuvan is linked to the amount of residual PAH activity [74] and patients with mild or moderate phenotypes (80% or 50%, respectively) respond much better than those with a severe phenotype (less than 10%) [72]. The daily dose is adjusted for each patient, allowing them to increase their Phe-intake, but not necessarily to go off the diet completely.

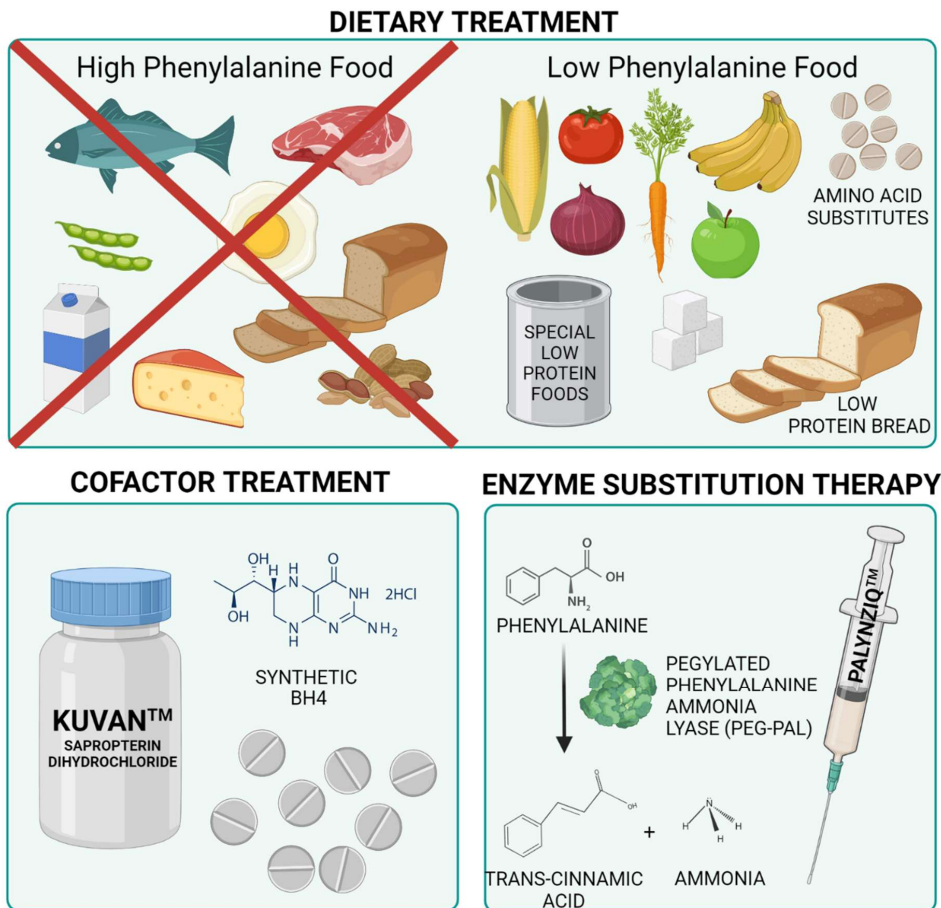


Figure 4. Current treatment options for PKU. The available treatment options are currently: dietary treatment, cofactor treatment, and enzyme substitution therapy. See main text for more details. The figure was created using Biorender.

The most recently approved PKU treatment is an enzyme substitution therapy using Pegvaliase (Palynziq). It contains an enzyme from plants, Phenylalanine Ammonia Lyase (PAL), that catalyzes the conversion of Phe to innocuous trans-cinnamic acid and metabolically minor amounts of ammonia, and thereby replaces the function of PAH [75]. As PAL is not a natural enzyme for the human body, it provokes strong immune reactions and is therefore pegylated, i.e., coated with polyethylene glycol (PEG) polymers, to reduce the immune response [76]. Contrary to Kuvan, Palynziq is highly

effective in most patients [77] and allows them to follow a normal diet. However, there are major disadvantages with this treatment; it must be administered by daily subcutaneous injections, and most patients experience adverse effects such as skin reactions, joint stiffness (arthralgia), and in rare cases anaphylactic reactions, despite pegylation of PAL [77, 78]. Most of the side-effects diminish after the first 6-months of on-going treatment. Palynziq is approved for adults (≥ 18 years) in the United States and for adolescents and adults in the European Union (≥ 16 years) [79, 80], and not for children, where effective treatment and Phe level control are most critical to avoid irreversible damage.

Unfortunately, none of the three available treatment options, low-Phe diet, Kuvan or Palynziq, are satisfactory as they only focus on the reduction of Phe levels. This might be effective in avoiding the neurological damage seen in untreated PKU patients but does not directly address the pathomechanisms of PKU, such as misfolding of PAH, which may challenge the proteostasis network and could contribute to comorbidities.

1.1.7 COMORBIDITIES IN PKU

The presence of comorbidities in PKU patients has been recognized for long but is complicated to study. With the many different mutations and phenotypes, combined with variations in dietary treatment compliance and control of blood Phe-levels during adolescence and adulthood, there are many factors to consider when mapping comorbidities. Several studies have indicated increased prevalence of disorders such as asthma and obesity [81], renal disease [82], cardiovascular complications [82], and multiple neuropsychiatric conditions [83] in PKU patients compared with non-PKU peers [83]. However, it should be mentioned that not all studies come to the same conclusion regarding PKU and its comorbidities, e.g., obesity [84]. A reason for the varying results may be that these comorbidity-studies have grouped all PKU patients together, while based on mutation types or metabolic phenotype (e.g., off-diet blood Phe levels) might be more reasonable, as well as good/poor compliance to diet and control of blood Phe-levels. Such a grouping, on the other hand, posts new challenges as the number of patients for each mutation is small, and it would be difficult to gather significant data.

Even well-treated PKU patients with good compliance to their diet and low average Phe-levels have higher incidences of specific learning disabilities and symptoms comparable to attention-deficit-hyperactivity disorder (ADHD) compared to non-PKU peers [85, 86]. The ADHD symptoms have also been described in other IEMs [87], implying that high Phe-levels are not the sole explanation for PKU comorbidities.

The first PKU patients benefitting from dietary treatment are now reaching their 50s and 60s, and there is a need for more knowledge about comorbidities in PKU and the effects of aging. In a recent review, Vardy et al [88] looked closer at conditions relevant to aging in early-treated adults with PKU. They focused (among other things) on obesity, kidney disease, osteoporosis, cardiovascular disease, cognitive deficits, neurodegeneration, and auto-immune diseases, many of which are expected to increase with aging also in the healthy population. They found an increased prevalence or earlier onset of disease in early-treated adults with PKU in several studies. However, most of the studies included patients with mixed age and treatment-history, and a confirmation of any comorbid association with the disease in question and PKU is challenging. Vardy et al concluded that there is a need for a large and detailed PKU-register, as well as longitudinal studies, to answer the many questions related to PKU, comorbidity and aging [88].

1.1.8 PKU IS A PARADIGM DISEASE

PKU is considered a paradigm disease for IEMs and discoveries done in PKU research have been at the front for other genetic diseases [4, 89]. Compared to many other IEMs PKU is a relatively uncomplicated disease to work with; it is easily diagnosed, has a clearly defined biomarker, available treatment options, and there are relatively many patients with well-documented phenotypes. Although PKU is more complex than the oversimplified ‘one gene-one disease’ model it originally seemed to be [4, 89], it has set an example for other IEMs as PKU was the first disease where: (i) severe intellectual disability was explained biochemically; (ii) a dietary treatment could prevent the severe effects of the biochemical abnormality; (iii) newborn screening was developed, allowing diagnosis to be set in time to prevent the severe effects of the disease; (iv) patients needed personalized dietary treatment with varying strictness due to variability in the

disease-severity; (v) dietary treatment could be replaced (or at least downscaled) using drugs in some patients (notably Kuvan) [1].

Today, we see how the discoveries in PKU research have paved the way for other genetic disorders, notably IEMs. Newborn screening has evolved to diagnose more than just PKU; in Norway 26 rare diseases are screened for, of which 21 are IEMs. Several IEMs are treated with low protein diets, some such as maple syrup urine disease, galactosemia, urea cycle disorders and tyrosinemia type I [90-92], in combination with other treatment modules.

1.2 PROTEOSTASIS NETWORK

1.2.1 PROTEIN FOLDING AND AGGREGATION

A protein consists of a long chain of amino acids in a specific sequence that folds into an intricate three-dimensional structure. This conformational state is the native state of the protein associated with its biological activity. Proteins are dynamic structures that fluctuate between conformational states, driven by their thermodynamic properties. The native state of a protein represents the ensemble of low-energy conformations resulting in a thermodynamically stable and functional structure with a low free energy [93].

The cell's ability to properly balance protein synthesis, folding and degradation, i.e., protein homeostasis or simply proteostasis, is crucial to the protein quality control and to maintain cellular health [94]. Unfolded, misfolded or aggregated proteins need to be managed and controlled, which require a complicated balancing job, performed by the proteostasis network [95-97]. Main players in this network are the molecular chaperones (heat shock proteins: Hsp60, Hsp70, Hsp90, Hsp100 and the small Hsps) and their cochaperones (in particular DNAJ/Hsp40 proteins, HIP and CHIP), in addition to the ubiquitin dependent proteasome (UPS) and autophagy systems [98, 99].

A correctly folded soluble protein is typically organized with hydrophobic amino acid residues inside their conformational structure to avoid aggregation and unintended hydrophobic interactions. By taking random folding-steps that are favorable in free energy, the proteins reach their low-energy, native-like conformations where they are biologically active [100]. Even a small error in the protein synthesis or folding process, can result in an inactive misfolded protein [101]. When the folding process fails,

hydrophobic areas are exposed and can attract other molecules, which may result in aggregation [102]. Other errors, such as mutations, can also shift the thermodynamic landscape so that other non-native conformational states or aggregates are more stable than the native states [100].

Abnormal protein folding is linked to an increasing list of pathologies, where it has traditionally been distinguished between loss-of-function and toxic gain-of-function diseases. PKU has been considered an example of a loss-of-function genetic disease, where catalytic activity is not only impaired due to mutations in residues directly involved in catalysis, but mainly through destabilization of the PAH structure that results in loss of protein and residual activity [45, 48]. Gain-of-function, on the other hand, usually refers to more common neurodegenerative diseases – both of familial and idiopathic origin – such as Alzheimer’s and Parkinson’s disease, where severe protein aggregation with formation of oligomers, amyloids and fibrils is associated with cellular toxicity and disease progression [102-104]. Recently, there seems to be an increasing consensus to view the concurrence of gain- and loss-of function in the pathogenesis of these type of diseases [105], as well as the implication of the age-dependent decline in proteostasis network capacity [97].

While most nonnative proteins accumulate in unstructured amorphous aggregates some can also create large amyloid fibrils, defined by β strands running across the long fibril axes [98]. These fibrils can display a tensile strength close to that of steel [106], and it is therefore not surprising that the amyloid form of a protein can be more stable than the native state [102]. Oligomeric aggregates often precede the formation of amyloid fibrils, and these oligomers are thought to have an important part as disease instigators [98, 103, 104].

The proteostasis network is intricately arranged and several of its components are tailored to specific cells or tissues, reflecting the need for tight regulation [107]. Even slight dysregulation of the proteostasis network and small variations in the relative levels of its components can have profound consequences for disease progression as the cells defenses against misfolded and damaged proteins can be altered [97, 108].

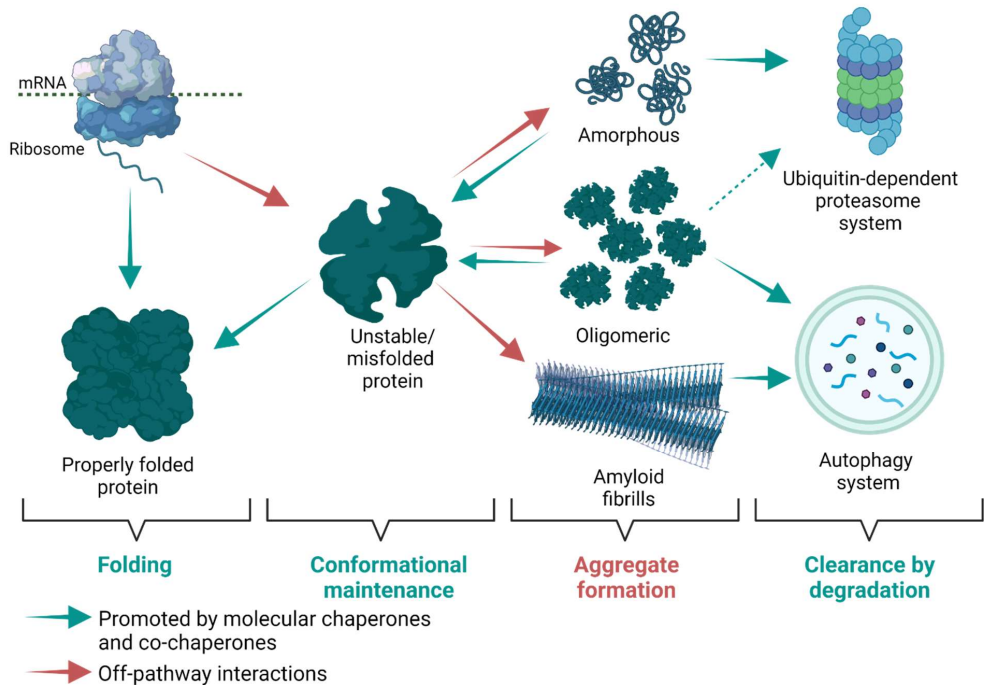


Figure 5. Simplified representation of the proteostasis network. From their initial folding and throughout their lifetime in the cell, proteins are dynamic structures that fluctuate between conformational states. Molecular chaperones and cochaperones play an important role in the cellular proteostasis network, working in several ways to keep the proteome balanced. They help with folding of newly synthesized proteins, the upkeep of conformational maintenance, and preventing potentially toxic aggregation. The removal of terminally misfolded and aggregated proteins is done in cooperation between the ubiquitin-dependent proteasome and autophagy. The illustration was adapted from [98] and created using Biorender.

1.2.2 MOLECULAR CHAPERONES

To ensure proteostasis and avoid the dangers of toxic protein species, cells invest in an intricate network of molecular chaperones [109]. These chaperones are proteins that help other proteins acquire and maintain their functionally active form without being part of their native structure [110]. They play an important role in the proteostasis network, either alone or combined with cochaperones, as they are involved in folding, refolding, disaggregation, degradation, and trafficking within the cell [98]. Chaperones are usually divided into different groups based on their sequence homology. As many chaperones are induced under conditions of stress (such as heat shock or oxidative

stress) they are called stress proteins or heat shock proteins (Hsps). The concentration of aggregation-prone folding-intermediates increases under these conditions, and upregulation of chaperones is needed [109]. Molecular chaperones were initially named by their molecular weight: Hsp40, Hsp60, Hsp70, Hsp90, Hsp100 and the small Hsps.

The first tier of chaperones interacts with the nascent chain of amino acids as it emerges from the ribosome. They recognize exposed hydrophobic sequences and act to prevent premature (mis)folding until the nascent chain is long enough to fold properly. Many proteins only need these chaperones to obtain their native form, but complex multidomain proteins require a chain of additional chaperones [111]. Proper folding is then promoted during ATP- and cochaperone-regulated cycles of binding and release [112]. If the rate of folding is slower than the rate of aggregation or chaperone-rebinding, the protein may be transferred to a different chaperone system or to the degradation machinery.

Heat shock 70 kDa proteins (Hsp70s) are essential for protein folding, disaggregation, and degradation [113], and they are one of the most ubiquitous classes of chaperones. Considering their diverse cellular functions, Hsp70s show surprisingly low sequence variability. Their functional diversity can be explained by the fact that they never work alone, but collaborate with many cochaperones, especially DNAJ-proteins (also known as Hsp40s) [114]. DNAJ-proteins are a diverse family with more than 40 members in humans and are usually selective to the clients they target for Hsp70s. Due to their diversity they provide both versatility and specificity to the Hsp70 function [114].

DNAJC12/Hsp40 has been identified as the specific cochaperone of the AAAs and plays a key role in their correct folding and conformational maintenance, in concert with Hsp70 [33] (See 1.1.3.3). Mutations in DNAJC12 have been found to result in mild HPA, dystonia, intellectual disability, and parkinsonism [33], but more recent results have shown a broader clinical spectrum depending on the mutation involved [115, 116]. Results from Gallego et al. [36] indicate that mutations in DNAJC12 have a greater negative impact on the stability of TH and PAH than on TPH. These authors also found that overexpression of DNAJC12 increased PAH levels in several misfolded PAH

mutations, but not in all. This mutation-dependent result can reflect a selective function of DNAJC12 with different PAH mutations.

1.2.3 UBIQUITIN-DEPENDENT PROTEASOME SYSTEM

Misfolded or aggregated proteins that cannot be restored are redirected towards degradation pathways by chaperones [110]. Short-lived, misfolded, and damaged proteins are usually degraded individually by the UPS, while long-lived and insoluble proteins are degraded in groups or aggregates by autophagy [117].

The UPS has two consecutive steps: ubiquitylation and proteolytic degradation. Ubiquitylation entails a three-step process catalyzed by the ubiquitin-activating enzyme E1, the ubiquitin-conjugating enzyme E2, and the ubiquitin ligase E3. The end result is the addition of the small protein ubiquitin to the target protein. In this way the target protein gets marked with a ubiquitin-chain, ready for degradation by the 26S proteasome complex [118]. The marked protein is then unfolded by the proteasome and kept in a non-aggregated state by chaperones [112]. The protein is chopped into smaller fragments and in the end cleaved into single amino acids ready to be reused in protein synthesis.

The proteasome is limited by the size of its central pore, and large protein complexes must therefore be degraded by other mechanisms.

1.2.4 AUTOPHAGY SYSTEM

There are three forms of autophagy: macroautophagy, microautophagy, and chaperone-mediated autophagy. They all end in lysosomal degradation but are mechanistically different. In microautophagy the cytosol is directly engulfed at the lysosome membrane, while chaperone-mediated autophagy requires the contribution of a chaperone (Hsp70) to deliver proteins across the lysosomal membrane [119]. In macroautophagy, organelles (or regions of the cytosol) are isolated into a double-membrane vesicle structure; the autophagosome. This structure is then transported to and fused with, the lysosome, making autolysosomes [119] (Figure 6). The content of the autolysosome is then degraded by lysosomal hydrolases, and the building blocks (amino acids) are returned to the cytosol for reuse in protein synthesis. In this work we focus on macroautophagy (herein autophagy).

Aggregated proteins are marked for degradation by ubiquitin and then detected by autophagy receptors, like the p62 protein, that specifically address ubiquitinated and aggregated protein. p62 is targeted by LC3 proteins, and together they act as an adaptor between the autophagy membrane and its substrates (Figure 6) [120]. There is a large and complex machinery involved in the autophagy process, but the interaction between p62 and LC3 is at the center of the process when large misfolded and/or aggregated ubiquitinated proteins are degraded [120].

There exist intricate connections and crosstalk between the UPS and autophagy [117, 121], leading to a compensatory balance between them to maintain cellular homeostasis.

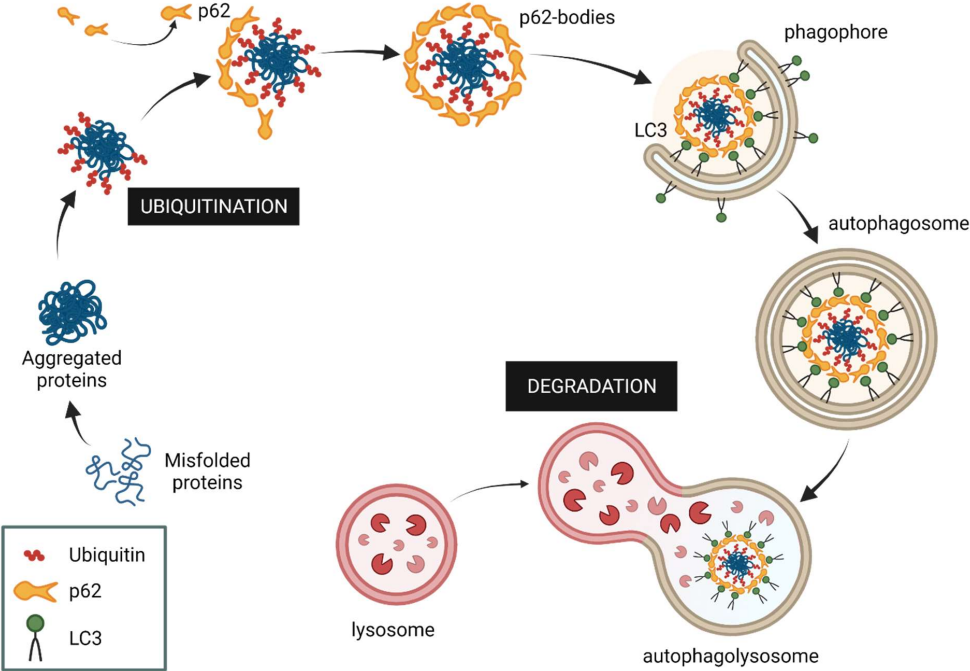


Figure 6. Involvement of p62 and LC3 in the degradation of ubiquitinated and misfolded proteins through selective autophagy. Together p62 and LC3 act as adaptors between the autophagy membrane and the ubiquitinated substrates that will be degraded. The p62 proteins bind to the ubiquitinated aggregated protein and is then targeted by LC3 that connects the substrate to the phagophore. The phagophore encapsulates the substrate generating the autophagosome which fuses with lysosomes to create autolysosomes where the substrate is degraded. The illustration was adapted from [120] and created using Biorender.

1.2.5 PROTEOSTASIS REGULATION OF PAH MUTANTS IN PKU

Protein misfolding has been established as the molecular mechanism in HPA/PKU, and decreased stability, oligomerization, and aggregation, as well as increased degradation of several PAH variants have been documented [64, 122, 123]. These misfolded variants of PAH are clear targets for the proteostasis network and its molecular chaperones [98].

Several studies indicate that this degradation of misfolded PAH proteins is performed by the UPS machinery. In the late 90s, PAH from rat liver was found conjugated with mono- and poly-ubiquitination [32]. Later, PAH from *Enu1/2* mice was found to be highly ubiquitinated and increasingly degraded compared to *WT* mice [124]. The molecular chaperones Hsp70/Hsp40 and Hsp90 inhibit the formation of oligomers and aggregates in the PKU mutation p.G46S-PAH, suggesting that PAH, at least in some mutated forms, is a client protein of the molecular chaperone system [63].

Scheller et al. [125] studied several PKU mutations associated with increased degradation rates and found that cellular PAH levels were increasing in the presence of proteasome inhibitors, indicating these variants as proteasome targets. Furthermore, the results supported the notion that PKU in many instances can be explained by a small destabilization of the PAH protein triggering the proteasomal degradation, leading to a lower amount of PAH, a loss-of-function phenotype, and manifestation of HPA/PKU [125].

PAH mutants, e.g., p.G46S-PAH, p.I65T-PAH, p.243Q-PAH, and p.L348V-PAH, as well as p.V106A-PAH (in the *Enu1* mouse model) have been observed to aggregate when expressed in prokaryote (See 1.1.5) and eukaryote systems [126]. Despite these observations, severe amyloid aggregates have earlier not been considered to be involved in the pathogenesis of the disease, and previous to this thesis autophagy has not been reported to be involved in the proteostasis regulation of PAH and mutants so far.

1.3 ANIMAL MODELS

1.3.1 ANIMAL MODELS FOR HUMAN DISEASE

The concept of using animal models was recognized over 2400 years ago, when the ancient Greeks observed animals to better understand different aspects of the human nature [127]. Since then, animal models have greatly contributed to advance human

medicine, from the development of new surgical techniques, drugs, and vaccines, to increased understanding of human pathophysiology [128].

The goal of a model is always to mimic the system it is modelling as accurately as possible; however, this is also the main challenge with animal models for human disease. Differences in the animal's biology can often lead to "errors in translation" both during planning of experiments and when interpreting research data involving animals [129, 130]. In the last century, with the possibility to genetically manipulate animals into transgenic models, the use of specialized animal models has increased. New tools like CRISPR/Cas9 enable us to create transgenic animals expressing human genes. These humanized models can more accurately mimic specific human mutations and associated diseases and are great assets in biomedical research when used correctly. There are of course differences between mice and men, the most obvious being size, which is closely linked to metabolic rate as well as life history strategy and rate of aging [129]. But with their short lifespan, small size, short breeding cycle, high tolerance of inbreeding, and relatively easy genetic manipulation, mice have by far become the most widely used mammalian animal model in biomedical research [131].

As the use of animal models in research has increased, so has the attention to ethical aspects of using animals. Today, most countries have strict guidelines that must be followed to be allowed to perform animal experiments. These guidelines are built on the concept of the 3Rs (Replace, Reduce, and Refine) for animal research that Russel and Birch developed in the late 1950s [132]. When following the 3Rs one should aspire to use methods that avoid or replace the use of animals (replace), minimize the number of animals used (reduce), and minimize animal suffering as well as improve animal welfare (refine).

Still, there are too many examples where poor experimental design, incorrect statistical methods, or lack of adherence to guidelines lead to non-reproducible and/or false positive results [130, 133]. Explanatory reasons could be that animals were subjected to unnecessary harm or stress, too few animals were used, or the incorrect breed or strain of animal was used in the study [134, 135].

1.3.2 PKU MOUSE MODELS

The first PKU animal models were rats where experimental HPA was induced by the administration of Phe together with PAH inhibitors. By achieving high Phe levels in newborn rats, these studies demonstrated the changes in learning and activity associated with PKU, and some studies reported enduring behavioral abnormalities after ended administration of Phe [136, 137]. However, these chemically induced PKU rat models presented with several difficulties: grossly elevated Tyr levels and large urinary Phe clearance, as well as problems with toxic PAH inhibitors [138]. The decision was then made to produce a heritable PKU model, as this would enable research previously hindered by the PKU animal model being chemically induced and the heterogeneity of the PKU patient population [139]. The first mouse models for PKU were developed in the 90s by phenotype driven N-ethyl-N-nitrosourea (Enu) germline mutagenesis and selection by HPA detection, and named *Enu1*, *Enu2* and *Enu3* [140, 141]. *Enu1* harbors the missense mutation p.V106A-PAH. In humans, the mutation has only been reported in one patient, in a single allele [142]. The *Enu1* mouse shows signs of mild BH₄-responsive HPA, reduced PAH levels and enzyme activity, and a moderately elevated Phe-level corresponding to mild HPA [143]. *Enu2* and *Enu3* are suitable models for severe BH₄-non-responsive PKU with high Phe-levels (>1200 µmol/L). *Enu2* carries the missense mutation p.F263S-PAH, which also presents a very low allele frequency in the PKU patient population worldwide (0.01%; [41]) and is associated with normal protein stability but no PAH activity [143, 144]. *Enu3* has a splice site mutation in the *PAH* gene (at the exon 11– exon 12 junction), generating a frameshift of amino acids and a premature termination codon, thus showing a total absence of expressed PAH protein and activity [141]. As observed in untreated PKU patients with severe phenotype, a pronounced hypopigmentation is seen in *Enu2* (Figure 7) and *Enu3* mice starting at 2 weeks of age. They also display abnormal behavior, grow slower and exhibit a severe maternal effect, referring to a reduced survival of pups from homozygous mutant mothers when kept on a normal diet, none of which are found in the *Enu1* mouse model [144].

These models have been indispensable for PKU research the last 30 years, both for basic investigations and in the search of novel treatments. But as research shows that the

severity of the phenotype is closely linked to the specific mutations and degree of instability they cause in the PAH enzyme [45], there is also a need for mouse models that specifically represent PKU mutations with high allele frequency and moderate/mild phenotype.



Figure 7. Mouse models of PKU and non-PKU HPA. A: control BTBR/Pas mouse. B: *Pah^{enu1/WT}* heterozygous carrier/wild-type mouse. C: *Pah^{enu1/1}* non-PKU HPA mouse. D: *Pah^{enu2/WT}* heterozygous carrier/wild-type mouse. E: *Pah^{enu2/2}* PKU mouse. F: *Pah^{enu1/2}* heteroallelic mouse. The hypopigmentation is clearly seen in E, the *Pah^{enu2/2}* PKU mouse (Photo from [143]).

1.3.3 PHENOTYPING ANIMAL MODELS

When a new animal model is generated, it is important to thoroughly study its phenotype before using it in research. It is crucial to gather enough information about possible unwanted side-effects of the mutation, such as off-target mutation or any events that affect the phenotype, as this can influence how accurate the model is and also to lead to wrong interpretations [145].

Ideally one would do a large-scale high-throughput phenotyping study with multiple standardized tests looking for clinical, physiological, morphological, or behavioral differences between mutant mice and their wild type (WT) siblings [146]. But as this is very costly, the characterization studies are often compromised to initially include a few tests covering a broad area and then focus the study on factors and parameters for which a difference is found or expected to be found.

The only experimental variable in these studies should be the introduced mutation, and measures need to be taken to avoid unintended variables like strain and background, genetic drift, sex ratio, age, concurrent disease, or environmental changes [145].

1.4 METABOLOMIC STUDIES

Metabolites are small endogenous molecules that are the intermediates and end products of metabolism in organisms, and metabolomics is the study of metabolite profiles. From a sample of biofluids, cells, or tissue, it is possible to measure and analyze many different metabolites in one single experiment [147]. A metabolic profile produces a snapshot of the physiological state of an organism at a given timepoint [148].

Metabolites often have a wide range of functions in the cell and organism and their specific functions are not always known. Alterations in metabolite profile can generate downstream effects on diverse processes in cells and tissues and may be signs of disease, genetic differences, and environmental changes. Under normal conditions the adverse effects are counteracted by homeostatic controls, but these can be impaired during aging or disease, resulting in functional decline and failure to return to steady state [149]. Due to new methods and technologies, there is now a focus not only on discovering and recognizing biomarkers, but also on detection of physiological effects of altered metabolite levels.

Untargeted metabolomic analyses measure the broadest range of metabolites in a sample with no prior knowledge and allow for an unbiased investigation of the relationship between interconnected metabolites. Novel and unanticipated discoveries linking cellular pathways to biological mechanisms can be revealed with this approach [148], but it is still not possible to examine all metabolite classes at the same time due to variables in sample extraction and analytic method [149]. If one or more related

pathways are of specific interest, targeted metabolomics is a better approach. Usually driven by a specific question or hypothesis, targeted metabolomics is based on prior information and provides higher sensitivity and selectivity [149]. The main methods used in metabolomic analyses are nuclear resonance spectroscopy (NMR) and, mainly, different versions of mass spectroscopy (MS), e.g., liquid chromatography-MS (LC-MS) and gas chromatography MS (GC-MS) [149, 150].

Metabolic and physiologic changes in mice can also be analyzed using metabolic cages: Comprehensive Lab Animal Monitoring System (CLAMS, Columbus Instruments) can measure several parameters with 12-minute intervals over several days. Among others, indirect calorimetry, metabolic gas exchange (O₂ consumption and CO₂ production), activity level, and feeding are measured. Based on these measurements one can calculate energy expenditure, and respiratory exchange ratio (RER). RER is based on the metabolic gas exchange and reflects the metabolic fuel utilization, revealing if fat, proteins, or carbohydrates are used as sole metabolic fuel [151]. CLAMS cages produce a broad analysis of an animal's metabolic status, and the results provide a basis for choosing more targeted metabolomics.

1.4.1 METABOLOMICS IN PKU

Many studies have analyzed metabolic profiles in patients with PKU, some of them searching for biomarkers associated with the disease while others looked for a link between metabolic disorders and PKU [152]. Most of these studies had a small group of participants (often not reporting past and present diet/treatment status) and differed in study design, sampling method and analysis technique, and their results have a low comparability [153].

There has also been a focus on metabolic effects from following the strict dietary treatment. Due to the low intake of natural protein, there is usually a high caloric intake of carbohydrates in PKU patients, possibly altering their metabolic profile [154]. This can lead to higher risk of carbohydrate intolerance and insulin resistance [155], especially when combined with overweight. PKU patients with excess weight also seems to be vulnerable to the development of metabolic syndrome [152].

In PKU mice, Lu et al. [156] found that several metabolic pathways in cerebral cortex were disturbed (e.g., phenylalanine, tyrosine, and tryptophan biosynthesis; valine, leucine, and isoleucine biosynthesis, and alanine, aspartate, and glutamate metabolism), and they suggest that this can contribute to neurodevelopmental impairment and brain dysfunction found in PKU.

1.5 OXIDATIVE STRESS

Reduction-oxidation (redox) processes are fundamentally important in biology, affecting practically all essential organismal processes. Redox homeostasis is maintained by balancing the prooxidant and antioxidant systems. Prooxidants are mainly reactive oxygen species (ROS), although there are several other reactive species that also have notable impacts on the redox homeostasis, such as reactive nitrogen, sulfur, or carbonyl species [157]. ROS can include free-radical species and non-radical species and play important roles in physiological redox signaling [158, 159]. Even if free radicals are a minor part of the ROS pool [157], their unpaired electron(s) make them highly reactive with high damage potential. The non-radical species of ROS, on the other hand, are more selective in their reactions [160].

An overproduction of prooxidants leads to oxidative stress, which can cause damage to biomolecules (proteins, lipids, carbohydrates, and DNA), leading to cell injury or death [161]. The origin of oxidative stress is usually multifactorial and there is seldom a singular mechanism behind it. ROS are produced internally when the antioxidant mechanisms are overwhelmed due to internal factors, e.g., mitochondria dysfunction or proteostasis dysregulation, or as a consequence of external factors, e.g., pollution or smoking (Figure 8) [162]. Excessive amounts of ROS and their damaging effects have been found to contribute to many human diseases, such as Alzheimer's, cardiovascular diseases, diabetes, and cancer [162, 163].

Organisms have several ways to defend themselves against oxidative stress: The damaging effects of prooxidants can be counteracted by antioxidants, or the autophagy degradation pathway can be initiated [164]. Antioxidants are either low-molecular-weight molecules or larger-molecular-weight enzymes, and both types hinder the formation of ROS and neutralize or mend the ROS-caused oxidative damage [157, 165].

Autophagy is induced by several cellular events, among them oxidative stress [166], and can delay cell death by engulfing organelles and proteins damaged by oxidative stress [167]. The cell is then able to survive under stress conditions by degrading proteins and damaged organelles to recycle nutrients [168].

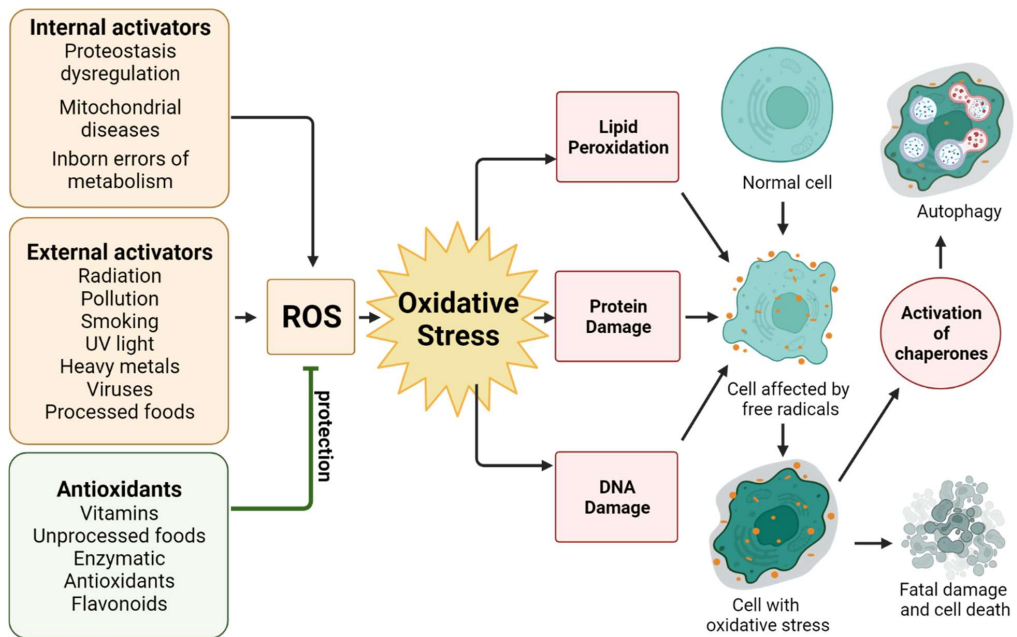


Figure 8: Simplified figure of the link between ROS, oxidative stress, and their cellular effects. Oxidative stress occurs when there is an imbalance between the prooxidant and antioxidant systems and the production of reactive oxygen species (ROS) increases faster than the organism capacity to neutralize them. The production of ROS is influenced by both external and internal factors (activators of ROS). Intracellular structures like proteins, lipids, and DNA are affected and intrinsic mechanisms are disrupted. Cells with oxidative stress will in the worst cases be fatally damaged, but oxidative stress can activate the autophagy system and thereby avoid cell death. The illustration was adapted from [162] and created using Biorender.

1.5.1 OXIDATIVE STRESS IN PKU

In the last decades, several studies have examined oxidative stress in PKU patients and animal models [161, 169]. These studies have strengthened the theory that oxidative stress is one of the pathophysiological processes responsible for brain damage in PKU patients. It is supposed that the two main causes for oxidative stress in PKU are either

nutritional restrictions due to the strict dietary treatment or the toxic Phe levels itself (or associated metabolites) [170]. No matter the cause, it is believed that the oxidative stress causes cell damage and can be linked to impaired antioxidant defenses and increased ROS production [169]. Oxidative damage to biomolecules has been observed in both patients and animal models for PKU, and several studies have found increased lipid and protein oxidation in the brain of a chemically induced rat model of PKU [171-173].

Other studies have reported Phe-induced oxidative stress in several tissues, e.g., brain, blood, and liver, supporting that mitochondrial impairment and oxidative stress can play a role in the pathophysiology of PKU and other HPA conditions [169, 174]. Sanayama et al. [175] found considerably increased oxidative stress when a patient's blood Phe-levels rose above 700–800 $\mu\text{mol/L}$, linking poor metabolic control to increased oxidative stress.

2 AIMS

The overall aim of this Industrial PhD project was to better understand the mechanisms leading to enzyme destabilization and accelerated protein degradation in PKU. This knowledge is essential to undertake the development of novel mechanistic therapies alternative to the Phe-free diet, which is the long-term goal of the present project. As a response to the need for mouse models with PAH mutations found frequently in patients with mild/moderate PKU we included as a specific objective the generation and characterization of a knock-in mouse with the mutation p.R261Q-PAH, expected to reveal enhanced mechanistic insights and be useful in therapy developments. The overall aim was achieved through three subprojects with following specific aims:

1. To further study the role of DNAJC12, the specific HSP40 cochaperone of the aromatic amino acid hydroxylases, in the proteostasis regulation of PAH by characterizing its interaction with PAH (wild-type and mutants) and its effect on enzyme stability by using transient expression of PAH mutants in COS cells and the PAH mouse model *Enu1*.
2. To generate a novel knock-in PKU mouse, *Pah-R261Q*, and perform its thorough characterization, including metabolic and behavioral phenotyping, as well as investigation of the effect of the mutation at the molecular, cellular, and organismal level to obtain insights on the mechanisms that maintain protein quality control and proteostasis of mutant PAH.
3. As the proteostasis network tends to be less effective with age, we aimed to expand the characterization of the *Pah-R261Q* mouse model to include old mice to study the effect of aging on the metabolic and behavioral phenotype.

3 SUMMARY OF RESULTS

Paper I

Phenylalanine hydroxylase variants interact with the co-chaperone DNAJC12.

Kunwar Jung-KC, Nastassja Himmelreich, Karina S. Prestegård, Tie-Jun Sten Shi, Tanja Scherer, Ming Ying, Ana Jorge-Finnigan, Beat Thöny, Nenad Blau, and Aurora Martinez

Human Mutat. 2019 Jan 22; 40(4): 483-494. doi: 10.1002/humu.23712

Paper II

The Pah-R261Q mouse reveals oxidative stress associated with amyloid-like hepatic aggregation of mutant phenylalanine hydroxylase.

Oscar Aubi*, Karina S. Prestegård*, Kunwar Jung-KC, Tie-Jun Sten Shi, Ming Ying, Ann Kari Grindheim, Tanja Scherer, Arve Ulvik, Adrian McCann, Endy Spriet, Beat Thöny, and Aurora Martinez.

*These authors contributed equally.

Nat Commun. 2021 Apr 6; 12(1):2073. doi: 10.1038/s41467-021-22107-1

Paper III

Aging Pah-R261Q mouse model of phenylketonuria suggests that unknown compensatory mechanisms may limit progression of metabolism related comorbidities

Karina S. Prestegård, Altanchimeg Altankhuyag, Arve Ulvik, Adrian McCann, Ann Kari Grindheim, and Aurora Martinez.

Manuscript in preparation.

3.1 PAPER I

In this study we aimed to investigate the role of DNAJC12 in folding and degradation of PAH, both WT and mutants. Endogenous expression of DNAJC12 was studied in COS-7 cells transiently expressing PAH WT or mutants associated with different severity of HPA/PKU. Our results revealed a positive correlation between the levels of immunoquantified PAH and endogenous DNAJC12. The immunodetected levels of endogenous DNAJC12 were reduced for the most unstable PAH mutants associated with highly unstable and misfolded PAH, which result in low immunodetection levels most probably due to rapid degradation of the enzyme.

For *in vivo* studies of the relationship between DNAJC12 and mutant PAH, we used the mouse model *Enu1*, that express the unstable and misfolded PAH mutant p.V106A-PAH. Similar to the observation for the unstable PAH mutants in COS-7 cells, we also measured a substantial reduction of both mutant PAH and DNAJC12 in liver lysates from *Enu1* compared with *WT*. In *Enu1* lysates, most PAH seemed to be mono-ubiquitinated, whereas *WT* PAH was mainly non-ubiquitinated. Nuclear and cytosolic fractions of liver lysates of *WT*, heterozygote (*Enu1^{1/WT}*), and homozygote (*Enu1^{1/1}*) mice were prepared and revealed that nuclear accumulation was not the cause of the apparent large reduction of DNAJC12 in *Enu1* liver lysates.

We measured mRNA levels of *Dnajc12*, *Pah*, and other selected genes based on their possible interactions with DNAJC12, searching for differences between *WT* and *Enu1* in the transcriptional regulation. No significant differences were found when comparing the mRNA expression of these genes in *WT* and *Enu1* mouse liver samples. An intracellular coaggregation of PAH and DNAJC12 could cause a reduced immunodetection, and to test this possibility we prepared lysates using buffer with lower ionic strength to diminish hydrophobic interaction. In addition to this, solubility was enhanced by treating with Triton X-100 (1%) before subjecting the samples to SDS-PAGE. These improvements resulted in a larger detection of mutant PAH and DNAJC12 in the *Enu1* liver lysates, still showing reduced levels compared to *WT* mice. Immunohistochemistry data after improved solubilization by Triton X-100 also gave

increased detection of total PAH and DNAJC12 for *Enu1*, showing larger decreases for mutant PAH than for DNAJC12 when compared to *WT*.

A possible complex formation between PAH and DNAJC12 was studied by immunoprecipitation assays, confirming that PAH was mostly non-ubiquitinated in *WT*, as opposed to *Enu1* where most PAH was mono-ubiquitinated. DNAJC12 and Hsc70/Hsp70 were co-immunoprecipitated in both samples.

This study reveals a role of DNAJC12 in the processing of misfolded ubiquitinated PAH and supports that this Hsp40 cochaperone plays an important part both for proper folding and degradation of its PAH client.

3.2 PAPER II

In paper 2, our goal was to characterize a new animal model for PKU, the *Pah-R261Q* mouse model. This mutation was selected due to its abundance in PKU patients, and the model was custom made by introducing the c.782G>A mutation in the *Pah* gene by CRISPR/Cas9 technology.

Pah-R261Q mice were similar to their *WT* and heterozygous siblings in length, pigmentation, breeding performance and behavior. Characterization of young (3 months old) *Pah-R261Q* showed that the males were significantly heavier than their *WT* counterparts. Otherwise, the mice appeared normal, without apparent anatomic abnormalities or changes in pigmentation. Further characterization was also performed with young mice. The *Pah-R261Q* mice had Phe levels corresponding to mild HPA, significantly different compared to their *WT* and heterozygous *Pah^{R261Q/WT}* siblings (*Pah-R261Q*, 108±36.6 μM; *WT*, 59.9±7.7 μM; *Pah^{R261Q/WT}*, 71.22±21.86 μM). Compared to *WT* and heterozygotes *Pah-R261Q* mice showed a massive increase in Phe concentrations (990±220 μM) 40 minutes after an i.p. injection with 200 μg Phe/g body weight, before returning to basal levels ca. 300 min later. When *Pah-R261Q* mice were pre-treated with BH₄ before the Phe challenge this resulted in a 28% decrease in Phe content, consistent with a BH₄-responsive phenotype.

Comprehensive Laboratory Animal Monitoring System (CLAMS) were used to test various physiological murine parameters in *Pah-R261Q* and *WT* mice for 36 hours. No

significant difference was found between both groups in food intake, activity, or movement patterns. *Pah-R261Q* showed a decrease in the rates of O₂ consumption and CO₂ production normalized to body mass (V_{O₂} and VCO₂), as well as the respiratory exchange ratio (RER= V_{O₂}/ VCO₂). RER values reflect metabolic fuel utilization and are most accurate during periods of rest. During rest we measured that RER for *Pah-R261Q* mice was closer to 0.8 while closer to 1 for *WT*, indicating an increased utilization of fat and protein as a fuel source among the mutant mice. Furthermore, 72 metabolic biomarkers were measured in blood serum and 17 of these showed differences at $p < 0.1$ level between *Pah-R261Q* and *WT* mice. These measurements showed metabolic differences that point to an altered lipid metabolism and oxidative stress in the mutant mice.

When tested on the rotarod, *Pah-R261Q* mice performed comparable to *WT*, indicating no impact on neuromuscular function or motor coordination, at least in young mice. The levels of aromatic amino acids, monoamine neurotransmitters and BH₄ in the brain were also normal. However, BH₄ concentration in the liver showed a 50% reduction in *Pah-R261Q* compared with *WT*.

We also studied how the function and stability of PAH in the mouse liver were affected by the mutation. Western blot of liver lysates showed a reduction of total p.R261Q-PAH protein levels and increased ubiquitination in *Pah-R261Q* compared to *WT* mice, indicative of instability and/or misfolding of this PAH mutant. For further investigation of mutation-specific aggregation by immunohistochemistry, samples from the *Enu1* mice, expressing the unstable p.V106A-PAH mutation, were also included. This method revealed that mutant PAH aggregates were larger in *Pah-R261Q* compared with *Enu1* mice, and that only the aggregates in *Pah-R261Q* were excluded from the nucleus. An Amytracker™ assay and transmission electron microscopy (TEM) indicated formation of amyloid-like amorphous aggregates for purified p.R261Q-PAH compared to p.WT-PAH. Also, the p.R261Q-PAH mutant, but not p.V106A-PAH, was predicted to form intermolecular cross-β (amyloid-like) aggregates by *in silico* evaluation (TANGO software). Interestingly, the autophagy markers LC3 and p62 were elevated and colocalized with PAH only in *Pah-R261Q*. Altogether these results indicate different

mechanisms of protein misfolding and aggregation of the two mutations, and that only the larger amyloid-like PAH aggregates in *Pah-R261Q* engage the autophagic system.

Lastly, gene (mRNA) expression of 10 selected genes related to the PAH system, protein quality control, and oxidative stress pathways was analyzed by quantitative PCR analysis in liver extracts from *WT* and *Pah-R261Q* mice. The results indicated no significant change in *Pah* expression, but upregulation in the expression of *GCHI-feedback regulatory (Gchf)* and *DNAJC12* genes in the mutant mice, as well as a downregulation of the expression of the transcription factor *Hsfl* and the molecular chaperone Hsp70.

To summarize, our findings point to a relation between the altered lipid metabolism and increased oxidative stress observed in the *Pah-R261Q* mice and the accumulation of mutant amyloid-like PAH aggregates in their livers, introducing the concept of toxic gain-of-function for specific PKU mutations. The *Pah-R261Q* mice thus represents an optimal model for new mechanistic and therapeutic discoveries in PKU research, as well as in studies of mutation-specific comorbidities.

3.3 PAPER III

Following the findings in paper 2, revealing oxidative stress caused by amyloid-like aggregates of PAH in young *Pah-R261Q* mice, we wanted to examine how this mouse model developed as it reached old age. Based on the link between oxidative stress and the age-dependent development of disease, we hypothesized that the aging *Pah-R261Q* mice might show decreased general health due to comorbidities, and possibly early death. In this paper, we therefore used old *Pah-R261Q* and *WT* mice, aged between 18 and 23 months, and compared our findings with the results reported on young *Pah-R261Q* mice in **Paper 2**, aged between 3 and 4 months. No apparent abnormalities were observed between old mutant and *WT* mice in the shape, appearance, or size of organs, nor in the survival rate.

Serum Phe was, as expected, significantly increased in old *Pah-R261Q* compared to their *WT* controls but we also found a significant 2-fold increase of Phe level in the old *Pah-R261Q* mice compared to their younger counterparts. Another unexpected result was the increase in Tyr in old mutant mice compared to both old *WT* and young mutant

mice, as a decrease in Tyr concentrations are typically found in classic PKU. The blood Phe:Tyr ratio, which is considered a better measure of neuronal penetrance in PKU than Phe, was found to be increased in both old and young *Pah-R261Q* mice but, interestingly, an increase in Tyr for the old mice led to a reduced difference in Phe:Tyr ratio compared with the relative increase in blood Phe on aging.

The metabolic analyses provided similar values for the concentration of metabolic biomarkers for old *Pah-R261Q* and *WT*, and the differences obtained in several metabolites that were linked to oxidative stress and an altered lipid metabolism in the young mice (**Paper 2**) were not observed in the old mice. However, specific correlation analysis of metabolites vital to the energy turnover in the cell showed a clear difference between old *Pah-R261Q* and *WT*. Thus, although the concentration profiles were remarkably similar, the differences in biomarker interrelations were very apparent.

As the old *Pah-R261Q* mice showed 2-fold higher blood Phe level and a lower but significant increase in Phe:Tyr ratio when compared with old *WT* mice, we tested them thoroughly to reveal any motor deficits in the mutant mice. Progression of neurodegeneration, loss of motor tone or function, ataxia, and gait abnormalities were all measured by a spectrum of tests. It was clear that the old *Pah-R261Q* mice did not suffer from any motor deficits, as they scored similar to or even better than their *WT* siblings.

In summary, old *Pah-R261Q* mice did not present any sign of deleterious health or additional comorbidities to the HPA. Indeed, these mice revealed a possible adaptation and/or compensatory mechanism reducing the signs of oxidative stress. A possible explanation for this finding might be linked to the activation of autophagy from an early age and could explain the improved motor function and lack of early death and comorbidities.

4 GENERAL DISCUSSION

PKU has been a paradigm disease for IEMs for almost a century and may at first glance seem like a well understood disease for which both pathophysiology and treatment were established a long time ago. Recent research by us and other groups has however unraveled new aspects of mechanisms and phenotypic traits of PKU, as well as new treatments, some already approved and others in development, demonstrating that further basic research is crucial to discover unknown aspects and improved therapies for PKU.

Through in-depth study of two mouse models with different PAH mutations, *Enu1* and *Pah-R261Q*, and also focusing on the effect of age for the latter, the work presented in this thesis contributes with new knowledge about the quality control and degradation pathways of specific PAH mutants. The deeper understanding obtained on the role of the molecular chaperone DNAJC12 in these processes and how mutations that lead to unstable PAH may form large aggregates that eventually engage the autophagy system. These findings provide new answers to why PKU patients present such a complex and heterogenous phenotypic landscape and paves the way for the development of mechanistic therapies.

4.1 MOUSE MODELS OF PKU – HOW TO MODEL A COMPLEX DISEASE

The vast number of mutations (more than 1200) combined with the fact that most patients are heterozygotes result in the large variety of phenotypes presented in patients [14]. Since the 1990s three mouse models for PKU, *Enu1* (used in **Paper 1**), *Enu2* and *Enu3* [140, 141], have been available, enabling basic research on the disease as well as development of the approved treatments BH₄-supplementation (Kuvan) [176] and pegylated PAL (Palynziq) [177]. Additionally, studies on the effects of BH₄ have also been performed on the compound heterozygous *Enu1/2* mouse [124, 178]. Nevertheless, none of the *Enu* models represent a mutation with high prevalence in the patient population, which was the reason why we generated the custom made novel *Pah-R261Q* knock-in model with the frequent PKU mutation p.R261Q-PAH [14, 41] and studied it in detail (**Papers 2 and 3**). In the characterization we focused on the elucidation of the pathogenic mechanisms of the mutation, which revealed a reduced stability, misfolding

and amyloid-like aggregation. We also investigated the systems involved in handling and degradation of the mutant protein to reduce deleterious effects in mouse liver. Although *Enu1* and *Pah-R261Q* present a similar mild HPA phenotype, caused by the unstable mutant PAH leading to reduced steady state activity levels in both cases (**Paper 1 and 2**), the pathogenic mechanisms of each mutation and the systems engaged for mutant degradation differ (**Paper 2**).

The complex proteostasis network involves a large number of proteins and maintains the protein quality control, degrades aggregates, and counteracts the gain-of-function effect [94, 99]. The ensemble of proteostasis network proteins represents additional polymorphic modifier variants that may explain the broader phenotypic spectrum (blood Phe levels) in patients with the p.R261Q-PAH mutant [53], though not in the mouse model, since all mice have identical genetic background. The human phenotypic variability seems to reflect the influence of genetic variation on the susceptibility to mutant protein aggregation in gain-of-function misfolding diseases [179, 180]. On the other hand, patients harboring other frequent mutations associated with mild PKU, such as p.I65T-PAH, p.L48S-PAH, p.A403V-PAH, p.V388M-PAH, p.A300S-PAH (Table 1), which according to the TANGO predictions (**Paper 2**) do not show propensity for β -cross amyloid-like aggregation, present a more homogeneous phenotype [41]. These mutant proteins are expected to form small aggregates, as seen in *Enu1* (**Paper 2** and [126]), and expected to be effectively processed by the UPS [125], leading to loss-of-function and better correlations between the severity of mutation-induced PAH destabilization and the reported metabolic phenotype for homozygous patients [47].

Even though we see an almost doubling in blood Phe levels in old vs. young *Pah-R261Q* mice (**Paper 3**), in both cases the values correspond to HPA and are below the PKU threshold for patients. The residual PAH activity is similar in homozygous patients (~15% of *WT*) and *Pah-R261Q* mice (**Paper 2**), however, the blood Phe levels are much lower in the mutant mice. A lower steady-state level of hepatic PAH in humans can explain this difference in metabolic phenotype in mice and men [181]. Nonetheless, this difference does not preclude the use of the knock-in mouse to model mild or moderate PKU. In **Paper 2**, we demonstrate that Phe levels in the *Pah-R261Q* mouse can be

modulated by the Phe-challenge to represent a mild or moderate phenotype, and that the mice respond to treatment with the cofactor BH₄, as expected from results in patients homozygous for the p.R261Q-PAH mutation [41].

4.2 PAH INSTABILITY AND AGGREGATION

Mutations in proteins normally result in unstable conformations with tendency to misfold and form aggregates. These may be small and relatively soluble or large and oligomeric, formed via amyloid-like stable β -cross intersubunit interactions, while some misfolded mutants can accumulate in amyloid fibrils [182]. The smaller aggregates are degraded by the UPS and autophagy is engaged to degrade the larger aggregates [117] (Figure 5), while fibrillar conformations engage the chaperone-triggered disaggregase system, but also form deposits in the cells [183]. A diverse range of diseases are associated with aggregates and the proteostasis dysregulation they trigger, e.g., amyloidosis, diabetes and neurodegenerative disorders like Alzheimer's disease and Parkinson's disease [98]. In this work we have, for the first time, shown the presence of large PAH aggregates in the liver of PKU mouse models (**Paper 2**).

Misfolded PAH variants of PKU have been found to oligomerize and aggregate both *in vitro* and *in vivo* [56, 123, 126]. These misfolded PAH variants result in a dysregulation of the normal proteostasis and an increased degradation of mutant PAH [124]. PAH from the *Enu1* mouse model has previously been found to aggregate [126], as we also show in our work both by Western blot when applying different lysis buffers (**Paper 1**) and by immunofluorescence (**Paper 2**). The Western blot experiments also revealed that the majority of mutated PAH in *Enu1* mice was mono-ubiquitinated, while *WT* mice appeared to mostly contain non-ubiquitinated PAH, indicating that unstable and misfolded mutant PAH is marked for degradation (**Paper 1**). This was also the case for *Pah-R261Q*, and parallel immunoquantification and PAH activity indicated that non-ubiquitinated PAH levels correlated with the remaining PAH activity measured in liver lysates, revealing for the first time that ubiquitinated PAH is not active.

In *Pah-R261Q*, immunofluorescence microscopy of liver verified the reduction of PAH protein and showed the scattered PAH aggregates colocalizing with an increased ubiquitination signal (**Paper 2**). When compared with *Enu1* mouse liver, the differences

in aggregation pattern of the two mouse models became obvious, as aggregates in *Enul* were smaller and evenly distributed in cytoplasm and nucleus while aggregates in *Pah-R261Q* were larger and appeared to be unable to penetrate the nuclear membrane (**Paper 2**). Large aggregates could hinder uptake to the nuclear quality control system by inhibiting nucleocytoplasmic transport [184] and lead to toxic accumulation in the cytoplasm, which has been shown to overload the autophagy system and increase oxidative stress [108, 185]. Larger aggregates can thus be cytotoxic, especially the oligomeric aggregates that may progress to amyloid fibrils [98], however, the fibers themselves are more stable and less cytotoxic than the oligomeric intermediates [186]. Immunofluorescence images revealed large amorphous aggregates of PAH in *Pah-R261Q*, that colocalized with autophagy markers p62 and LC3, but no fibrillar structures were found, neither by immunohistochemistry nor by transmission electron microscopy (**Paper 2**).

Beyond the metabolic changes directly related to HPA (e.g., Phe, Tyr, and Trp), other metabolic and pathophysiological changes encountered in young adult mice (3–4 months old), e.g., oxidative stress, altered lipid metabolism, and decreased BH₄ content, appeared most probably related to the presence of the large amyloid-like large aggregates (as discussed in **Paper 2**). As diseases linked to amyloid aggregation tend to worsen with age [106], combined with the expected decrease in the proteostasis network effectiveness, we predicted to see a deterioration of general health in the old *Pah-R261Q* mice (18–23 months old). However, no sign of deterioration with age or clear comorbidities were seen in the old mutant mice compared to their *WT* controls (**Paper 3**). In particular, and similarly to that observed in the young mice, no motor dysfunction could be found, and although further experiments and measurements of amino acids and neurotransmitters in brain of old mice should be performed, the results so far indicate that the presence of the large aggregates does not result in a neurological impairment at any age.

4.3 METABOLIC PROFILE AND OXIDATIVE STRESS

In this work we also examined and compared the effect of the *PAH* mutation on the metabolism in young and old *Pah-R261Q* mice (**Papers 2 and 3**). The young mice

presented an altered lipid metabolism when tested in metabolic cages and several metabolites, previously shown to be increased in adiposity and altered lipid metabolism in humans [187], showed a trend towards higher values in mutant mice (**Paper 2**). Also, young mice displayed reduced BH4 and alterations in metabolic parameters and biomarkers associated with oxidative stress, as well as activation of the antioxidant response and total antioxidant capacity. Several inborn errors of metabolism are associated with lipid disorders, obesity and diabetes, comorbidities which are associated with the metabolic dysregulation [188, 189]. Although some recent studies have revealed an increased predisposition to diabetes in the patients [190], this association is less clear for PKU, where the adiposity may be explained by the reduction of BH4 and consequent dysfunction of the BH4-dependent alkylglycerol monooxygenase, an enzyme involved in the degradation of ether lipids [191]. On the other hand, the oxidative stress certainly appears related to the large amyloid-like PAH aggregation and their interference with the nucleocytoplasmic transport (**Paper 2**), as found in so many metabolic and neurodegenerative disorders associated with protein aggregates [192].

As mentioned above, disease states involving protein aggregation often worsen with age in humans. Interestingly, metabolic studies in older *Pah-R261Q* mice did not show indications of increased oxidative stress (**Paper 3**), on the contrary, several of the biomarker concentrations were more similar in old *WT* and mutant mice than in the younger mice. Despite the more equal concentrations in the old *Pah-R261Q* and *WT* there is a noticeably clear difference in biomarker interrelations, possibly a sign of dysmetabolism in the mutant mice. The normalization of biomarker concentrations in mutant mice combined with the difference in biomarker interrelations suggest a compensation or correction mechanism leading to the reduction of the oxidative stress and altered metabolism that was observed in the young mutant mice.

As proven in **Paper 2**, the production of large PAH aggregates engages the autophagy system, which is known to be activated as a response to counteract oxidative stress [164, 193], especially in disorders associated with oligomeric aggregates [194, 195]. Increasing the cellular degradative capacity through activation of autophagy is obtaining increased interest as a therapeutic strategy to suppress age-related pathologies, notably

neurodegenerative diseases [196]. We therefore hypothesize in **Paper 3** that the activation of autophagy observed in young age, and probably maintained and/or increased towards aging, could be beneficial to not merely counteract the aggregate-induced oxidative stress and process p.R261Q-PAH aggregates, but also to degrade other damaged proteins and organelles. Autophagy activation may thus explain the prevention of the expected comorbidities due to the combination of age and oxidative stress, and also contribute to the modest improvement of motor function in the old *Pah-R261Q* mice.

4.4 DNAJC12

DNAJC12 is a cochaperone of the Hsp40 family and is expected to work together with Hsp/Hsc70 in the folding of the AAAHs [33, 36]. In **Paper 1**, immunoquantification results indicated decreased levels of both DNAJC12 and PAH in COS-7 cells expressing unstable PAH mutants and in the *Enu1* mouse model, where DNAJC12 was detected in liver lysates when these were prepared under solubilizing conditions. As the levels of *Dnajc12* and *Pah* mRNA were found to be similar for *WT* and *Enu1* –with a ratio of about 1:100 for *Dnajc12:Pah* for both mice groups – the observed decrease in protein levels suggests coaggregation of DNAJC12 and mutant PAH in *Enu1* (**Paper 1**). Comparative Western blots and co-immunoprecipitations using mouse liver lysates also revealed that only a small fraction of PAH is mono-ubiquitinated in *WT* mice, while most mutant PAH in *Enu1* is mono-ubiquitinated (**Paper 1**). DNAJC12 co-immunoprecipitated with this ubiquitinated fraction in *Enu1*, indicating that the cochaperone is engaged in targeting misfolded PAH for degradation, probably through initial attempts for solubilization, delivery to HSP70 and final degradation at the UPS [197].

Differently to the observations in *Enu1*, *Dnajc12* mRNA was found to be increased in young *Pah-R261Q* mice compared with *WT* counterparts (**Paper 2**). This upregulation of *Dnajc12* adds to the physiological and metabolic indications of oxidative stress and activation of the antioxidant response in the young *Pah-R261Q* mice (**Paper 2** and 4.3), as DNJC12 has long been known to be upregulated by different cellular stresses, notably oxidative stress [198]. In the last years, DNAJC12 has been found to be overexpressed

in a number of cancers, where expression levels are associated with tumor aggressiveness and where DNAJC12 may represent a promising predictor for patient prognosis [198, 199]. It appears that this role of DNAJC12 is not associated with its HSP40 co-chaperone function in the proteostasis regulation of its specific clients, the AAAHs, including PAH, but rather a strategy of cancer cells to respond to the proteotoxic stress caused by increased translation rates, dysregulated metabolism and production of mutated proteins, and in that way avoid apoptosis [200].

4.5 A NEW UNDERSTANDING OF MOUSE MODELS OF PKU

As more details about diverse mutation effects and molecular pathogenic mechanisms are observed and documented, PKU presents as a much more complex disease than the monogenic disorder it first appears to be. To model PKU in its various phenotypes there are now 4 mouse models available: (1) *Enu3*, with a splice site mutation (at the exon 11– exon 12 junction) generating frameshifted amino acids, premature termination codon and complete loss of PAH activity [141]; (2) *Enu2*, with a severe missense catalytic mutation (p.F263S-PAH) around the active site that results in almost total loss of PAH activity [140]; (3) *Enu1*, with a missense mutation (p.V106A-PAH) that causes PAH instability and small aggregates, resulting in reduced PAH and activity in liver (loss-of function misfolding) [140]; (4) *Pah-R261Q* with a missense mutation (p.R261Q-PAH) that causes PAH instability, misfolding and large aggregates, resulting in reduced PAH and activity in liver and oxidative stress in the young mice (gain-of-function misfolding) (**Paper 2**). Another classification could be based on severity of the phenotype, with *Enu2* and *Enu3* presenting with classic PKU [141] and *Enu1* and *Pah-R261Q* with mild HPA (**Paper 2**) [143], although the p.R261Q-PAH mutation corresponds to a broad phenotype in patients, varying from mild to classic PKU based on their Phe levels when off the low-Phe diet [41, 53].

Our work has contributed with novel information on the *Enu1* mouse model, such as the engagement of DNAJC12 by ubiquitinated mutant p.V106A-PAH (**Paper 1**), visualization of small PAH aggregates in liver lysates, and degradation of the mutant PAH by the UPS, as there is no engagement of the autophagy machinery in these mice (**Paper 2**). Furthermore, our work on the *Pah-R261Q* mouse model has revealed the

unexpected existence of a toxic misfolding, with gain-of-function aggregation mechanism, elicited by the mutant p.R261Q-PAH (**Paper 2**), as well as a possible adaptation and/or compensatory mechanism reducing the signs of oxidative stress in old mice, potentially due to early activation of autophagy (**Paper 3**). We believe this knowledge and the new mouse model generated in this work represent a large contribution to the PKU field and are expected to facilitate the selection of more robust and precise mouse models for development of mechanistic therapies for patient/mutation tailored therapies.

5 CONCLUDING REMARKS AND FUTURE PERSPECTIVES

In this work we have revealed new knowledge about the aggregation and degradation of mutant PAH using the *Enu1* and the novel *Pah-R261Q* mice as models for HPA/PKU. In *Enu1* mice we found coaggregation of DNAJC12 and ubiquitinated PAH, indicating the involvement of cochaperones in degradation of mutant PAH. Small PAH aggregates in *Enu1* livers are most likely degraded by the UPS. In the knock-in *Pah-R261Q* mouse model we found an unexpected molecular mechanism, with gain-of-function misfolding and amyloid-like aggregation in addition to HPA, where the large PAH aggregates are degraded by autophagy. This new knock-in mouse contributes to a deeper understanding of the mutation-associated mechanisms and complexity of PKU and complements the spectrum of mouse models for testing novel therapies in patient-tailored models.

Today, the cornerstone treatment of PKU is still the low-Phe diet, but other therapeutic options have been approved or are under development to be used alone or in combination with the diet. The phenotypic variety in PKU complicates the treatment of the disease, and the need for patient-tailored therapies is great. Kuvan, a synthetic form of the BH₄ cofactor, and Palynziq, an enzyme substitution therapy, are approved in the US and Europe, only for adults in the case of Palynziq. Whereas Kuvan is mostly used in combination to a less strict diet, Palynziq may substitute the dietary treatment for many patients, although both have limitations (see 1.1.6). Based on the results of this work two potential therapies appear promising for patients harboring unstable and misfolding mutations in PKU, i.e., pharmacological chaperones and DNAJC12-based therapies. Pharmacological chaperones are small molecules that aid to fold and stabilize mutant proteins, have shown promise for HPA/PKU and appear as effective alternatives to be tested in *Enu1* and *Pah-R261Q* [201]. Another interesting possibility could be to increase the levels of DNAJC12 through e.g., RNA therapies or activators of expression, as this co-chaperone seems limiting in *Enu1* (**Paper 1**). Higher amounts of the co-chaperone could provide increased folding and protection towards aggregation for unstable and misfolding mutations, as shown for neurodegenerative diseases [202]. Treatment aimed at correcting the unstable and misfolded PAH could thus target both elevated Phe levels and comorbidities.

Oxidative stress has been reported both in animal models of PKU as well as in PKU patients. Nevertheless, the toxic gain-of-function associated with the p.R261Q-PAH mutation reported in this thesis has never been seen before. In light of these findings, it would be interesting to perform focused studies on patient samples with specific mutations, and specifically to investigate the presence of biomarkers indicative of oxidative stress in patients homozygous for the p.R261Q-PAH mutation.

The aging *Pah-R261Q* mice performed better than initially expected, and even seemed to have adapted and/or compensated for the oxidative stress found in the young mutant mice. Several studies have focused on aging PKU patients, but none of them on specific mutations. For aging PKU patients homozygous for p.R261Q-PAH, it would be interesting to investigate if the same trends of increased Phe and Tyr levels, as well as normalization of biomarker concentrations and biomarker correlations is observed in both mice and men.

To better understand the aging of *Pah-R261Q* mice we have planned several additional experiments. We want to visualize the size of PAH aggregates in the old *Pah-R261Q* mice, and also compare the state of autophagy in the young and old mice. By analyzing the same biomarkers in young mutant and *WT* mice and run the same correlation analysis, we are eager to see how the interrelation profiles of young mice compares with the ones from old mice presented in this work. Moreover, further fundamental studies will be directed to proof the interesting hypothesis that the long-life activation of autophagy may be the driver of the oxidative stress compensation in old *Pah-R261Q* mice. If correct, this finding could pave the way for studies on therapeutic benefits of using autophagy activators in aging-related diseases [203].

It is now evident that it is not only the metabolic phenotype that varies between the different PAH mutations and that more of the research on pathophysiology and comorbidities should include the specific mutation as a variable, even if it is difficult due to the substantial number of mutations (more than 1200) and the rarity of the disease. In our work we demonstrate the importance of understanding molecular mechanisms for each type of mutation and the effect of PAH aggregates at the cellular and organismal level. A last point to consider is that even if the heterozygote carriers of PKU will not

reach toxic levels of Phe they are expressing mutant, and thus possibly aggregated, PAH. If we find signs of elevated oxidative stress in homozygote patients for p.R261Q-PAH, the next step will be to analyze the blood of their parents to see if they also show signs of toxic gain-of-function. Further studies will be needed to understand the consequences of oxidative stress for comorbidities and health on aging for carriers.

6 BIBLIOGRAPHY

1. van Spronsen, F.J., et al., *Phenylketonuria*. Nat Rev Dis Primers, 2021. **7**(1): p. 36.
2. Scriver, C.R. and P.J. Waters, *Monogenic traits are not simple: lessons from phenylketonuria*. Trends Genet, 1999. **15**(7): p. 267-72.
3. Dipple, K.M. and E.R. McCabe, *Phenotypes of patients with "simple" Mendelian disorders are complex traits: thresholds, modifiers, and systems dynamics*. Am J Hum Genet, 2000. **66**(6): p. 1729-35.
4. Argmann, C.A., et al., *A Next Generation Multiscale View of Inborn Errors of Metabolism*. Cell Metab, 2016. **23**(1): p. 13-26.
5. Folling, I., *The discovery of phenylketonuria*. Acta Paediatr Suppl, 1994. **407**: p. 4-10.
6. Penrose, L. and J.H. Quastel, *Metabolic studies in phenylketonuria*. Biochem J, 1937. **31**(2): p. 266-74.
7. Penrose, L., *Inheritance of Phenylperuvic Amentia (Phenylketonuria)*. The Lancet, 1935. **226**(5839): p. 192-194.
8. Daly, A., et al., *Protein Substitutes in PKU; Their Historical Evolution*. Nutrients, 2021. **13**(2).
9. Bickel, H., J. Gerrard, and E.M. Hickmans, *Influence of phenylalanine intake on phenylketonuria*. Lancet, 1953. **265**(6790): p. 812-3.
10. Levy, H.L., *Robert Guthrie and the Trials and Tribulations of Newborn Screening*. Int J Neonatal Screen, 2021. **7**(1).
11. Blau, N., N. Shen, and C. Carducci, *Molecular genetics and diagnosis of phenylketonuria: state of the art*. Expert Rev Mol Diagn, 2014. **14**(6): p. 655-71.
12. Blau, N., F.J. van Spronsen, and H.L. Levy, *Phenylketonuria*. Lancet, 2010. **376**(9750): p. 1417-27.
13. van Spronsen, F.J., et al., *Key European guidelines for the diagnosis and management of patients with phenylketonuria*. Lancet Diabetes Endocrinol, 2017. **5**(9): p. 743-756.
14. Hillert, A., et al., *The Genetic Landscape and Epidemiology of Phenylketonuria*. Am J Hum Genet, 2020. **107**(2): p. 234-250.
15. Werner, E.R., N. Blau, and B. Thony, *Tetrahydrobiopterin: biochemistry and pathophysiology*. Biochem J, 2011. **438**(3): p. 397-414.
16. Fitzpatrick, P.F., *The aromatic amino acid hydroxylases*. Adv Enzymol Relat Areas Mol Biol, 2000. **74**: p. 235-94.
17. Skjærven, L.T., K.; Martinez, A., *Structure-Function Relationships in the Aromatic Amino Acid Hydroxylases Enzyme Family: Evolutionary Insights*. eLS, 2014.
18. Fitzpatrick, P.F., *Mechanism of aromatic amino acid hydroxylation*. Biochemistry, 2003. **42**(48): p. 14083-91.
19. Arturo, E.C., et al., *First structure of full-length mammalian phenylalanine hydroxylase reveals the architecture of an autoinhibited tetramer*. Proc Natl Acad Sci U S A, 2016. **113**(9): p. 2394-9.
20. Flydal, M.I., et al., *Structure of full-length human phenylalanine hydroxylase in complex with tetrahydrobiopterin*. Proc Natl Acad Sci U S A, 2019. **116**(23): p. 11229-11234.
21. Kobe, B., et al., *Structural basis of autoregulation of phenylalanine hydroxylase*. Nat Struct Biol, 1999. **6**(5): p. 442-8.
22. Fusetti, F., et al., *Structure of tetrameric human phenylalanine hydroxylase and its implications for phenylketonuria*. J Biol Chem, 1998. **273**(27): p. 16962-7.
23. Liberles, J.S., M. Thorolfsson, and A. Martinez, *Allosteric mechanisms in ACT domain containing enzymes involved in amino acid metabolism*. Amino Acids, 2005. **28**(1): p. 1-12.
24. Andersen, O.A., et al., *2.0 Å resolution crystal structures of the ternary complexes of human phenylalanine hydroxylase catalytic domain with tetrahydrobiopterin and 3-(2-thienyl)-L-alanine or L-norleucine: substrate specificity and molecular motions related to substrate binding*. J Mol Biol, 2003. **333**(4): p. 747-57.

25. Panay, A.J., et al., *Evidence for a high-spin Fe(IV) species in the catalytic cycle of a bacterial phenylalanine hydroxylase*. *Biochemistry*, 2011. **50**(11): p. 1928-33.
26. Roberts, K.M., J.A. Pavon, and P.F. Fitzpatrick, *Kinetic mechanism of phenylalanine hydroxylase: intrinsic binding and rate constants from single-turnover experiments*. *Biochemistry*, 2013. **52**(6): p. 1062-73.
27. Flydal, M.I. and A. Martinez, *Phenylalanine hydroxylase: function, structure, and regulation*. *IUBMB Life*, 2013. **65**(4): p. 341-9.
28. Fitzpatrick, P.F., *Allosteric regulation of phenylalanine hydroxylase*. *Arch Biochem Biophys*, 2012. **519**(2): p. 194-201.
29. Mitnaul, L.J. and R. Shiman, *Coordinate regulation of tetrahydrobiopterin turnover and phenylalanine hydroxylase activity in rat liver cells*. *Proc Natl Acad Sci U S A*, 1995. **92**(3): p. 885-9.
30. Milstien, S., et al., *Hepatic phenylalanine 4-monoxygenase is a phosphoprotein*. *Proc Natl Acad Sci U S A*, 1976. **73**(5): p. 1591-3.
31. Miranda, F.F., et al., *Phosphorylation and mutations of Ser(16) in human phenylalanine hydroxylase. Kinetic and structural effects*. *J Biol Chem*, 2002. **277**(43): p. 40937-43.
32. Doskeland, A.P. and T. Flatmark, *Recombinant human phenylalanine hydroxylase is a substrate for the ubiquitin-conjugating enzyme system*. *Biochem J*, 1996. **319** (Pt 3): p. 941-5.
33. Anikster, Y., et al., *Biallelic Mutations in DNAJC12 Cause Hyperphenylalaninemia, Dystonia, and Intellectual Disability*. *Am J Hum Genet*, 2017. **100**(2): p. 257-266.
34. van Spronsen, F.J., et al., *Heterogeneous clinical spectrum of DNAJC12-deficient hyperphenylalaninemia: from attention deficit to severe dystonia and intellectual disability*. *J Med Genet*, 2017.
35. Veenma, D., et al., *DNAJC12-associated developmental delay, movement disorder, and mild hyperphenylalaninemia identified by whole-exome sequencing re-analysis*. *Eur J Hum Genet*, 2018. **26**(12): p. 1867-1870.
36. Gallego, D., et al., *Pathogenic variants of DNAJC12 and evaluation of the encoded cochaperone as a genetic modifier of hyperphenylalaninemia*. *Hum Mutat*, 2020. **41**(7): p. 1329-1338.
37. Dekker, S.L., H.H. Kampinga, and S. Bergink, *DNAJs: more than substrate delivery to HSPA*. *Front Mol Biosci*, 2015. **2**: p. 35.
38. Li, Y., et al., *A noncoding RNA modulator potentiates phenylalanine metabolism in mice*. *Science*, 2021. **373**(6555): p. 662-673.
39. Alderson, T.R., J.H. Kim, and J.L. Markley, *Dynamical Structures of Hsp70 and Hsp70-Hsp40 Complexes*. *Structure*, 2016. **24**(7): p. 1014-30.
40. Jaffe, E.K., *New protein structures provide an updated understanding of phenylketonuria*. *Mol Genet Metab*, 2017. **121**(4): p. 289-296.
41. *PAHvdb : Phenylalanine Hydroxylase Gene Locus-Specific Database*. [Accessed April 6th, 2022]; Available from: www.biopku.org.
42. Shen, N., et al., *Co-expression of phenylalanine hydroxylase variants and effects of interallelic complementation on in vitro enzyme activity and genotype-phenotype correlation*. *Mol Genet Metab*, 2016. **117**(3): p. 328-35.
43. Jennings, I.G., R.G. Cotton, and B. Kobe, *Structural interpretation of mutations in phenylalanine hydroxylase protein aids in identifying genotype-phenotype correlations in phenylketonuria*. *Eur J Hum Genet*, 2000. **8**(9): p. 683-96.
44. Marvit, J., et al., *GT to AT transition at a splice donor site causes skipping of the preceding exon in phenylketonuria*. *Nucleic Acids Res*, 1987. **15**(14): p. 5613-28.
45. Wettstein, S., et al., *Linking genotypes database with locus-specific database and genotype-phenotype correlation in phenylketonuria*. *Eur J Hum Genet*, 2015. **23**(3): p. 302-9.
46. Gamez, A., et al., *Expression analysis of phenylketonuria mutations. Effect on folding and stability of the phenylalanine hydroxylase protein*. *J Biol Chem*, 2000. **275**(38): p. 29737-42.

47. Pey, A.L., et al., *Predicted effects of missense mutations on native-state stability account for phenotypic outcome in phenylketonuria, a paradigm of misfolding diseases*. Am J Hum Genet, 2007. **81**(5): p. 1006-24.
48. Gersting, S.W., et al., *Loss of function in phenylketonuria is caused by impaired molecular motions and conformational instability*. Am J Hum Genet, 2008. **83**(1): p. 5-17.
49. Danecka, M.K., et al., *Mapping the functional landscape of frequent phenylalanine hydroxylase (PAH) genotypes promotes personalised medicine in phenylketonuria*. J Med Genet, 2015. **52**(3): p. 175-85.
50. Himmelreich, N., et al., *Relationship between genotype, phenylalanine hydroxylase expression and in vitro activity and metabolic phenotype in phenylketonuria*. Mol Genet Metab, 2018. **125**(1-2): p. 86-95.
51. Himmelreich, N., N. Blau, and B. Thony, *Molecular and metabolic bases of tetrahydrobiopterin (BH4) deficiencies*. Mol Genet Metab, 2021. **133**(2): p. 123-136.
52. Blau, N., et al., *DNAJC12 deficiency: A new strategy in the diagnosis of hyperphenylalaninemias*. Mol Genet Metab, 2018. **123**(1): p. 1-5.
53. Guldberg, P., et al., *A European multicenter study of phenylalanine hydroxylase deficiency: classification of 105 mutations and a general system for genotype-based prediction of metabolic phenotype*. Am J Hum Genet, 1998. **63**(1): p. 71-9.
54. Erlandsen, H., et al., *Correction of kinetic and stability defects by tetrahydrobiopterin in phenylketonuria patients with certain phenylalanine hydroxylase mutations*. Proc Natl Acad Sci U S A, 2004. **101**(48): p. 16903-8.
55. Waters, P.J., *How PAH gene mutations cause hyper-phenylalaninemia and why mechanism matters: insights from in vitro expression*. Hum Mutat, 2003. **21**(4): p. 357-69.
56. Gjetting, T., et al., *In vitro expression of 34 naturally occurring mutant variants of phenylalanine hydroxylase: correlation with metabolic phenotypes and susceptibility toward protein aggregation*. Mol Genet Metab, 2001. **72**(2): p. 132-43.
57. Pey, A.L., et al., *Phenylketonuria: genotype-phenotype correlations based on expression analysis of structural and functional mutations in PAH*. Hum Mutat, 2003. **21**(4): p. 370-8.
58. Vockley, J., et al., *Complex patterns of inheritance, including synergistic heterozygosity, in inborn errors of metabolism: Implications for precision medicine driven diagnosis and treatment*. Mol Genet Metab, 2019. **128**(1-2): p. 1-9.
59. Bjorgo, E., et al., *Partial characterization and three-dimensional-structural localization of eight mutations in exon 7 of the human phenylalanine hydroxylase gene associated with phenylketonuria*. Eur J Biochem, 1998. **257**(1): p. 1-10.
60. Eiken, H.G., et al., *PKU mutation G46S is associated with increased aggregation and degradation of the phenylalanine hydroxylase enzyme*. Hum Mutat, 1996. **7**(3): p. 228-38.
61. Leandro, J., et al., *PKU mutation p.G46S prevents the stereospecific binding of l-phenylalanine to the dimer of human phenylalanine hydroxylase regulatory domain*. FEBS Open Bio, 2017. **7**(2): p. 195-203.
62. Leandro, J., et al., *The G46S-hPAH mutant protein: a model to study the rescue of aggregation-prone PKU mutations by chaperones*. Mol Genet Metab, 2011. **104** Suppl: p. S40-4.
63. Leandro, J., et al., *Phenylketonuria as a protein misfolding disease: The mutation pG46S in phenylalanine hydroxylase promotes self-association and fibril formation*. Biochim Biophys Acta, 2011. **1812**(1): p. 106-20.
64. Muntau, A.C. and S.W. Gersting, *Phenylketonuria as a model for protein misfolding diseases and for the development of next generation orphan drugs for patients with inborn errors of metabolism*. J Inherit Metab Dis, 2010. **33**(6): p. 649-58.
65. Rocha, J.C. and A. MacDonald, *Dietary intervention in the management of phenylketonuria: current perspectives*. Pediatric Health Med Ther, 2016. **7**: p. 155-163.
66. Rubin, S., et al., *Sight-threatening phenylketonuric encephalopathy in a young adult, reversed by diet*. JIMD Rep, 2013. **10**: p. 83-5.

67. Jaulent, P., et al., *Neurological manifestations in adults with phenylketonuria: new cases and review of the literature*. J Neurol, 2020. **267**(2): p. 531-542.
68. Bilder, D.A., et al., *Systematic Review and Meta-Analysis of Neuropsychiatric Symptoms and Executive Functioning in Adults With Phenylketonuria*. Dev Neuropsychol, 2016. **41**(4): p. 245-260.
69. Jahja, R., et al., *Long-Term Follow-Up of Cognition and Mental Health in Adult Phenylketonuria: A PKU-COBESO Study*. Behav Genet, 2017. **47**(5): p. 486-497.
70. Guest, J.F., et al., *Costs and outcomes over 36 years of patients with phenylketonuria who do and do not remain on a phenylalanine-restricted diet*. J Intellect Disabil Res, 2013. **57**(6): p. 567-79.
71. Kure, S., et al., *Tetrahydrobiopterin-responsive phenylalanine hydroxylase deficiency*. J Pediatr, 1999. **135**(3): p. 375-8.
72. Fiege, B. and N. Blau, *Assessment of tetrahydrobiopterin (BH4) responsiveness in phenylketonuria*. J Pediatr, 2007. **150**(6): p. 627-30.
73. Blau, N., *Sapropterin dihydrochloride for the treatment of hyperphenylalaninemias*. Expert Opin Drug Metab Toxicol, 2013. **9**(9): p. 1207-18.
74. Dobrowolski, S.F., et al., *Molecular genetics and impact of residual in vitro phenylalanine hydroxylase activity on tetrahydrobiopterin responsiveness in Turkish PKU population*. Mol Genet Metab, 2011. **102**(2): p. 116-21.
75. Sarkissian, C.N., et al., *A different approach to treatment of phenylketonuria: phenylalanine degradation with recombinant phenylalanine ammonia lyase*. Proc Natl Acad Sci U S A, 1999. **96**(5): p. 2339-44.
76. Bell, S.M., et al., *Formulation and PEGylation optimization of the therapeutic PEGylated phenylalanine ammonia lyase for the treatment of phenylketonuria*. PLoS One, 2017. **12**(3): p. e0173269.
77. Burton, B.K., et al., *Pegvaliase for the treatment of phenylketonuria: Results of the phase 2 dose-finding studies with long-term follow-up*. Mol Genet Metab, 2020. **130**(4): p. 239-246.
78. Gupta, S., et al., *Association of immune response with efficacy and safety outcomes in adults with phenylketonuria administered pegvaliase in phase 3 clinical trials*. EBioMedicine, 2018. **37**: p. 366-373.
79. *FDA approves a new treatment for PKU, a rare and serious genetic disease* [May 24, 2018]; Available from: <https://www.fda.gov/news-events/press-announcements/fda-approves-new-treatment-pku-rare-and-serious-genetic-disease>.
80. *Palynziq* [May 29, 2019]; Available from: <https://www.ema.europa.eu/en/medicines/human/EPAR/palynziq#product-information-section>.
81. Hennermann, J.B., et al., *Chronic kidney disease in adolescent and adult patients with phenylketonuria*. J Inherit Metab Dis, 2013. **36**(5): p. 747-56.
82. Hermida-Ameijeiras, A., et al., *Arterial stiffness assessment in patients with phenylketonuria*. Medicine (Baltimore), 2017. **96**(51): p. e9322.
83. Burton, B.K., et al., *Prevalence of comorbid conditions among adult patients diagnosed with phenylketonuria*. Mol Genet Metab, 2018. **125**(3): p. 228-234.
84. Rocha, J.C., et al., *Dietary treatment in phenylketonuria does not lead to increased risk of obesity or metabolic syndrome*. Mol Genet Metab, 2012. **107**(4): p. 659-63.
85. Stevenson, M. and N. McNaughton, *A comparison of phenylketonuria with attention deficit hyperactivity disorder: do markedly different aetiologies deliver common phenotypes?* Brain Res Bull, 2013. **99**: p. 63-83.
86. Ashe, K., et al., *Psychiatric and Cognitive Aspects of Phenylketonuria: The Limitations of Diet and Promise of New Treatments*. Front Psychiatry, 2019. **10**: p. 561.
87. Cannon Homaei, S., et al., *ADHD symptoms in neurometabolic diseases: Underlying mechanisms and clinical implications*. Neurosci Biobehav Rev, 2021.

88. Vardy, E., et al., *Phenylketonuria, co-morbidity, and ageing: A review*. J Inherit Metab Dis, 2020. **43**(2): p. 167-178.
89. Scriver, C.R., *The PAH gene, phenylketonuria, and a paradigm shift*. Hum Mutat, 2007. **28**(9): p. 831-45.
90. Kabra, M., *Dietary management of inborn errors of metabolism*. Indian J Pediatr, 2002. **69**(5): p. 421-6.
91. Camp, K.M., M.A. Lloyd-Puryear, and K.L. Huntington, *Nutritional treatment for inborn errors of metabolism: indications, regulations, and availability of medical foods and dietary supplements using phenylketonuria as an example*. Mol Genet Metab, 2012. **107**(1-2): p. 3-9.
92. Barone, H., et al., *Tyrosinemia Type 1 and symptoms of ADHD: Biochemical mechanisms and implications for treatment and prognosis*. Am J Med Genet B Neuropsychiatr Genet, 2020. **183**(2): p. 95-105.
93. Wei, G., et al., *Protein Ensembles: How Does Nature Harness Thermodynamic Fluctuations for Life? The Diverse Functional Roles of Conformational Ensembles in the Cell*. Chem Rev, 2016. **116**(11): p. 6516-51.
94. Chen, B., et al., *Cellular strategies of protein quality control*. Cold Spring Harb Perspect Biol, 2011. **3**(8): p. a004374.
95. Diaz-Villanueva, J.F., R. Diaz-Molina, and V. Garcia-Gonzalez, *Protein Folding and Mechanisms of Proteostasis*. Int J Mol Sci, 2015. **16**(8): p. 17193-230.
96. Labbadia, J. and R.I. Morimoto, *The biology of proteostasis in aging and disease*. Annu Rev Biochem, 2015. **84**: p. 435-64.
97. Hipp, M.S., P. Kasturi, and F.U. Hartl, *The proteostasis network and its decline in ageing*. Nat Rev Mol Cell Biol, 2019. **20**(7): p. 421-435.
98. Balchin, D., M. Hayer-Hartl, and F.U. Hartl, *In vivo aspects of protein folding and quality control*. Science, 2016. **353**(6294): p. aac4354.
99. Jayaraj, G.G., M.S. Hipp, and F.U. Hartl, *Functional Modules of the Proteostasis Network*. Cold Spring Harb Perspect Biol, 2020. **12**(1): p. a033951.
100. Dill, K.A. and J.L. MacCallum, *The protein-folding problem, 50 years on*. Science, 2012. **338**(6110): p. 1042-6.
101. Anfinsen, C.B., *Principles that govern the folding of protein chains*. Science, 1973. **181**(4096): p. 223-30.
102. Hartl, F.U., *Protein Misfolding Diseases*. Annu Rev Biochem, 2017. **86**: p. 21-26.
103. Hayden, E.Y. and D.B. Teplow, *Amyloid beta-protein oligomers and Alzheimer's disease*. Alzheimers Res Ther, 2013. **5**(6): p. 60.
104. Klein, W.L., W.B. Stine, Jr., and D.B. Teplow, *Small assemblies of unmodified amyloid beta-protein are the proximate neurotoxin in Alzheimer's disease*. Neurobiol Aging, 2004. **25**(5): p. 569-80.
105. Kepp, K.P., *Alzheimer's disease due to loss of function: A new synthesis of the available data*. Prog Neurobiol, 2016. **143**: p. 36-60.
106. Chiti, F. and C.M. Dobson, *Protein Misfolding, Amyloid Formation, and Human Disease: A Summary of Progress Over the Last Decade*. Annu Rev Biochem, 2017. **86**: p. 27-68.
107. Powers, E.T., et al., *Biological and chemical approaches to diseases of proteostasis deficiency*. Annu Rev Biochem, 2009. **78**: p. 959-91.
108. Sala, A.J., L.C. Bott, and R.I. Morimoto, *Shaping proteostasis at the cellular, tissue, and organismal level*. J Cell Biol, 2017. **216**(5): p. 1231-1241.
109. Hartl, F.U., A. Bracher, and M. Hayer-Hartl, *Molecular chaperones in protein folding and proteostasis*. Nature, 2011. **475**(7356): p. 324-32.
110. Hartl, F.U., *Molecular chaperones in cellular protein folding*. Nature, 1996. **381**(6583): p. 571-9.
111. Klaiaps, C.L., G.G. Jayaraj, and F.U. Hartl, *Pathways of cellular proteostasis in aging and disease*. J Cell Biol, 2018. **217**(1): p. 51-63.

112. Kim, Y.E., et al., *Molecular chaperone functions in protein folding and proteostasis*. *Annu Rev Biochem*, 2013. **82**: p. 323-55.
113. Zuiderweg, E.R., L.E. Hightower, and J.E. Gestwicki, *The remarkable multivalency of the Hsp70 chaperones*. *Cell Stress Chaperones*, 2017. **22**(2): p. 173-189.
114. Kampinga, H.H. and E.A. Craig, *The HSP70 chaperone machinery: J proteins as drivers of functional specificity*. *Nat Rev Mol Cell Biol*, 2010. **11**(8): p. 579-92.
115. van Spronsen, F.J., et al., *Heterogeneous clinical spectrum of DNAJC12-deficient hyperphenylalaninemia: from attention deficit to severe dystonia and intellectual disability*. *J Med Genet*, 2017. **55**: p. 249-253.
116. Straniero, L., et al., *DNAJC12 and dopa-responsive nonprogressive parkinsonism*. *Ann Neurol*, 2017. **82**(4): p. 640-646.
117. Kocaturk, N.M. and D. Gozuacik, *Crosstalk Between Mammalian Autophagy and the Ubiquitin-Proteasome System*. *Front Cell Dev Biol*, 2018. **6**: p. 128.
118. Hershko, A. and A. Ciechanover, *The ubiquitin system*. *Annu Rev Biochem*, 1998. **67**: p. 425-79.
119. Yang, Z. and D.J. Klionsky, *Mammalian autophagy: core molecular machinery and signaling regulation*. *Curr Opin Cell Biol*, 2010. **22**(2): p. 124-31.
120. Puissant, A., N. Fenouille, and P. Auberger, *When autophagy meets cancer through p62/SQSTM1*. *Am J Cancer Res*, 2012. **2**(4): p. 397-413.
121. Lamark, T. and T. Johansen, *Autophagy: links with the proteasome*. *Curr Opin Cell Biol*, 2010. **22**(2): p. 192-8.
122. Sarodaya, N., et al., *Protein Degradation and the Pathologic Basis of Phenylketonuria and Hereditary Tyrosinemia*. *Int J Mol Sci*, 2020. **21**(14).
123. Underhaug, J., O. Aubi, and A. Martinez, *Phenylalanine hydroxylase misfolding and pharmacological chaperones*. *Curr Top Med Chem*, 2012. **12**(22): p. 2534-45.
124. Sarkissian, C.N., et al., *The mechanism of BH4 -responsive hyperphenylalaninemia--as it occurs in the ENU1/2 genetic mouse model*. *Hum Mutat*, 2012. **33**(10): p. 1464-73.
125. Scheller, R., et al., *Toward mechanistic models for genotype-phenotype correlations in phenylketonuria using protein stability calculations*. *Hum Mutat*, 2019. **40**(4): p. 444-457.
126. Eichinger, A., et al., *Secondary BH4 deficiency links protein homeostasis to regulation of phenylalanine metabolism*. *Hum Mol Genet*, 2018. **27**(10): p. 1732-1742.
127. Ericsson, A.C., M.J. Crim, and C.L. Franklin, *A brief history of animal modeling*. *Mo Med*, 2013. **110**(3): p. 201-5.
128. Robinson, N.B., et al., *The current state of animal models in research: A review*. *Int J Surg*, 2019. **72**: p. 9-13.
129. Perlman, R.L., *Mouse models of human disease: An evolutionary perspective*. *Evol Med Public Health*, 2016. **2016**(1): p. 170-6.
130. Frommlet, F., *Improving reproducibility in animal research*. *Sci Rep*, 2020. **10**(1): p. 19239.
131. Hickman, D.L.J., J.; Vemulapalli, T.H.; Crisler, J.R.; Shepherd, R., *Commonly Used Animal Models*. *Principles of Animal Research for Graduate and Undergraduate Students 2017*: p. 117-175.
132. Russel, W.M.S.B., R.L., *The Principles of Humane Experimental Technique*. 1959.
133. Begley, C.G. and J.P. Ioannidis, *Reproducibility in science: improving the standard for basic and preclinical research*. *Circ Res*, 2015. **116**(1): p. 116-26.
134. Bailey, K.R., N.R. Rustay, and J.N. Crawley, *Behavioral phenotyping of transgenic and knockout mice: practical concerns and potential pitfalls*. *ILAR J*, 2006. **47**(2): p. 124-31.
135. Ghosal, S., et al., *Mouse handling limits the impact of stress on metabolic endpoints*. *Physiol Behav*, 2015. **150**: p. 31-7.
136. Schalock, R.L., et al., *Model phenylketonuria (PKU) in the albino rat: behavioral, biochemical, and neuroanatomical effects*. *J Comp Physiol Psychol*, 1975. **89**(6): p. 655-66.
137. Andersen, A.E., V. Rowe, and G. Guroff, *The enduring behavioral changes in rats with experimental phenylketonuria*. *Proc Natl Acad Sci U S A*, 1974. **71**(1): p. 21-5.

138. Lane, J.D., et al., *Characterization of Experimental Phenylketonuria - Augmentation of Hyperphenylalaninemia with Alpha-Methylphenylalanine and Para-Chlorophenylalanine*. *Biochimica Et Biophysica Acta*, 1980. **627**(2): p. 144-156.
139. McDonald, J.D., *The PKU mouse project: its history, potential and implications*. *Acta Paediatrica*, 1994. **83**(407): p. 122-123.
140. McDonald, J.D. and C.K. Charlton, *Characterization of mutations at the mouse phenylalanine hydroxylase locus*. *Genomics*, 1997. **39**(3): p. 402-5.
141. Haefele, M.J., G. White, and J.D. McDonald, *Characterization of the mouse phenylalanine hydroxylase mutation Pah(enu3)*. *Mol Genet Metab*, 2001. **72**(1): p. 27-30.
142. Okano, Y., et al., *Molecular characterization of phenylketonuria and tetrahydrobiopterin-responsive phenylalanine hydroxylase deficiency in Japan*. *J Hum Genet*, 2011. **56**(4): p. 306-12.
143. Sarkissian, C.N., et al., *A heteroallelic mutant mouse model: A new orthologue for human hyperphenylalaninemia*. *Mol Genet Metab*, 2000. **69**(3): p. 188-94.
144. Shedlovsky, A., et al., *Mouse Models of Human Phenylketonuria*. *Genetics Society of America*, 1993. **134**.
145. Zeiss, C.J., J.M. Ward, and H.G. Allore, *Designing phenotyping studies for genetically engineered mice*. *Vet Pathol*, 2012. **49**(1): p. 24-31.
146. Svenson, K.L., et al., *Multiple trait measurements in 43 inbred mouse strains capture the phenotypic diversity characteristic of human populations*. *J Appl Physiol* (1985), 2007. **102**(6): p. 2369-78.
147. Shen, C.H., *Diagnostic Molecular Biology*. Vol. 1. 2019: Academic Press.
148. Patti, G.J., O. Yanes, and G. Siuzdak, *Innovation: Metabolomics: the apogee of the omics trilogy*. *Nat Rev Mol Cell Biol*, 2012. **13**(4): p. 263-9.
149. Johnson, C.H., J. Ivanisevic, and G. Siuzdak, *Metabolomics: beyond biomarkers and towards mechanisms*. *Nat Rev Mol Cell Biol*, 2016. **17**(7): p. 451-9.
150. Wishart, D.S., *Metabolomics for Investigating Physiological and Pathophysiological Processes*. *Physiol Rev*, 2019. **99**(4): p. 1819-1875.
151. Even, P.C. and N.A. Nadkarni, *Indirect calorimetry in laboratory mice and rats: principles, practical considerations, interpretation and perspectives*. *Am J Physiol Regul Integr Comp Physiol*, 2012. **303**(5): p. R459-76.
152. Kanufre, V.C., et al., *Metabolic syndrome in children and adolescents with phenylketonuria*. *J Pediatr* (Rio J), 2015. **91**(1): p. 98-103.
153. Bakkali Aissaoui, H., *Metabolomics in Phenylketonuria disease: A systematic review, in Faculty of Pharmacy and Food Sciences*. 2021, University of Barcelona: Diposit Digital.
154. Moretti, F., et al., *Dietary glycemic index, glycemic load and metabolic profile in children with phenylketonuria*. *Nutr Metab Cardiovasc Dis*, 2017. **27**(2): p. 176-182.
155. Couce, M.L., et al., *Carbohydrate status in patients with phenylketonuria*. *Orphanet J Rare Dis*, 2018. **13**(1): p. 103.
156. Lu, L.H., et al., *Metabolomics analysis reveals perturbations of cerebrocortical metabolic pathways in the Pah(enu2) mouse model of phenylketonuria*. *CNS Neurosci Ther*, 2020. **26**(4): p. 486-493.
157. Sies, H., C. Berndt, and D.P. Jones, *Oxidative Stress*. *Annu Rev Biochem*, 2017. **86**: p. 715-748.
158. Roy, J., et al., *Physiological role of reactive oxygen species as promoters of natural defenses*. *FASEB J*, 2017. **31**(9): p. 3729-3745.
159. Zuo, J., et al., *Redox signaling at the crossroads of human health and disease*. *MedComm* (2020), 2022. **3**(2): p. e127.
160. Huang, C., Zhang, Y., *Oxidative Stress, Human Diseases and Medicine*. Vol. 1. 2021: Springer, Singapore.
161. Ribas, G.S., et al., *Oxidative stress in phenylketonuria: what is the evidence?* *Cell Mol Neurobiol*, 2011. **31**(5): p. 653-62.



162. Sharifi-Rad, M., et al., *Lifestyle, Oxidative Stress, and Antioxidants: Back and Forth in the Pathophysiology of Chronic Diseases*. Front Physiol, 2020. **11**: p. 694.
163. Poprac, P., et al., *Targeting Free Radicals in Oxidative Stress-Related Human Diseases*. Trends Pharmacol Sci, 2017. **38**(7): p. 592-607.
164. Filomeni, G., D. De Zio, and F. Cecconi, *Oxidative stress and autophagy: the clash between damage and metabolic needs*. Cell Death Differ, 2015. **22**(3): p. 377-88.
165. Clark, I.A., W.B. Cowden, and N.H. Hunt, *Free radical-induced pathology*. Med Res Rev, 1985. **5**(3): p. 297-332.
166. Khandia, R., et al., *A Comprehensive Review of Autophagy and Its Various Roles in Infectious, Non-Infectious, and Lifestyle Diseases: Current Knowledge and Prospects for Disease Prevention, Novel Drug Design, and Therapy*. Cells, 2019. **8**(7).
167. Gao, Q., *Oxidative Stress and Autophagy*. Adv Exp Med Biol, 2019. **1206**: p. 179-198.
168. Codogno, P. and A.J. Meijer, *Autophagy and signaling: their role in cell survival and cell death*. Cell Death Differ, 2005. **12 Suppl 2**: p. 1509-18.
169. Bortoluzzi, V.T., C.S. Dutra Filho, and C.M.D. Wannmacher, *Oxidative stress in phenylketonuria-evidence from human studies and animal models, and possible implications for redox signaling*. Metab Brain Dis, 2021. **36**(4): p. 523-543.
170. Rocha, J.C. and M.J. Martins, *Oxidative stress in phenylketonuria: future directions*. J Inherit Metab Dis, 2012. **35**(3): p. 381-98.
171. Martinez-Cruz, F., et al., *Oxidative stress induced by phenylketonuria in the rat: Prevention by melatonin, vitamin E, and vitamin C*. J Neurosci Res, 2002. **69**(4): p. 550-8.
172. Mazzola, P.N., et al., *Regular exercise prevents oxidative stress in the brain of hyperphenylalaninemic rats*. Metab Brain Dis, 2011. **26**(4): p. 291-7.
173. Moraes, T.B., et al., *Lipoic acid prevents oxidative stress in vitro and in vivo by an acute hyperphenylalaninemia chemically-induced in rat brain*. J Neurol Sci, 2010. **292**(1-2): p. 89-95.
174. Wyse, A.T.S., et al., *Insights from Animal Models on the Pathophysiology of Hyperphenylalaninemia: Role of Mitochondrial Dysfunction, Oxidative Stress and Inflammation*. Mol Neurobiol, 2021. **58**(6): p. 2897-2909.
175. Sanayama, Y., et al., *Experimental evidence that phenylalanine is strongly associated to oxidative stress in adolescents and adults with phenylketonuria*. Mol Genet Metab, 2011. **103**(3): p. 220-5.
176. Gersting, S.W., et al., *Pahenu1 is a mouse model for tetrahydrobiopterin-responsive phenylalanine hydroxylase deficiency and promotes analysis of the pharmacological chaperone mechanism in vivo*. Hum Mol Genet, 2010. **19**(10): p. 2039-49.
177. Sarkissian, C.N., et al., *Preclinical evaluation of multiple species of PEGylated recombinant phenylalanine ammonia lyase for the treatment of phenylketonuria*. Proc Natl Acad Sci U S A, 2008. **105**(52): p. 20894-9.
178. Scherer, T., et al., *Tetrahydrobiopterin treatment reduces brain L-Phe but only partially improves serotonin in hyperphenylalaninemic ENU1/2 mice*. J Inherit Metab Dis, 2018. **41**(4): p. 709-718.
179. Gidalevitz, T., et al., *Natural genetic variation determines susceptibility to aggregation or toxicity in a C. elegans model for polyglutamine disease*. BMC Biol, 2013. **11**: p. 100.
180. Tank, E.M., et al., *Prion protein repeat expansion results in increased aggregation and reveals phenotypic variability*. Mol Cell Biol, 2007. **27**(15): p. 5445-55.
181. Ledley, F.D., et al., *Mouse phenylalanine hydroxylase. Homology and divergence from human phenylalanine hydroxylase*. Biochem J, 1990. **267**(2): p. 399-405.
182. Chiti, F. and C.M. Dobson, *Protein misfolding, functional amyloid, and human disease*. Annu Rev Biochem, 2006. **75**: p. 333-66.
183. Franco, A., et al., *All-or-none amyloid disassembly via chaperone-triggered fibril unzipping favors clearance of alpha-synuclein toxic species*. Proc Natl Acad Sci U S A, 2021. **118**(36).
184. Woerner, A.C., et al., *Cytoplasmic protein aggregates interfere with nucleocytoplasmic transport of protein and RNA*. Science, 2016. **351**(6269): p. 173-6.

185. Levine, B. and G. Kroemer, *Autophagy in the pathogenesis of disease*. Cell, 2008. **132**(1): p. 27-42.
186. Lee, S.J., et al., *Towards an understanding of amyloid-beta oligomers: characterization, toxicity mechanisms, and inhibitors*. Chem Soc Rev, 2017. **46**(2): p. 310-323.
187. Strand, E., et al., *Serum Carnitine Metabolites and Incident Type 2 Diabetes Mellitus in Patients With Suspected Stable Angina Pectoris*. J Clin Endocrinol Metab, 2018. **103**(3): p. 1033-1041.
188. Vantyghem, M.C., et al., *Endocrine manifestations related to inherited metabolic diseases in adults*. Orphanet J Rare Dis, 2012. **7**: p. 11.
189. Hwang, W.J., et al., *Pancreatic involvement in patients with inborn errors of metabolism*. Orphanet J Rare Dis, 2021. **16**(1): p. 37.
190. Trefz, K.F., et al., *Clinical burden of illness in patients with phenylketonuria (PKU) and associated comorbidities - a retrospective study of German health insurance claims data*. Orphanet J Rare Dis, 2019. **14**(1): p. 181.
191. Watschinger, K., et al., *Tetrahydrobiopterin and alkylglycerol monooxygenase substantially alter the murine macrophage lipidome*. Proc Natl Acad Sci U S A, 2015. **112**(8): p. 2431-6.
192. Levy, E., et al., *Causative Links between Protein Aggregation and Oxidative Stress: A Review*. Int J Mol Sci, 2019. **20**(16).
193. White, E., *Deconvoluting the context-dependent role for autophagy in cancer*. Nat Rev Cancer, 2012. **12**(6): p. 401-10.
194. Pankiv, S., et al., *p62/SQSTM1 binds directly to Atg8/LC3 to facilitate degradation of ubiquitinated protein aggregates by autophagy*. J Biol Chem, 2007. **282**(33): p. 24131-45.
195. Lamark, T. and T. Johansen, *Aggrephagy: selective disposal of protein aggregates by macroautophagy*. Int J Cell Biol, 2012. **2012**: p. 736905.
196. Bjedov, I., et al., *Fine-tuning autophagy maximises lifespan and is associated with changes in mitochondrial gene expression in Drosophila*. PLoS Genet, 2020. **16**(11): p. e1009083.
197. Abildgaard, A.B., et al., *Co-Chaperones in Targeting and Delivery of Misfolded Proteins to the 26S Proteasome*. Biomolecules, 2020. **10**(8).
198. Choi, J., et al., *The co-chaperone DNAJC12 binds to Hsc70 and is upregulated by endoplasmic reticulum stress*. Cell Stress Chaperones, 2014. **19**(3): p. 439-46.
199. He, H.L., et al., *Overexpression of DNAJC12 predicts poor response to neoadjuvant concurrent chemoradiotherapy in patients with rectal cancer*. Exp Mol Pathol, 2015. **98**(3): p. 338-45.
200. Cyran, A.M. and A. Zhitkovich, *Heat Shock Proteins and HSF1 in Cancer*. Front Oncol, 2022. **12**: p. 860320.
201. Pey, A.L., et al., *Identification of pharmacological chaperones as potential therapeutic agents to treat phenylketonuria*. J Clin Invest, 2008. **118**(8): p. 2858-67.
202. Rozales, K., et al., *Differential roles for DNAJ isoforms in HTT-polyQ and FUS aggregation modulation revealed by chaperone screens*. Nat Commun, 2022. **13**(1): p. 516.
203. Vilchez, D., I. Saez, and A. Dillin, *The role of protein clearance mechanisms in organismal ageing and age-related diseases*. Nat Commun, 2014. **5**: p. 5659.

I

RESEARCH ARTICLE

Phenylalanine hydroxylase variants interact with the co-chaperone DNAJC12

Kunwar Jung-KC¹ | Nastassja Himmelreich² | Karina S. Prestegård¹ |
Tie-Jun Sten Shi¹ | Tanja Scherer³ | Ming Ying¹ | Ana Jorge-Finnigan¹ |
Beat Thöny³ | Nenad Blau^{2,3}  | Aurora Martinez¹ 

¹Department of Biomedicine, University of Bergen, Bergen, Norway

²Dietmar-Hopp-Metabolic Center, University Children's Hospital, Heidelberg, Germany

³Division of Metabolism, University Children's Hospital Zürich, Zürich, Switzerland

Correspondence

Aurora Martinez, Department of Biomedicine, University of Bergen, Bergen, Norway.

Email: aurora.martinez@uib.no

Nenad Blau, Dietmar-Hopp-Metabolic Center, University Children's Hospital, Heidelberg, Germany.

Email: Nenad.Blau@med.uni-heidelberg.de

Funding information

This work was supported by Research Council of Norway grants FRIMEDBIO 261826/F20 and FORNY 248889/O30, the K.G. Jebsen Centre for Neuropsychiatric Disorders, and the Western Norway Regional Health Authorities (Helse-Vest project 912246) (to A.M.), and by the European Commission FP7-HEALTH-2012-INNOVATION-1 EU Grant No. 305444 (to N.B.).

Communicated by David S. Rosenblatt

Kunwar Jung-KC and Nastassja Himmelreich have contributed equally to this work.

Abstract

DNAJC12, a type III member of the HSP40/DNAJ family, has been identified as the specific co-chaperone of phenylalanine hydroxylase (PAH) and the other aromatic amino acid hydroxylases. DNAJ proteins work together with molecular chaperones of the HSP70 family to assist in proper folding and maintenance of intracellular stability of their clients. Autosomal recessive mutations in *DNAJC12* were found to reduce PAH levels, leading to hyperphenylalaninemia (HPA) in patients without mutations in *PAH*. In this work, we investigated the interaction of normal wild-type DNAJC12 with mutant PAH in cells expressing several PAH variants associated with HPA in humans, as well as in the *Enu*^{1/1} mouse model, homozygous for the *V106A-Pah* variant, which leads to severe protein instability, accelerated PAH degradation and mild HPA. We found that mutant PAH exhibits increased ubiquitination, instability, and aggregation compared with normal PAH. In mouse liver lysates, we showed that DNAJC12 interacts with monoubiquitin-tagged PAH. This form represented a major fraction of PAH in the *Enu*^{1/1} but was also present in liver of wild-type PAH mice. Our results support a role of DNAJC12 in the processing of misfolded ubiquitinated PAH by the ubiquitin-dependent proteasome/autophagy systems and add to the evidence that the DNAJ proteins are important players both for proper folding and degradation of their clients.

KEYWORDS

HSP40 co-chaperones, hyperphenylalanine, molecular chaperones, protein aggregation, protein misfolding

1 | INTRODUCTION

The aromatic amino acid hydroxylases (AAAHs) are a family of non-heme iron- and tetrahydrobiopterin (BH₄)-dependent enzymes that catalyze the hydroxylation of their respective aromatic amino acid substrates using O₂ as an additional substrate (Fitzpatrick, 2015; Skjærven, Teigen, & Martinez, 2014). In vertebrates, four genes code for the AAAHs: phenylalanine hydroxylase (*PAH*), tyrosine hydroxylase (*TH*), and tryptophan hydroxylases 1 and 2 (*TPH1* and *TPH2*). The AAAHs catalyze physiologically and clinically important reactions, as the hydroxylation of L-Phe to L-Tyr, which is the first step in the catabolic degradation of L-Phe (by *PAH*), the hydroxylation of L-Tyr to L-DOPA, the rate-limiting step in the biosynthesis of catecholamines

(by *TH*), and the hydroxylation of L-Trp to 5-hydroxytryptophan, the rate-limiting reaction in the synthesis of serotonin (by the *TPHs*). Dysfunction of the AAAHs is associated with serious neurometabolic disorders, such as phenylketonuria (PKU), which is caused by the hyperphenylalaninemia (HPA) that results from variants in *PAH*, and neurological and neuropsychiatric disorders caused by malfunction and dysregulation of *TH* or the *TPHs* (Waløen, Kleppe, Martinez, & Haavik, 2017).

Recent work has shown that mutations in *DNAJC12*—a co-chaperone of the HSP40/DNAJ family, type III—lead to HPA, dystonia, and intellectual disability (Anikster et al., 2017; Blau, Martinez, Hoffmann, & Thony, 2018; Bouchereau et al., 2018; Straniero et al., 2017; van Spronsen et al., 2017; Veenma, Cordeiro,

Sondheimer, & Mercimek-Andrews, 2018). Moreover, affinity capture-mass spectrometry analysis in human cells has shown direct interactions of DNAJC12 with PAH, TH, and the TPHs (Anikster et al., 2017; Huttlin et al., 2015), which indicates that DNAJC12 is a specific co-chaperone for the AAAHs that contributes to the maintenance of their intracellular stability. The function of the DNAJ proteins in the quality control machinery is believed to be the transfer of its specific protein clients to the molecular chaperone HSC70/HSP70-HSP90 network for proper folding (Kampinga & Craig, 2010), and PAH protein level and activity are indeed reduced in cells that express mutant DNAJC12 (Anikster et al., 2017). Nevertheless, the complex molecular chaperone machinery is essential to maintain proteostasis in eukaryotic cells not only by assisting in the folding of client proteins but also in the intertwined triage decisions that affect the disposition of misfolded proteins, which are degraded to avoid toxic aggregation and cellular damage (Dekker, Kampinga, & Bergink, 2015; Pratt, Morishima, Peng, & Osawa, 2010). In this context, the DNAJ-co-chaperones appear essential for ubiquitin (Ub)-tagging and further degradation of the clients by the Ub-dependent proteasome (Kampinga & Craig, 2010). Furthermore, DNAJ and HSC70/HSP70 also participate in the degradation of aggregated proteins by autophagy (Kaushik & Cuervo, 2012). Proteins such as PAH, which do not include a specific sequence motif for chaperone-mediated autophagy allowing direct translocation across the lysosome membrane, usually follow a mechanism known as selective autophagy (Kaushik & Cuervo, 2012). This selective autophagosomal-lysosomal system also requires Ub-tagging of the clients and collaborates with the Ub-proteasome in the degradation of misfolded and aggregated proteins, where HSP70s and DNAJs play an important role in the crosstalk between both systems (Fernandez-Fernandez, Gragera, Ochoa-Ibarrola, Quintana-Gallardo, & Valpuesta, 2017; Kraft, Peter, & Hofmann, 2010).

PAH mutants often form amorphous aggregates when expressed in *Escherichia coli* (Björge, Knappskog, Martínez, Stevens, & Flatmark, 1998), and fibril formation has also been observed in vitro (Leandro, Simonsen, Saraste, Leandro, & Flatmark, 2011). However, in vivo amyloid or other fibrillary deposits, which are the pathological manifestation of other protein folding defects via gain-of-function toxicity (Gregersen, 2006), have not been reported for PKU-associated variants. The misfolded PAH mutants are considered to be effectively degraded by the cellular quality control system when they are expressed in eukaryote cells (Himmelreich et al., 2018; Pey, Desviat, Gamez, Ugarte, & Perez, 2003; Waters, Parniak, Akerman, & Sriver, 2000) or as observed in mammalian liver of mouse models of HPA (Gersting et al., 2010; Sarkissian, Boulais, McDonald, & Sriver, 2000; Sarkissian, Ying, Scherer, Thony, & Martinez, 2012). PKU is therefore considered a paradigm of misfolding disorders in which the metabolic phenotype is mainly related to the conformational destabilization caused by the mutation in the PAH structure, which in turn is associated to the remaining PAH protein expression and activity (Pey, Stricher, Serrano, & Martinez, 2007; Wettstein et al., 2015). Recently, the aggregation of the unstable PAH variant p.V106A, which is expressed by the *Enu*^{1/1} mouse model of mild HPA (Sarkissian et al., 2000), has also been observed when the mutant protein is expressed in primary hepatocytes and COS-7 cells (Eichinger et al.,

2018). Furthermore, studies with both, the *Enu*^{1/1} and the *Enu*^{1/2} heteroallelic mouse models, which carry both the unstable V106A-PAH (*enu1* allele) and/or the catalytically deficient but stable F263S-PAH (*enu2* allele) variants, have shown that mutant forms of PAH, notably p.V106A, are highly ubiquitinated and very unstable in vivo, indicating that they are targets for proteasome-mediated degradation and selective autophagy (Sarkissian et al., 2012).

To further investigate the involvement of DNAJC12 in the degradation of mutant PAH, we studied the interactions of the wild-type (wt) co-chaperone with normal and mutant PAH forms expressed in COS cells and in mouse liver. To study the interactions in vivo, we selected the homozygote *Enu*^{1/1} mouse model. Despite the fact that the *PAH* variant carried by these mice is extremely rare in human subjects (0.2% of alleles in Japan) (Okano, Kudo, Nishi, Sakaguchi, & Aso, 2011), the *Enu*^{1/1} is a model for pathological states associated with human PAH instability and accelerated degradation (Gersting et al., 2010; Sarkissian et al., 2000). We demonstrated that in the livers of these mice, mutant p.V106A-PAH is found largely in a mono-ubiquitinated state and forms a complex with DNAJC12, which supports the functional association of the co-chaperone with PAH degradation.

2 | MATERIALS AND METHODS

2.1 | Generation of plasmids for cellular expression of PAH and DNAJC12

Generation of plasmids for recombinant expression of the PAH variants was performed as described (Himmelreich et al., 2018; Shen et al., 2016) (Supporting Information Table S1). To generate an expression plasmid for DNAJ12 (based on pCiNeo-Myc), total RNA was extracted from 1×10^6 cells (control fibroblasts) using the MasterPure RNA purification kit (Epicentre Biotechnologies). Using random hexamer primers (Invitrogen) and RevertAid reverse transcriptase (Thermo Scientific), 1 μ g of total RNA was reverse transcribed into cDNA, using manufacturer's protocol (5 min at 25°C, 60 min at 42°C, and 5 min at 70°C). Nested-PCR for human DNAJC12 (NM_021800.2; CDS: 169–765) was performed with the following parameters: Step 1: 98°C, 1 min; Step 2: 98°C, 15 s; Step 3: 55°C, 30 s; Step 4: 72°C, 40 s; Step 5: 72°C, 5 min; Step 6: 4°C, indefinitely. Steps 2–4 were repeated 35 times. The amplification primers for DNAJC12 were F1_hDNAJC12: 5'-₄GTCTAGGATGACATCTGGTGTATTG₂₉-3' together with R1_hDNAJC12: 5'-₈₈₄GTACTCAGCAATTCACAGACATGAC₈₅₉-3' and F2_hDNAJC12: 5'-₁₁₁TTCGAAGCTCACTGTGCCCTCTTG₁₃₃-3' together with R2_hDNAJC12: 5'-₈₁₃GCATAGGGGACAGTCTTGCTCTT₇₉₁-3'. After gel extraction (Bioline) and Sanger sequencing of the DNAJC12-PCR fragment, a third PCR was performed to attach flanking *NotI* endonuclease restriction sites for ligation with T4-DNA-ligase (Fermentas) into vector pCiNeo-Myc (Promega) (F3_hDNAJC12_NOT_ATG: 5'-ACGCGGCCG CATGGATGCAACTACT together with R4_hDNAJC12_Not_STOP: 5'-TACGCGCCGCTATTTTCATAGTTTCT-3'). The *NotI* restriction fragment was ligated into vector pCiNeo-Myc overnight at room temperature before transformation into *E. coli* DH5a cells. The constructs were rechecked after plasmid miniprep (Bioline) and

thereafter stably transfected into the COS-7 cell line upon selection with Neomycin in the cell culture medium (225 $\mu\text{g}\cdot\text{ml}^{-1}$ G418, Life Technologies).

2.2 | Cell culture, transient transfection of PAH-expressing plasmids, PAH and DNAJC12 expression, and cell lysate preparation

COS-7 cells were used for transient transfection of human PAH-expressing plasmids. Cells were cultured in Dulbecco's Modified Eagle Medium, enriched with a 10% fetal calf serum plus 1% Pen/Strep under standard conditions (37°C with 5% CO₂) in a sterile environment. One day before transfection, 10⁶ COS-7 cells were seeded in 10 cm culture dishes (Sarstedt). For the transfection with Fugene HD reagent (Promega), the cells had a density of 50–70% confluence, and the experiments were carried out according to the manufacturer's manual. Plasmids pCMV-Flag-PAH (10 μg) expressing either the wt or a PAH-variant were co-transfected with 2 μg of pSV- β -Galactosidase control vector (Promega) using 30 μl of liposomal transfection reagent in antibiotic-free media. After culturing the transfected cells for 72 hr, the cells were harvested with trypsin, washed with 1 \times PBS, pH 6.8, and shock-frozen in liquid N₂ for storage at –80°C. COS-7 cells stably expressing DNAJC12 were used in three different variants, that is, as “un-transfected” controls, and transfected with either wt or one of the mutant PAH. Cell lysates were prepared by macerating the cells in 1 M Sucrose, 1 \times PBS buffer, pH 6.8, containing protease inhibitor cocktail (Roche Applied Science) (except DNAJC12 overexpressing cells, which were lysed in water) 20 times through a 20 G needle followed by 3 \times 20 s sonification and centrifugation for 30 min at 13,000 rpm at 4°C. The cell extracts were desalted and further purified using Zebra Desalt Spin columns (Pierce Biotechnology). The Myc-Tagged DNAJC12 was also used as a marker for immunodetection of the antigen, and to validate the antibody, which was selected based on its highest selectivity for DNAJC12 toward other DNAJ-proteins.

2.3 | Mice husbandry and genotyping

Heterozygous C57BL/6-*enu1* mice (*Enu1*^{1/wt}) were kindly donated by Dr. Soren W. Gersting from the Ludwig-Maximilians-University in Munich to the University of Zurich (Beat Thöny) for colony forming, and thereafter transferred to the laboratory animal facility at the University of Bergen. The here presented animal studies received approval from the National committee for the use of animals in research (Norwegian Food Safety Authority) and were conducted in accordance with the International and National regulations on the use of animals in research. Homozygote mutant mice *enu1/enu1* (*Enu1*^{1/1}) were generated by cross-breeding heterozygous females with homozygous males. C57BL/6 mice were used as wt controls. Animals used for experiments were between 18 and 21 weeks of age with a body weight of 25–35 g. Animals were housed in a controlled temperature room maintained under alternating 12 hr light and dark cycles and, in between experiments, had free access to food (standard chow) and water. Ear biopsies were collected for genotyping following a method as described (McDonald & Charlton, 1997).

2.4 | Preparation of mouse liver lysates

Immediately after the sacrifice with CO₂, the entire liver was resected, frozen in liquid nitrogen, and stored at –80°C. The liver tissue was manually ground into fine powder and stored in aliquots at –80°C until analysis. Liver lysate preparation was performed at 4°C. For standard initial immunodetection experiments, liver powder aliquots were homogenized with a Tissue Lyser II (Qiagen) in PBS buffer, pH 7.4, containing a protease inhibitor cocktail (Roche). The lysates were clarified by centrifugation at 13,000 \times g for 20 min, and the supernatants were collected and stored in liquid nitrogen prior to use. To improve the solubilization of aggregates, the liver powder aliquots were homogenized with a Tissue Lyser II in 4 \times volumes of 20 mM Hepes, pH 7.4, 125 mM NaCl, 1 mM EDTA, 2 mM PMSF supplemented with protease inhibitor cocktail (Roche Applied). The lysates were clarified by centrifugation at 16,000 \times g for 20 min. The supernatants were collected and treated with 1% Triton X-100 for 1 hr with rotation, and centrifuged at 20,000 \times g for 15 min. The protein concentrations were measured using a Direct Detect® Infrared Spectrometer (Merck Life Science). These conditions were also used for the preparation of lysates for co-immunoprecipitation. Subcellular fractionation of nuclear and cytoplasmic fraction of liver extracts was performed using a nuclear extraction kit (Merck Life Science) on the liver powder.

2.5 | mRNA quantification

Quantification of selected mouse mRNAs by RT-qPCR was performed as described (Scherer et al., 2018), using the ABI assay number Mm00500918_m1 (NCBI nucleotide sequence number NM_008777.3) for *Pah*-mRNA, Mm01731394_gH (NM_031165.4) for *Hspa8*-mRNA, Mm00517691_m1 (NM_001163434.1) for *Hspa5(BIP)*-mRNA, Mm01322973_m1 (NM_008102.3) for *Gch1*-mRNA, Mm00433149_m1 for *Esr1*-mRNA, Mm01201402_m1 (NM_008296.2) for *Hsf1*-mRNA, Mm00490634_m1 (NM_019719.3) for *Stub1*-mRNA, Mm00622819_m1 (NM_177157.4) for *Gchfr*-mRNA, Mm00497038_m1 (NM_001253685.1) for *Dnajc12*-mRNA, Mm01729741_g1 (NM_001285429.1) for *Eef1d*-mRNA, Mm00517691_m1 (NM_010478.2) for *Hspa1b(Hsp70)*-mRNA, Mm02620446_s1 (NM_029771.3) for *Gper1*-mRNA, and Mm00599821_m1 (NM_010157.3) for *Esr2*-mRNA. The murine *Gapdh* gene was used as a control (ABI assay ID Mm9999915_g1; NCBI nucleotide sequence number NM_008084.3).

2.6 | Expression and immunoblotting of PAH and DNAJC12

Western blotting of the cell lysates was performed as described (Himmelreich et al., 2018); 20 μg of the total protein from the supernatant was resolved in a 12 % SDS-PAGE, blotting for 50 min to a nitrocellulose membrane (GE Healthcare) using a semidry transfer method and blocking for 1 hr at room temperature in 5% milk powder either in TBST with 0.1% (v/v) Tween (for DNAJC12 or M2-Flag) or PBST 0.1 with 0.1% (v/v) Tween (for PAH, HSP70, and β -actin). Primary antibodies against DNAJC12 (1:500 dilution, Abcam ab167425),

PAH (1:1,000 dilution, Millipore MAB5278), M2-Flag (1:1,000 dilution, Sigma F1804), HSP70 (1:1,000 dilution, ab2787), and β -actin (1:10,000, Sigma A5441) were incubated overnight at 4°C under constant movement. The secondary antibodies against rabbit (Dianova) and against mouse (Santa Cruz) were labeled with a horseradish peroxidase tag, and detection with an ECL reagent (Pierce) was performed according to manufacturer's recommendations. Western blots of the liver lysates were performed using SDS-PAGE 10% TGX™ gels (Bio-Rad) with 15 μ g total protein in sample buffer consisting of 1% SDS and 100 mM DTT (final concentration) in each lane. The samples were transferred onto PVDF membranes using a Transblot Turbo system (Bio-Rad) and immunostained using as primary antibodies: anti-PAH (clone PH8) (1:5,000, mouse; Merck Life Science), anti-DNAJC12 (1:300, rabbit; Abcam), anti-ubiquitin (1:1,000, mouse; Thermo Fisher Scientific), anti- β -actin (1:1,000, mouse; Merck Life Science), anti-HSC70/HSP70 (1:5,000, mouse; Enzo; this antibody recognizes both HSC70 and HSP70), anti-GAPDH (1:1,000, rabbit; Abcam). Secondary antibodies for both goat anti-rabbit IgG (H+L) horseradish peroxidase conjugate and goat anti-mouse IgG (H+L) horseradish peroxidase conjugate were from Bio-Rad. The membranes were developed by enhanced chemiluminescence and visualized using a ChemiDoc instrument (Bio-Rad). The band intensities were quantified using Image Lab software v 5.1 (Bio-Rad).

2.7 | Immunohistochemistry

Enu^{1/1} and wt mice (male, 6-month-old) were deeply anesthetized with sodium pentobarbital (Mebumal; 20 mg·kg⁻¹, ip), and then transcardially perfused with 20 ml of warm saline solution (0.9%; 37°C), followed by 20 ml of a warm mixture of paraformaldehyde (4%; 37°C) with 0.4% picric acid in 0.16 M phosphate buffer, pH 7.2, and finally with 50 ml of the same, but ice-cold, fixative. After perfusion, the livers were dissected and post-fixed in the same fixative for 90 min at 4°C and subsequently stored in 20% sucrose in PBS, pH 7.4, containing 0.01% sodium azide (Merck Life Science) and 0.02% bacitracin (Merck Life Science) at 4°C for 4 days. The tissues were then embedded in OCT compound (Tissue Tek, Miles Laboratories), frozen, cut into 20- μ m-thick sections in a cryostat (Microm) and mounted on Superfrost Plus microscope slides (Thermo Fisher Scientific). The sections were dried at room temperature (RT) for 30 min and rinsed with PBS for 10 min. The sections were pretreated with 0.5 or 1% Triton X-100 (as indicated) in PBS for 1 hr at RT, and then incubated for 24 hr at 4°C in a humid chamber with rabbit anti-PAH (1:200; Abcam) or rabbit anti-DNAJC12 (1:400; Abcam) antisera diluted in PBS containing 5% (w/v) normal goat serum. After incubation, the slides were rinsed with PBS for 15 min at RT followed by a 2 hr incubation with donkey anti-rabbit IgG-H&L (Alexa Fluor® 488; 1:100; Abcam) diluted in 5% normal goat serum in PBS, then washed in PBS for 15 min. Finally, the sections were mounted with glycerol/PBS (9:1) containing 2.5% DABCO (Merck Life Science). The specimens were analyzed using a Leica TCS SP5 microscope (Leica Microsystems) equipped with X10 (0.5 numerical aperture, NA) and X20 water (0.75 NA) objectives, and images were acquired with the LasAF software from Leica.

2.8 | Co-immunoprecipitation

The supernatants from the liver lysates treated with 1% Triton X-100 (see above) were incubated with an antibody against PAH (clone PH8) (mouse; Merck Life Science), control IgGs (Merck Life Science), or no antibody (only beads) with overnight rotation. Protein A/G PLUS-agarose beads (Santa Cruz Biotechnology, Inc.) were incubated with gentle rotation for 1 hr with the samples. The immunoprecipitates were then pelleted, washed, and incubated at 95°C for 10 min in 50 μ l of sample buffer. The samples were analyzed using SDS-PAGE and immunoblotting with anti-PAH (1:1,000, mouse, Merck Life Science), anti-DNAJC12 (1:300, rabbit; Abcam), anti-ubiquitin (1:1,000, mouse; Thermo Fisher Scientific), and anti-HSC70/HSP70 (1:5,000, mouse; Enzo) antibodies as primary antibodies; anti-mouse kappa light chain (HRP) (Abcam) and anti-rabbit IgG heavy chain (HRP) (Abcam) antibodies were used as secondary antibodies for the detection of primary antibodies to prevent unspecific recognition of accumulated heavy and light chain from the immunoprecipitation. Also, for PAH immunodetection, both in input and immunoprecipitation, samples from wt mice were diluted 10 times compared to *Enu*^{1/1} samples to prevent obscuring of the weak PAH signal in the latter due to dynamic range.

2.9 | Statistical analysis

Using Student's *t*-test, two-way comparison was performed for statistical analysis, considering *p*-value <0.05 statistically significant. The sample size *n* was in all cases ≥ 3 .

3 | RESULTS

3.1 | Immunodetection of DNAJC12 in lysates of COS cells expressing different PAH variants

To investigate the relative expression of PAH variants and endogenous DNAJC12, we chose COS-7 cells as they have recently been used to express PKU-associated PAH variants (Himmelreich et al., 2018). COS-7 cells expressed low amounts of endogenous DNAJC12 (Figure 1a, first lane) until they were subjected to transient transfection of PAH (wt and variants) (Figure 1a), and we also observed that the endogenous DNAJC12 also increased in stably transfected COS-7 cells expressing DNAJC12 with a Myc-Tag (Supporting Information Figure S1, last lane). Normal COS-7 cells are thus a useful system to overexpress human PAH-wt and PKU associated variants, as COS-7 cells with stable expression of DNAJC12 appeared to result in the overexpression of the endogenous form of the co-chaperone that may cause alteration of mechanisms and interaction with partners, such as PAH. We selected 11 PAH variants characterized by different relative residual PAH activity for inclusion in the present study according to PAHvdb: Phenylalanine Hydroxylase Gene Locus-Specific Database (www.biopku.org), that is, p.A47V, p.V190A, p.A300S, p.A313T and p.A403V associated with mild HPA; p.R68G, p.E76 and p.R297H with mild PKU; and p.G218V and p.R408W, associated with severe, classic PKU (Figure 1a). Cell lysates were analyzed by Western blotting for immunodetection of overexpressed PAH variants, both

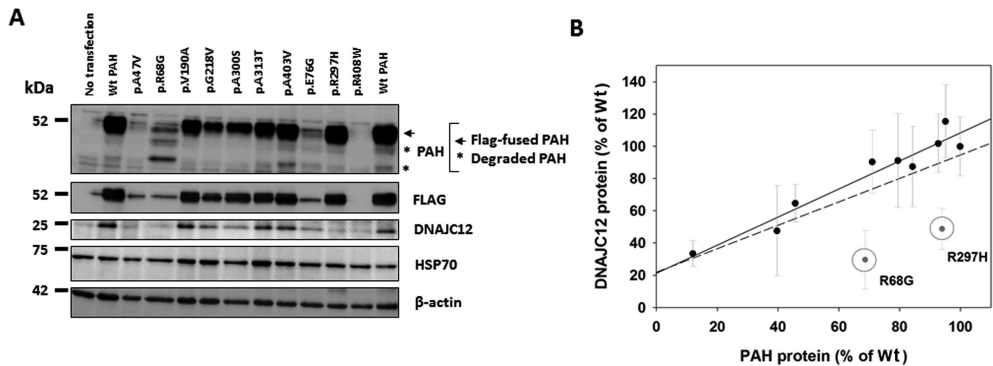


FIGURE 1 Expression analyses of the transient transfection of a subset of PAH-variants in COS-7 cells and endogenous DNAJC12 and HSP70. (a) Western blots of PAH wt and variants (Himmelreich et al., 2018), the Flag-tag, DNAJC12, and HSP70 ($n \geq 3$). (b) Correlations between immunoquantified DNAJC12 and PAH for each PAH variant expressed in the COS-7 cells, relative to immunoquantified DNAJC12 and PAH in the wt-PAH sample normalized against β -actin, respectively. A moderate positive correlation was measured between the levels of immunoquantified PAH with the PAH antibody (on the ~52-kDa Flag-fused PAH) and endogenous DNAJC12 (~24 kDa) ($R^2 = 0.51$; dashed line). A stronger relationship was measured for a subset of variants, excluding p.R68G and p.R297H ($R^2 = 0.93$; solid line)

with antibodies against PAH itself and Flag-tagged PAH, and for endogenous DNAJC12 and HSP70 (Figure 1a). For PAH-wt, the immunodetection pattern showed a strong 52-kDa full-length band, corresponding to PAH with a fused Flag-tag, some minor degradation bands of lower molecular weight, as well as bands of higher molecular weight associated in previous studies with post-translationally modified PAH (Doskeland & Flatmark, 1996; Sarkissian et al., 2012) (see also Supporting Information Figure S1, showing results from a different experiment; $n = 7$ performed). Moreover, a similar band pattern was found for several of the PAH variants, with most revealing decreased levels of the full-length PAH, whereas other variants, such as p.R68G, presented stronger degradation bands (Figure 1a and Supporting Information Figure S1). The immunoquantification of the PAH variants relative to PAH-wt provided very similar values by using either PAH or Flag antibodies. The immunodetected levels of DNAJC12 were reduced for the most unstable PAH variants. In particular, the expression of p.R408W, which produces a strongly misfolded PAH enzyme, results in degraded PAH and provided very low levels of immunodetected PAH protein and of endogenous DNAJC12 (Figure 1a). As depicted in Figure 1b, we observed a moderate positive correlation between the levels of immunoquantified PAH with the PAH antibody (on the ~52-kDa Flag-tagged PAH) and endogenous DNAJC12 (~24 kDa) ($R^2 = 0.51$). Similar positive correlations were obtained between the immunoquantified Flag epitope and endogenous DNAJC12 (data not shown). The relationship was actually very strong for a subset of variants excluding p.R68G and p.R297H ($R^2 = 0.93$). On the other hand, the immunodetected endogenous HSP70 was not affected by the PAH variant expressed, and the levels of this molecular chaperone appeared rather constant (Figure 1a).

The correlation between PAH and DNAJC12 levels supports an association between both proteins, and indicates a specific interaction of the co-chaperone with the most severely misfolded PAH mutants.

We aimed to investigate the underlying molecular mechanisms for the interaction, but in order to avoid any differences in expression of endogenous DNAJC12 due to transcriptional and translational interference from the transient expression of PAH, we selected the *Enu*^{1/1} HPA mouse model for analysis of endogenous expression of DNAJC12 and variant PAH.

3.2 | Immunodetection of PAH, DNAJC12 and HSC70/HSP70, and ubiquitination state of PAH in liver lysates of wild-type and *Enu*^{1/1} mice prepared under standard conditions

We investigated the interactions between DNAJC12 and PAH in liver of *Enu*^{1/1} mice as they express the highly unstable PAH variant p.V106A-PAH. Western blot analyses of liver lysates showed the expected reduction of PAH levels in the *Enu*^{1/1} compared with wt mice (Gersting et al., 2010; Sarkissian et al., 2000) (Figure 2). We also performed Western blot analysis of ubiquitin in livers, where wt mice showed a major fraction of full-length non-ubiquitinated-PAH (~50 kDa) and a smaller fraction of monoubiquitinated-PAH, whereas a large proportion of mutant PAH appeared to be monoubiquitinated (55 kDa) in *Enu*^{1/1} livers (Figure 2a). These bands have previously been identified based on immunodetection in *Enu*^{1/1} and *Enu*^{1/2} and immunoprecipitation in *Enu*^{1/2} liver lysates (Sarkissian et al., 2000; Sarkissian et al., 2012). Weak polyubiquitinated bands were observed for both wt and *Enu*^{1/1} mice. As observed in the lysates of COS-7 cells expressing wt and the most unstable PAH mutants (Figure 1a), DNAJC12 was immunodetected in the liver lysates from wt mice but not in lysates from *Enu*^{1/1} (Figure 2a). On the other hand, the expression levels of HSC70/HSP70 were not affected by the PAH genotype and these molecular chaperones presented very similar levels in wild-type and *Enu*^{1/1} mice samples (Figure 2a).

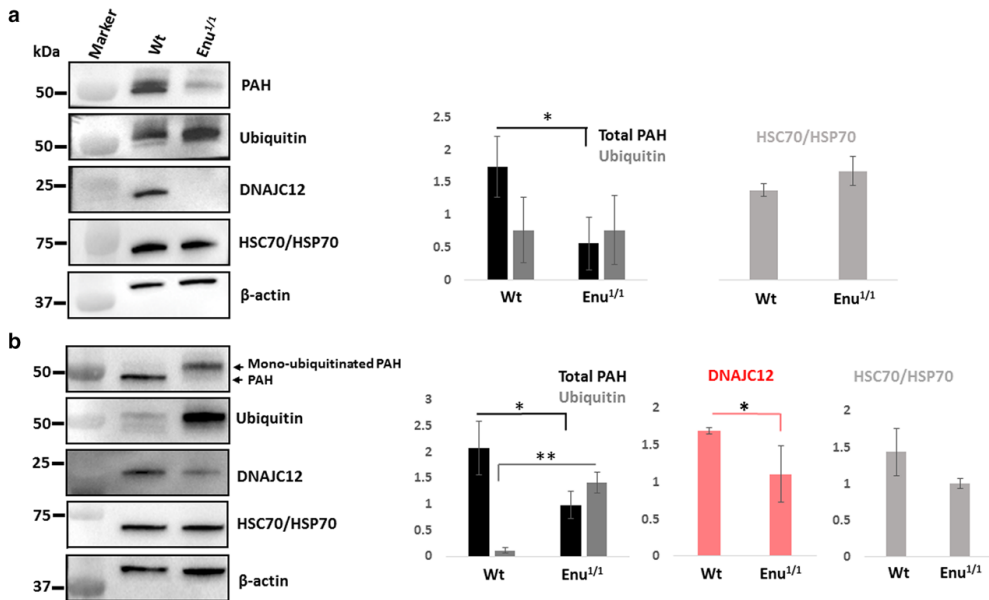


FIGURE 2 Immunodetection of PAH, ubiquitinated protein, DNAJC12, and HSC70/HSP70 from liver lysates of wt and *Enu*^{1/1} mice prepared in PBS buffer (a) and solubilizing buffer (b). β -actin was used as a loading control in both cases ($n = 3$). The histograms in both panels represent immunoquantified protein levels by densitometric analysis; * $p < 0.05$; ** $p < 0.0005$

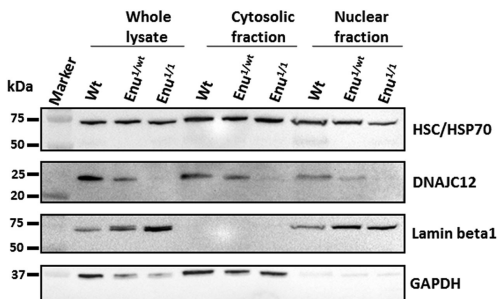


FIGURE 3 Cellular distribution of DNAJC12 and HSC70/HSP70 in wt, *Enu*^{1/wt}, and *Enu*^{1/1} mice. DNAJC12 and HSC70/HSP70 were detected in the whole lysate, nuclear, and cytosolic fractions. The purity of the fractions was tested with lamin beta1 (nuclear fraction marker) and GAPDH (cytosolic fraction marker)

DNAJC12 is mainly a cytoplasmic protein with a minor nuclear localization (Choi, Djebbar, Fournier, & Labrie, 2014), and since nuclear proteins are often poorly detected in whole tissue lysates, we investigated whether a different cytoplasmic/nuclear distribution of DNAJC12 in the normal and HPA mice could explain the different immunodetected levels. The liver lysates of wt, heterozygous *Enu*^{1/wt}, and *Enu*^{1/1} were fractionated into cytosolic and nuclear fractions prior to the SDS-PAGE and immunodetection. Lamin beta 1 and GAPDH were used as the nuclear and cytoplasmic markers, respectively, to validate the purity of the fractions obtained (Figure 3). PAH is mainly

distributed in the cytoplasmic fraction (data not shown), but DNAJC12 was detected in both the cytoplasmic and nuclear fractions, preferentially in the former. The levels of DNAJC12 were in any case strongly reduced in heterozygous mice compared with wt, and almost absent in both fractions in the homozygote *Enu*^{1/1} (Figure 3), which indicated that a change in the subcellular distribution is probably not the main reason for the lack of immunodetected DNAJC12 in *Enu*^{1/1} mice.

We then considered two possibilities for the observed reduction of immunodetected DNAJC12 in the liver lysates of *Enu*^{1/1} mice (Figure 2a): (i) a possible transcriptional down-regulation of the co-chaperone, or (ii) aggregation of the mutant p.V106A-PAH, leading to concomitant aggregation of DNAJC12 in this case complexed with PAH. We proceeded first with analysis of the *Dnajc12*-mRNA level and a few associated genes.

3.3 | Quantification of gene expression of *Pah*, *Dnajc12*, and associated players in liver of wild-type and *Enu*^{1/1} mice

Possible differences in the transcriptional regulation between wt and *Enu*^{1/1} mice were determined by mRNA quantification (RT-qPCR). We measured the mRNA levels of *Dnajc12* and *Pah*, as well as those for other selected genes based on their possible interactions with DNAJC12, including (i) the molecular chaperones Hsp70 (*Hspa1b*), Hsc70 (*Hspa8*), HSF1 (*Hsf1*), and BIP (*Hspa5*), the latter being an endoplasmic reticulum chaperone that is associated with DNAJC12 in situations of cellular stress (Choi et al., 2014), and the

TABLE 1 Relative mRNA quantification for *Dnajc12*-mRNA, *Pah*-mRNA, and other selected genes in liver of wt and *Enu*^{1/1} mice

Gene	<i>Pah</i> genotype	Relative to <i>Dnajc12</i> in wt mice defined as 1	p-Value
<i>Pah</i>	wt/wt	111.99 (86.84 ± 144.42)	0.45
(n = 5)	<i>Enu</i> ^{1/1}	98.14 (74.59 ± 129.13)	
<i>Hspa8 (Hsc70)</i>	wt/wt	415.85 (298.88 ± 578.60)	0.57
(n = 5)	<i>Enu</i> ^{1/1}	374.13 (295.79 ± 473.22)	
<i>Hspa5 (Bip)</i>	wt/wt	237.25 (153.15 ± 367.54)	0.89
(n = 5)	<i>Enu</i> ^{1/1}	250.38 (117.99 ± 531.33)	
<i>Gch1</i>	wt/wt	39.48 (28.74 ± 54.23)	0.83
(n = 11)	<i>Enu</i> ^{1/1}	38.24 (26.03 ± 56.18)	
<i>Esr1</i>	wt/wt	19.77 (10.70 ± 36.53)	0.86
(n = 5)	<i>Enu</i> ^{1/1}	21.25 (10.56 ± 42.79)	
<i>Hsf1</i>	wt/wt	7.35 (5.90 ± 9.15)	0.21
(n = 6)	<i>Enu</i> ^{1/1}	5.90 (4.21 ± 8.27)	
<i>Stub1</i>	wt/wt	4.48 (3.54 ± 5.66)	0.49
(n = 6)	<i>Enu</i> ^{1/1}	3.98 (2.85 ± 5.56)	
<i>Gchfr</i>	wt/wt	3.47 (2.49 ± 4.83)	0.58
(n = 11)	<i>Enu</i> ^{1/1}	3.76 (2.68 ± 5.27)	
<i>Dnajc12</i>	wt/wt	1.00 (0.45 ± 2.23)	0.78
(n = 11)	<i>Enu</i> ^{1/1}	0.82 (0.29 ± 2.29)	
<i>Eef1d</i>	wt/wt	1.11 (1.01 ± 1.23)	0.76
(n = 5)	<i>Enu</i> ^{1/1}	1.07 (0.81 ± 1.41)	
<i>Hspa1b (Hsp70)</i>	wt/wt	0.13 (0.07 ± 0.26)	0.73
(n = 5)	<i>Enu</i> ^{1/1}	0.11 (0.05 ± 0.26)	
<i>Gper1</i>	wt/wt	0.03 (0.02 ± 0.05)	0.61
(n = 11)	<i>Enu</i> ^{1/1}	0.04 (0.02 ± 0.07)	
<i>Esr2</i>	wt/wt	0.02 (0.01 ± 0.02)	0.91
(n = 5)	<i>Enu</i> ^{1/1}	0.02 (0.01 ± 0.02)	

co-chaperone/E3 ubiquitin-protein ligase CHIP (*Stub1*); (ii) the eukaryotic translation elongation factor 1 delta EEF1D (*Eef1d*), which has been found to interact with DNAJC12 in a transcription factor interaction network (Miyamoto-Sato et al., 2010); (iii) the estrogen receptors 1 and 2 ESR1 and 2 (*Esr1*, *Esr2*), and the G protein-coupled estrogen receptor 1 (*Gper1*), which were analyzed because DNAJC12 expression has been associated with estrogen receptor status in breast cancers (De Bessa et al., 2006); and (iv) GTP cyclohydrolase 1 (*Gch1*) and GTP cyclohydrolase 1 feedback regulatory protein (*Gchfr*), which are involved in the synthesis of the PAH-cofactor tetrahydrobiopterin (BH₄). The results are presented in Table 1. *Esr2* was not expressed, *Gper1* was faintly expressed, and *Hsp70* also showed low expression. Both *Dnajc12* and *Pah*, notably the latter, were abundantly expressed in mouse livers, with ~112-fold higher expression of *Pah* with respect to *Dnajc12*, and no difference in the mRNA levels for these two genes between wt and *Enu*^{1/1} samples. Overall, no significant differences on mRNA expression were measured for any of the studied genes upon *Pah* mutation.

3.4 | Immunodetection of PAH, DNAJC12, and HSC70/HSP70, and ubiquitination state of PAH in liver lysates of wild-type and *Enu*^{1/1} mice prepared using improved solubilization conditions

We then investigated whether an intracellular co-aggregation of PAH and DNAJC12 might lead to decreased immunodetection. Aggregated proteins and complexes are often poorly solubilized by 1% SDS and are therefore prone to low detection in SDS-PAGE and Western blotting due to precipitation upon sample preparation, notably under the heat pretreatment (Juenemann, Wiemhoefer, & Reits, 2015). We thus optimized the lysis of liver tissue and sample preparation steps by reducing the ionic strength of the buffers to diminish hydrophobic interactions and favor the extraction and immunodetection of proteins that may form intracellular aggregates. We also included treatment with the non-ionic detergent Triton X-100 (1%) before subjecting the samples to SDS-PAGE (see Section 3.2 for details). Following immunoblotting, it was indeed observed that these conditions lead to the detection of DNAJC12 in the *Enu*^{1/1} liver lysates, at almost similar levels as for the wt mice (Figure 2b). The use of the improved solubilization lysis conditions also resulted in an increased level of immunodetected PAH in the *Enu*^{1/1} mice relative to the wt (Figure 2a,b), but densitometric analysis still revealed the expected reduction of total PAH and the increased proportion of ubiquitinated-PAH in *Enu*^{1/1} when compared to wt mice. Immunoquantification of HSC70/HSP70 showed similar levels of this molecular chaperone in both mice.

3.5 | Expression and distribution of PAH and DNAJC12 analyzed by immunohistochemistry in livers of wild-type and *Enu*^{1/1} mice

Further analyses of the DNAJC12 protein were performed using immunohistochemistry in livers of the wt and *Enu*^{1/1} mice, which also supported a preferential cytoplasmic localization of both PAH and DNAJC12-like immunoreactivities (Figure 4). With the standard protocol in which 0.5% Triton X-100 was included, the PAH signal was largely decreased in the *Enu*^{1/1} livers compared to the wt (Figure 4, a,a1-a3,e,f), whereas DNAJC12, although strongly reduced in the *Enu*^{1/1} mice, was clearly detected (Figure 4, b,b1-b3). Furthermore, despite the fact that higher concentrations of Triton X-100 may alter the organelle integrity and protein distribution, the ability of the detergent to solubilize possible complexes that include DNAJC12 and to facilitate its interaction with the anti-DNAJC12 antibody was investigated. As seen in Figure 4c,c1-c3 and d,d1-d3, treatment with a higher concentration (1%) of Triton X-100 did not alter the relative proportions of PAH-like immunoreactivity, but reduced the difference between levels of DNAJC12-like immunoreactivity in the livers of the wt and *Enu*^{1/1} mice.

3.6 | PAH ubiquitination state and co-immunoprecipitation of DNAJC12

We next performed immunoprecipitation assays to study a possible complex formation between PAH and DNAJC12 in mice liver. PAH was

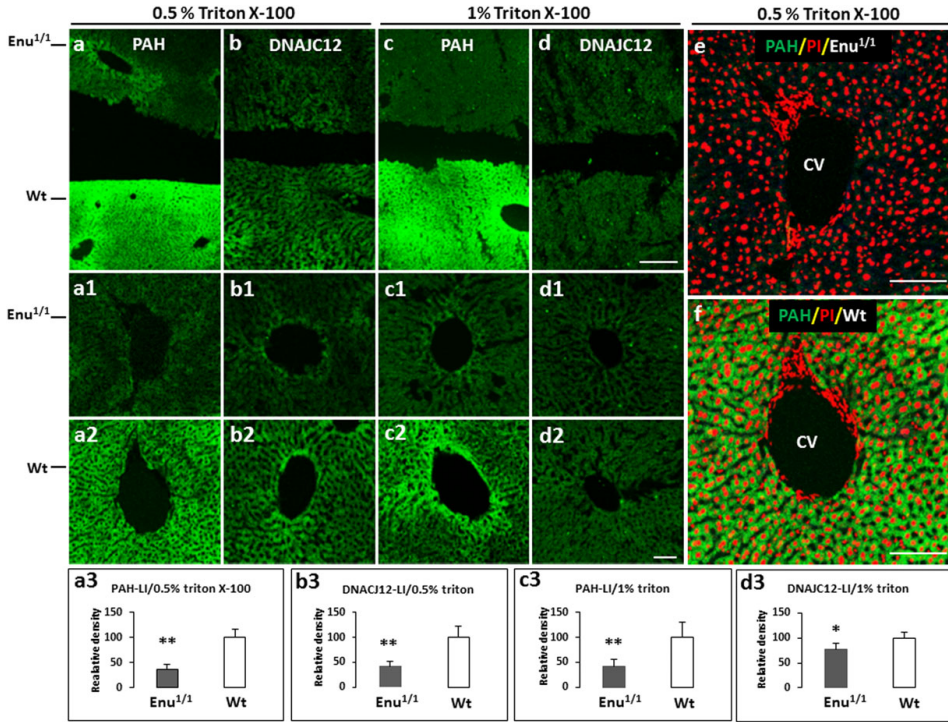


FIGURE 4 Expression of PAH and DNAJC12-like immunoreactivities (LIs) in the liver tissues of Enu^{1/1} and wt mice. Low-magnification (a–d), high-magnification (a1–d1, a2–d2) and high magnification merged images (e, f). PAH-LI (green; a, a1, a2 and c, c1, c2, e, f) and DNAJC12-LI (green; b, b1, b2 and d, d1, d2) are mainly expressed in the cytoplasm of the liver cells. In the samples processed with 0.5% Triton X-100, significant reduction of PAH and DNAJC12-LIs was observed in Enu^{1/1} compared to wt (a3, b3). With a higher concentration of Triton X-100 (1%), the relative levels of PAH-LI were not affected (a3, c3) and the level of DNAJC12 was increased in Enu^{1/1} and reduced in wt, though the difference between both samples was still significant (b3, d3). Hepatocyte nuclei were counterstained with propidium iodide (PI; red; e, f). Lumen like sub-structures are central vein (CV; a1–d1, a2–d2, e, f). Scale bars 250 μ m (a–d) and 75 μ m (a1–d1, a2–d2, e, f)

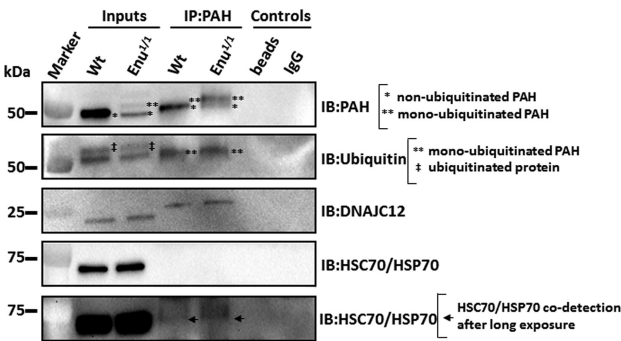


FIGURE 5 Immunoprecipitation (IP) of PAH and co-IP of ubiquitinated proteins, DNAJC12, and HSC70/HSP70 in the livers of the wt and Enu^{1/1} mice. PAH-IP was performed in liver lysates of wt and Enu^{1/1} mice prepared at the improved solubilizing conditions (see main text). Ubiquitinated proteins and DNAJC12 were co-detected by immunoblotting (IB) with the indicated antibodies. HSC70/HSP70 was faintly detected as a co-immunoprecipitant and required longer exposure of the blot for the detection. Lysates incubated with only beads and IgGs were used as controls

immunoprecipitated (IP) from liver lysates of wt and Enu^{1/1} prepared at the improved solubilizing conditions and the samples were examined for PAH, ubiquitination, DNAJC12, and HSC70/HSP70 by Western blot (Figure 5). The IP-PAH in wt liver is mainly non-ubiquitinated, but a monoubiquitinated fraction is also present, whereas in the Enu^{1/1} mice a similar monoubiquitinated fraction was obtained, which for these mice corresponds with the major IP-PAH form (Figure 5). Fur-

thermore, co-IP DNAJC12 was obtained in the IP-PAH samples from both mice livers. It should be noted that the shift in the band pattern of DNAJC12 in the co-IP sample compared with the migration of the endogenous protein in the input (tissue lysate) (Figure 5) is due to the often observed higher apparent molecular weight for the more purified proteins, as is the case in IP samples. On the other hand, HSC70/HSP70 was faintly immunodetected in the IP-PAH samples (Figure 5), which

suggested that HSC70 and/or HSP70, most probably have transient interactions in complexes with both wt and mutant PAH. Furthermore, all attempts to perform IP of DNAJC12 and detect co-IP PAH were unsuccessful due to the inadequacy of the available DNAJC12 antibodies for this procedure (data not shown).

4 | DISCUSSION

The function of the HSP70 family of molecular chaperones requires the binding both of DNAJ/HSP40 co-chaperones that stimulate the ATPase activity and facilitate client capture and of nucleotide exchange factors that promote the dissociation of the ADP and the release of the client protein (Dekker et al., 2015; Kampinga & Craig, 2010). The binding of DNAJ to the HSP70s involves the conserved His-Pro-Asp motif in the J-domain, and this interaction is a requirement for the function of the molecular chaperones. Stimulation of ATP hydrolysis by HSP70s as well as the coordination of client binding for proper folding, refolding, and release, are considered to be the main functions of the DNAJ/HSP40 proteins. However, as more DNAJ proteins are characterized, their varied involvement in many aspects of proteostatic control, in addition to folding, is being revealed, including protection of misfolded clients from aggregation and contribution to the ubiquitination and delivery of terminally misfolded proteins to the ubiquitin-proteasome or autophagy systems for degradation (Kampinga & Craig, 2010; Kraft et al., 2010; Shiber & Ravid, 2014; Zarouchlioti, Parfitt, Li, Gittings, & Cheetham, 2018).

Except for the common J-domain (Hageman & Kampinga, 2009; Kampinga et al., 2009), the large number of DNAJ proteins (50 annotated DNAJ/HSP40 proteins compared with the 11 HSC70/HSP70s as of October 2018) present a highly variable sequence that contributes to the additional role of these proteins. In particular, type III (class C) DNAJ-proteins present very little sequence similarity or domain sharing, which seems to be associated to a high selectivity in client binding. DNAJC12 was earlier classified as a DNAJ protein with client-independent function (Kampinga & Craig, 2010), but its interaction with the AAAHs and its important role in proper folding of PAH has recently been demonstrated (Anikster et al., 2017). Our present results provide additional insights into the DNAJC12 role on PAH folding. By analyzing a number of PAH variants associated with HPA/PKU of different severity, we observed a moderate positive correlation between the immunodetected contents of soluble PAH and DNAJC12. Subsequent immunodetection of PAH and DNAJC12 levels in both wt and *Enu*^{1/1} mice, the latter expressing the unstable and misfolded p.V106A-PAH variant (Gersting et al., 2010), contributed to reveal the mechanisms behind the correlation. Thus, the immunodetected content of both proteins increased in the mutant mice upon application of solubilizing conditions to prepare the liver lysates, strongly indicating a co-aggregation of DNAJC12 both in lysates of COS-7 cells expressing unstable PAH variants and in liver lysates of *Enu*^{1/1} mice. Furthermore, the IP and co-IP experiments with *Enu*^{1/1} mice liver lysates showed an interaction of DNAJC12 with the monoubiquitinated PAH variant, pointing to a major role of the co-chaperone in targeting the degradation of misfolded PAH.

It has been suggested that the proteostatic pathways in disease states differ from those in the normal cellular cycles (Klaips, Jayaraj, & Hartl, 2018). Our results, on the other hand, suggest that— notwithstanding an increased aggregation and accelerated degradation for the PAH mutants (Figures 1 and 2)—the pathways may be similar for both normal and variant PAH, since lysates from wt mice, in addition to their specific major non-ubiquitinated PAH form, also present monoubiquitinated PAH at comparable levels as for the *Enu*^{1/1} mice. Quantification of *Dnajc12*- and *Pah*-mRNA levels (Table 1) supports a much lower expression of DNAJC12 compared with PAH, as also indicated by the relation of protein levels (Figure 4). This lower expression of DNAJC12 may be associated to a regulatory role of the co-chaperone in the folding/degradation of PAH. Together with ubiquitination, DNAJC12 binding may determine the upper value for the degradation-competent fraction of PAH, contributing to regulate the steady-state levels of this enzyme, as also described for DNAJB members interacting with wild-type and mutants of parkin (Kakkar, Kuiper, Pandey, Braakman, & Kampinga, 2016). One can expect a challenged proteostatic regulation in *Enu*^{1/1} liver, biased toward the degradation of ubiquitinated misfolded mutant PAH, which recruits most of the available DNAJC12.

The fact that DNAJC12 was co-immunoprecipitated with monoubiquitinated IP-PAH from the *Enu*^{1/1} liver also provides information on the possible mechanism for the degradation of PAH. The general mechanism for the DNAJ- and HSC70/HSP70-assisted degradation of misfolded client proteins with a tendency to aggregate is believed to be the recognition of the non-ubiquitinated misfolded client by the DNAJ followed by the recruitment of the HSP70 machinery (Dekker et al., 2015; Houck, Singh, & Cyr, 2012). This phase is actually similar to the complex formation for folding or refolding of the clients. However, in the case of misfolding, CHIP or other specific E3-ubiquitin ligases can be recruited to the complex for polyubiquitination and targeting to the proteasome or, if the aggregation is severe, to the autophagy system (Dekker et al., 2015; Houck et al., 2012; Kampinga & Craig, 2010; Shiber & Ravid, 2014). Nevertheless, there is also evidence that DNAJ proteins can recognize and bind clients that are already mono- or polyubiquitinated, or that may be ubiquitinated while bound to the co-chaperone, previous to complex formation with the HSP70 machinery for further polyubiquitination (Dekker et al., 2015; Kampinga & Craig, 2010; Shiber, Breuer, Brandeis, & Ravid, 2013). In particular, if the client tends to aggregate, it is expected that the DNAJ:ubiquitinated-client complexes are more stable. On the other hand, the dynamic complexes that engage HSP70 present a quick dissociation of the HSPs and release the client toward degradation as fast as the ATP is hydrolyzed (Misselwitz, Staeck, Matlack, & Rapoport, 1999). Thus, these complexes including DNAJ:client:HSP70 are very transient, unstable, and difficult to isolate and characterize (Alderson, Kim, & Markley, 2016; Malinverni, Jost Lopez, De Los Rios, Hummer, & Barducci, 2017), probably explaining that in our IP experiments we mainly isolated the stable DNAJC12:monoubiquitinated PAH complexes, whereas HSP70 is only present in a minor proportion in the immunoprecipitated sample (Figure 5).

The direct interaction of DNAJ proteins with ubiquitinated clients has been studied for DNAJB2 (alternatively known as HSJ1),

which has an important role determining the fate of the clients prior to the interaction with HSP70 and sorting to the proteasome (Kampinga & Craig, 2010; Westhoff, Chapple, van der Spuy, Hohfeld, & Cheetham, 2005). The selectivity of DNAJB2 toward mono- and polyubiquitinated clients is provided by its ubiquitin interacting motifs (UIMs). DNAJC12 does not have a canonical UIM, and it is therefore not possible to speculate if it has an inherent higher affinity for ubiquitinated-PAH than for non-ubiquitinated-PAH. DNAJC12 is actually one of the shortest DNAJ proteins and does not contain identifiable domains other than the J-domain (Kampinga & Craig, 2010). Further structural and biophysical studies on the interaction between DNAJC12 and PAH and the other AAAHs are required to increase our understanding on the selectivity and the mechanisms for folding and degradation of these clients, both in health and in AAAH-associated diseases (Blau et al., 2018; Bouchereau et al., 2018; Straniero et al., 2017).

Knowledge on the proteostatic pathways and the chaperone networks that regulate the intracellular stability of PAH appears to be essential to understand how the system is affected by PKU-associated mutations and other factors. Because PKU is known to be a complex trait disease (Scriver & Waters, 1999), it is expected that mutations and polymorphisms in genes that control the intracellular stability of PAH, such as DNAJC12, may contribute to understanding the deviations from the general genotype-phenotype correlations in PKU. Not much is yet known about the interactions of DNAJC12 with the proteasome and autophagy systems, and such knowledge may promote the research on novel therapies for disorders associated to the AAAHs. Nevertheless, previous attempts to regulate HSP40 and HSP70 levels pharmacologically have not been very successful and have shown the complexity of the proteostatic regulation in health and disease, as well as particular differences for each disease (Labbadia & Morimoto, 2015). Specifically, whereas DNAJC12 has been shown to be upregulated by endoplasmic reticulum stress (Choi et al., 2014), which is known to induce protein misfolding and aggregation, this upregulation has not been observed for cellular stress in general (Vleminckx et al., 2002). In this work, we did not observe upregulation of either *Dnajc12* or *Hspa1b* expression (Table 1), which may indicate a mild stress effect caused by the *enu1* allele.

In conclusion, the present work showed the tight interaction of DNAJC12 with ubiquitinated, mutant PAH, which indicated the involvement of DNAJC12 in the degradation of PAH. Based on the myriad of different mechanisms by which the DNAJ-proteins can regulate the ubiquitination and degradation of proteins by the proteasome and/or autophagy, further studies are necessary to demonstrate the detailed mechanisms and interactions between DNAJC12 and the AAAHs clients at the molecular level. The work also reveals the complex quality control system implicated in the intracellular stability of PAH and contributes to the understanding of this disease as a complex trait disease.

ACKNOWLEDGMENTS

This work was supported by Research Council of Norway grants FRIMEDBIO 261826/F20 and FORNY 248889/O30, the K.G. Jeb-

sen Centre for Neuropsychiatric Disorders, and the Western Norway Regional Health Authorities (Helse-Vest project 912246) (to A.M.), and by the FP7-HEALTH-2012-INNOVATION-1 EU Grant No. 305444 (to N.B.).

CONFLICTS OF INTEREST

The authors have no conflict of interest to declare.

ORCID

Nejad Blau  <https://orcid.org/0000-0003-4347-3230>

Aurora Martinez  <https://orcid.org/0000-0003-1643-6506>

REFERENCES

- Alderson, T. R., Kim, J. H., & Markley, J. L. (2016). Dynamical structures of Hsp70 and Hsp70-Hsp40 complexes. *Structure (London, England)*, 24(7), 1014–1030.
- Anikster, Y., Haack, T. B., Vilboux, T., Pode-Shakked, B., Thony, B., Shen, N., ... Schiff, M. (2017). Biallelic mutations in DNAJC12 cause hyperphenylalaninemia, dystonia, and intellectual disability. *American Journal of Human Genetics*, 100(2), 257–266.
- Björge, E., Knappskog, P. M., Martínez, A., Stevens, R. C., & Flatmark, T. (1998). Partial characterization and three-dimensional-structural localization of eight mutations in exon 7 of the human phenylalanine hydroxylase gene associated with phenylketonuria. *European Journal of Biochemistry*, 257(1), 1–10.
- Blau, N., Martínez, A., Hoffmann, G. F., & Thony, B. (2018). DNAJC12 deficiency: A new strategy in the diagnosis of hyperphenylalaninemia. *Molecular Genetics and Metabolism*, 123(1), 1–5.
- Bouchereau, J., Huttlin, E. L., Guarani, V., Pichard, S., Anikster, Y., & Schiff, M. (2018). DNAJC12: A molecular chaperone involved in proteostasis, PKU, biogenic amines metabolism and beyond? *Molecular Genetics and Metabolism*, 123(3), 285–286.
- Choi, J., Djebbar, S., Fournier, A., & Labrie, C. (2014). The co-chaperone DNAJC12 binds to Hsc70 and is upregulated by endoplasmic reticulum stress. *Cell Stress & Chaperones*, 19(3), 439–446.
- De Bessa, S. A., Salaorni, S., Patrao, D. F., Neto, M. M., Brentani, M. M., & Nagai, M. A. (2006). JDP1 (DNAJC12/Hsp40) expression in breast cancer and its association with estrogen receptor status. *International Journal of Molecular Medicine*, 17(2), 363–367.
- Dekker, S. L., Kampinga, H. H., & Bergink, S. (2015). DNAJs: More than substrate delivery to HSPA. *Frontiers in Molecular Biosciences*, 2, 35.
- Doskeland, A. P., & Flatmark, T. (1996). Recombinant human phenylalanine hydroxylase is a substrate for the ubiquitin-conjugating enzyme system. *Biochemical Journal*, 319(Pt 3), 941–945.
- Eichinger, A., Danecka, M. K., Moglich, T., Borsch, J., Woidy, M., Buttner, L., ... Gersting, S. W. (2018). Secondary BH4 deficiency links protein homeostasis to regulation of phenylalanine metabolism. *Human Molecular Genetics*, 27(10), 1732–1742.
- Fernandez-Fernandez, M. R., Gragera, M., Ochoa-Ibarrola, L., Quintana-Gallardo, L., & Valpuesta, J. M. (2017). Hsp70: A master regulator in protein degradation. *FEBS Letters*, 591(17), 2648–2660.
- Fitzpatrick, P. F. (2015). Structural insights into the regulation of aromatic amino acid hydroxylation. *Current Opinion in Structural Biology*, 35, 1–6.
- Gersting, S. W., Lagler, F. B., Eichinger, A., Kemter, K. F., Danecka, M. K., Messing, D. D., ... Muntau, A. C. (2010). Pahenu1 is a mouse model for tetrahydrobiopterin-responsive phenylalanine hydroxylase deficiency

- and promotes analysis of the pharmacological chaperone mechanism in vivo. *Human Molecular Genetics*, 19(10), 2039–2049.
- Gregersen, N. (2006). Protein misfolding disorders: Pathogenesis and intervention. *Journal of Inherited Metabolic Disease*, 29(2–3), 456–470.
- Hageman, J., & Kampinga, H. H. (2009). Computational analysis of the human HSPH/HSPA/DNAJ family and cloning of a human HSPH/HSPA/DNAJ expression library. *Cell Stress & Chaperones*, 14(1), 1–21.
- Himmelreich, N., Shen, N., Okun, J. G., Thiel, C., Hoffmann, G. F., & Blau, N. (2018). Relationship between genotype, phenylalanine hydroxylase expression and in vitro activity and metabolic phenotype in phenylketonuria. *Molecular Genetics and Metabolism*, 125(1–2), 86–95. <https://doi.org/10.1016/j.jmgme.2018.06.011>
- Houck, S. A., Singh, S., & Cyr, D. M. (2012). Cellular responses to misfolded proteins and protein aggregates. *Methods in Molecular Biology*, 832, 455–461.
- Huttlin, E. L., Ting, L., Bruckner, R. J., Gebreab, F., Gygi, M. P., Szpyt, J., ... Gygi, S. P. (2015). The BioPlex network: A systematic exploration of the human interactome. *Cell*, 162(2), 425–440.
- Juenemann, K., Wiemhoefer, A., & Reits, E. A. (2015). Detection of ubiquitinated huntingtin species in intracellular aggregates. *Frontiers in Molecular Neuroscience*, 8, 1.
- Kakkar, V., Kuiper, E. F. E., Pandey, A., Braakman, I., & Kampinga, H. H. (2016). Versatile members of the DNAJ family show Hsp70 dependent anti-aggregation activity on RING1 mutant parkin C289G. *Scientific Reports*, 6, 34830.
- Kampinga, H. H., & Craig, E. A. (2010). The HSP70 chaperone machinery: J proteins as drivers of functional specificity. *Nature Reviews Molecular Cell Biology*, 11(8), 579–592.
- Kampinga, H. H., Hageman, J., Vos, M. J., Kubota, H., Tanguay, R. M., Bruford, E. A., ... Hightower, L. E. (2009). Guidelines for the nomenclature of the human heat shock proteins. *Cell Stress & Chaperones*, 14(1), 105–111.
- Kaushik, S., & Cuervo, A. M. (2012). Chaperones in autophagy. *Pharmacological Research*, 66(6), 484–493.
- Klaips, C. L., Jayaraj, G. G., & Hartl, F. U. (2018). Pathways of cellular proteostasis in aging and disease. *Journal of Cell Biology*, 217(1), 51–63.
- Kraft, C., Peter, M., & Hofmann, K. (2010). Selective autophagy: Ubiquitin-mediated recognition and beyond. *Nature Cell Biology*, 12(9), 836–841.
- Labbadia, J., & Morimoto, R. I. (2015). The biology of proteostasis in aging and disease. *Annual Review of Biochemistry*, 84, 435–464.
- Leandro, J., Simonsen, N., Saraste, J., Leandro, P., & Flatmark, T. (2011). Phenylketonuria as a protein misfolding disease: The mutation pG465 in phenylalanine hydroxylase promotes self-association and fibril formation. *Biochimica Et Biophysica Acta*, 1812(1), 106–120.
- Malinverni, D., Jost Lopez, A., De Los Rios, P., Hummer, G., & Barducci, A. (2017). Modeling Hsp70/Hsp40 interaction by multi-scale molecular simulations and coevolutionary sequence analysis. *Elife*, 6, pii: e23471; <https://doi.org/10.7554/eLife.23471>
- McDonald, J. D., & Charlton, C. K. (1997). Characterization of mutations at the mouse phenylalanine hydroxylase locus. *Genomics*, 39(3), 402–405.
- Misselwitz, B., Staack, O., Matlack, K. E., & Rapoport, T. A. (1999). Interaction of BiP with the J-domain of the Sec63p component of the endoplasmic reticulum protein translocation complex. *Journal of Biological Chemistry*, 274(29), 20110–20115.
- Miyamoto-Sato, E., Fujimori, S., Ishizaka, M., Hirai, N., Masuoka, K., Saito, R., ... Yanagawa, H. (2010). A comprehensive resource of interacting protein regions for refining human transcription factor networks. *Plos One*, 5(2), e9289.
- Okano, Y., Kudo, S., Nishi, Y., Sakaguchi, T., & Aso, K. (2011). Molecular characterization of phenylketonuria and tetrahydrobiopterin-responsive phenylalanine hydroxylase deficiency in Japan. *Journal of Human Genetics*, 56(4), 306–312.
- Pey, A. L., Desviat, L. R., Gamez, A., Ugarte, M., & Perez, B. (2003). Phenylketonuria: Genotype-phenotype correlations based on expression analysis of structural and functional mutations in PAH. *Human Mutation*, 21(4), 370–378.
- Pey, A. L., Stricher, F., Serrano, L., & Martinez, A. (2007). Predicted effects of missense mutations on native-state stability account for phenotypic outcome in phenylketonuria, a paradigm of misfolding diseases. *American Journal of Human Genetics*, 81(5), 1006–1024.
- Pratt, W. B., Morishima, Y., Peng, H. M., & Osawa, Y. (2010). Proposal for a role of the Hsp90/Hsp70-based chaperone machinery in making triage decisions when proteins undergo oxidative and toxic damage. *Experimental Biology and Medicine (Maywood, NJ)*, 235(3), 278–289.
- Sarkissian, C. N., Boulais, D. M., McDonald, J. D., & Scriver, C. R. (2000). A heteroallelic mutant mouse model: A new orthologue for human hyperphenylalaninemia. *Molecular Genetics and Metabolism*, 69(3), 188–194.
- Sarkissian, C. N., Ying, M., Scherer, T., Thony, B., & Martinez, A. (2012). The mechanism of BH4-responsive hyperphenylalaninemia—as it occurs in the ENU1/2 genetic mouse model. *Human Mutation*, 33(10), 1464–1473.
- Scherer, T., Allegri, G., Sarkissian, C. N., Ying, M., Grisch-Chan, H. M., Rassi, A., ... Thony, B. (2018). Tetrahydrobiopterin treatment reduces brain L-Phe but only partially improves serotonin in hyperphenylalaninemic ENU1/2 mice. *Journal of Inherited Metabolic Disease*, 41(4), 709–718.
- Scriver, C. R., & Waters, P. J. (1999). Monogenic traits are not simple: Lessons from phenylketonuria. *Trends in Genetics*, 15(7), 267–272.
- Shen, N., Heintz, C., Thiel, C., Okun, J. G., Hoffmann, G. F., & Blau, N. (2016). Co-expression of phenylalanine hydroxylase variants and effects of interallelic complementation on in vitro enzyme activity and genotype-phenotype correlation. *Molecular Genetics and Metabolism*, 117(3), 328–335.
- Shiber, A., Breuer, W., Brandeis, M., & Ravid, T. (2013). Ubiquitin conjugation triggers misfolded protein sequestration into quality control foci when Hsp70 chaperone levels are limiting. *Molecular Biology of the Cell*, 24(13), 2076–2087.
- Shiber, A., & Ravid, T. (2014). Chaperoning proteins for destruction: Diverse roles of Hsp70 chaperones and their co-chaperones in targeting misfolded proteins to the proteasome. *Biomolecules*, 4(3), 704–724.
- Skjærven, L., Teigen, K., & Martinez, A. (2014). *Structure-function relationships in the aromatic amino acid hydroxylases enzyme family: Evolutionary insights*. eLS. Chichester, United Kingdom: John Wiley & Sons.
- Straniero, L., Guella, I., Cilia, R., Parkkinen, L., Rimoldi, V., Young, A., ... Duga, S. (2017). DNAJC12 and dopa-responsive nonprogressive parkinsonism. *Annals of Neurology*, 82(4), 640–646.
- van Spronsen, F. J., Himmelreich, N., Rufenacht, V., Shen, N., Vliet, D. V., Al-Owain, M., ... Thöny, B. (2017). Heterogeneous clinical spectrum of DNAJC12-deficient hyperphenylalaninemia: From attention deficit to severe dystonia and intellectual disability. *Journal of Medical Genetics*, pii: jmedgenet-2017-104875; <https://doi.org/10.1136/jmedgenet-2017-104875>
- Veenna, D., Cordeiro, D., Sondheimer, N., & Mercimek-Andrews, S. (2018). DNAJC12-associated developmental delay, movement disorder, and mild hyperphenylalaninemia identified by whole-exome sequencing re-analysis. *European Journal of Human Genetics*, 26, 1867–1870.
- Vlemminckx, V., Van Damme, P., Goffin, K., Delye, H., Van Den Bosch, L., & Robberecht, W. (2002). Upregulation of HSP27 in a transgenic model of ALS. *Journal of Neuro pathology and Experimental Neurology*, 61(11), 968–974.

- Waløen, K., Kleppe, R., Martinez, A., & Haavik, J. (2017). Tyrosine and tryptophan hydroxylases as therapeutic targets in human disease. *Expert Opinion on Therapeutic Targets*, 21(2), 167–180.
- Waters, P. J., Parniak, M. A., Akerman, B. R., & Scriver, C. R. (2000). Characterization of phenylketonuria missense substitutions, distant from the phenylalanine hydroxylase active site, illustrates a paradigm for mechanism and potential modulation of phenotype. *Molecular Genetics and Metabolism*, 69(2), 101–110.
- Westhoff, B., Chapple, J. P., van der Spuy, J., Hohfeld, J., & Cheetham, M. E. (2005). HSF1 is a neuronal shuttling factor for the sorting of chaperone clients to the proteasome. *Current Biology*, 15(11), 1058–1064.
- Wettstein, S., Underhaug, J., Perez, B., Marsden, B. D., Yue, W. W., Martinez, A., & Blau, N. (2015). Linking genotypes database with locus-specific database and genotype-phenotype correlation in phenylketonuria. *European Journal of Human Genetics*, 23(3), 302–309.
- Zarouchlioti, C., Parfitt, D. A., Li, W., Gittings, L. M., & Cheetham, M. E. (2018). DNAJ proteins in neurodegeneration: Essential and protective factors. *Philosophical Transactions of the Royal Society of London. Series B: Biological Sciences*, 373(1738).






SUPPORTING INFORMATION

Additional supporting information may be found online in the Supporting Information section at the end of the article.

How to cite this article: Jung-KC K, Himmelreich N, Prestegård KS, et al. Phenylalanine hydroxylase variants interact with the co-chaperone DNAJC12. *Human Mutation*. 2019; 1–12. <https://doi.org/10.1002/humu.23712>

II

The *Pah-R261Q* mouse reveals oxidative stress associated with amyloid-like hepatic aggregation of mutant phenylalanine hydroxylase

Oscar Aubi ^{1,4}, Karina S. Prestegård ^{1,4}, Kunwar Jung-KC ¹, Tie-Jun Sten Shi¹, Ming Ying¹, Ann Kari Grindheim¹, Tanja Scherer², Arve Ulvik³, Adrian McCann³, Endy Spriet¹, Beat Thöny ² & Aurora Martinez ¹✉

Phenylketonuria (PKU) is caused by autosomal recessive variants in phenylalanine hydroxylase (PAH), leading to systemic accumulation of L-phenylalanine (L-Phe) that may reach neurotoxic levels. A homozygous *Pah-R261Q* mouse, with a highly prevalent misfolding variant in humans, reveals the expected hepatic PAH activity decrease, systemic L-Phe increase, L-tyrosine and L-tryptophan decrease, and tetrahydrobiopterin-responsive hyperphenylalaninemia. *Pah-R261Q* mice also present unexpected traits, including altered lipid metabolism, reduction of liver tetrahydrobiopterin content, and a metabolic profile indicative of oxidative stress. *Pah-R261Q* hepatic tissue exhibits large ubiquitin-positive, amyloid-like oligomeric aggregates of mutant PAH that colocalize with selective autophagy markers. Together, these findings reveal that PKU, customarily considered a loss-of-function disorder, can also have toxic gain-of-function contribution from protein misfolding and aggregation. The proteostasis defect and concomitant oxidative stress may explain the prevalence of comorbid conditions in adult PKU patients, placing this mouse model in an advantageous position for the discovery of mutation-specific biomarkers and therapies.

¹Department of Biomedicine, University of Bergen, Bergen, Norway. ²Division of Metabolism, University Children's Hospital Zürich and Children's Research Centre, Zürich, Switzerland. ³Bevital AS, Laboratoriebygget, Bergen, Norway. ⁴These authors contributed equally: Oscar Aubi, Karina S. Prestegård ✉email: aurora.martinez@uib.no

Phenylketonuria (PKU; MIM261600) is an autosomal recessive inborn error of metabolism characterized by the inability to break down the amino acid L-phenylalanine (L-Phe). PKU is primarily caused by mutations in the human *PAH* gene (NM_000277.2) encoding phenylalanine hydroxylase (PAH; EC 1.14.16.1). PAH is a tetrameric, non-heme iron aromatic amino acid hydroxylase that catalyzes the hydroxylation of L-Phe to L-tyrosine (L-Tyr) using molecular oxygen as additional substrate and the cofactor (6R)-5,6,7,8-tetrahydrobiopterin (BH₄)^{1,2}. This is the rate-limiting step in the catabolic degradation of L-Phe, which occurs predominantly in the cytoplasm of hepatic cells. A consequence of deficient PAH catalysis is the accumulation of L-Phe in the blood and ultimately in the brain of untreated patients, causing growth retardation, intellectual disability, and behavioral and neuropsychiatric disorders³. PKU has a prevalence of approximately 1:10,000 livebirths worldwide and can be classified, based on the off-diet blood L-Phe concentrations, as mild hyperphenylalaninemia (HPA) (120–600 μmol/L), mild PKU (600–1200 μmol/L), and classic PKU (>1200 μmol/L)³. The low-Phe diet is the cornerstone of PKU/HPA management and prevents the most severe consequences of the disease. However, controlled studies have shown that early treated PKU patients present several psychiatric disturbances as adults, notably depression and anxiety-related disorders⁴. Moreover, recent investigations have revealed an elevated risk of comorbidities with unexplained etiology in both early- and late-treated adult PKU patients, with a high prevalence of cardiovascular and renal diseases and overweight^{5,6}. In the last years, many new treatments for PKU have been approved or are in clinical development⁷. A fraction of patients typically with mild and moderate *PAH* mutations are responsive to synthetic formulations of BH₄ (Sapropterin, Kuvan®), which is often used in combination with a less restrictive diet⁸. Notwithstanding the considerable amount of accumulated knowledge on PKU, there is a need for a more profound mechanistic and pathophysiological understanding of the disease, as well as novel therapies. These required studies would greatly benefit from the availability of useful model organisms.

Mouse (*Mus musculus*) models are a powerful research tool owing to the small size, high reproductive rate, and relative ease of genetic manipulation, compared to other mammals, and are therefore most commonly selected to study human disease⁹. There are evident differences between mice and humans, primarily related to evolutionary divergences, for instance in size, metabolic rate, life expectancy, and immune system, but overall, the genetic and physiological similarities are high⁹. The first generation of mouse models of PKU were created by phenotype-driven N-ethyl-N-nitrosourea (*ENU*) germline mutagenesis. In this manner, three HPA/PKU mouse models have previously been established; namely, (i) *Enu1* (*enu*¹ allele), with the p.V106A-PAH mutation, located in the PAH regulatory domain¹⁰; (ii) *Enu2* (*enu*² allele), with the p.F263S-PAH mutation, located in the catalytic domain¹⁰; and (iii) *Enu3* (*enu*³ allele), with a splice site mutation generating frameshifted amino acids and premature termination codon¹¹. *Enu2* and *Enu3* mice exhibit high blood L-Phe concentrations (>1200 μmol/L) and appear as suitable models for severe, classic PKU, with a total absence of PAH activity albeit normal protein stability (*Enu2*), or total absence of expressed PAH protein and activity (*Enu3*)¹¹. In contrast, *Enu1* mice present reduced PAH stability and thus decreased steady-state levels of PAH protein and enzymatic activity (approximately 5% of normal controls), leading to mild HPA¹². The available mouse models have undoubtedly contributed to a better understanding of PKU at a biochemical and behavioral level and have allowed testing of novel therapies such as enzyme substitution¹³ or genome base editing¹⁴. An increasing body of evidence

indicates that PKU is a prototypic genetic conformational disorder wherein the principal pathogenic determinant is the degree of PAH protein instability caused by the specific mutations¹⁵. The available strains do not adequately represent this primary pathogenic mechanism (*Enu2* and *Enu3*) or include murine mutations that are non-existent or low recurrent in the human *PAH* gene (*Enu1*), prompting us to generate a PKU mouse model with a common *PAH* mutant associated with protein misfolding.

There are over 1100 registered human PAH variants (<http://www.biopku.org/>), among which the nucleotide aberration c.782 G > A in *Pah* exon 7 coding for p.Arg261Gln (p.R261Q) mutation seems to be an optimal candidate to generate a knock-in mouse model. The *R261Q* mutation is one of the most abundant among PKU patients, with an average allele frequency of approx. 6% (9–14% in Mediterranean countries and the Middle East) and ~2% of patients homozygous for this mutation (up to 12% in Mediterranean countries and the Middle East)^{15,16} (<http://www.biopku.org/>). The associated phenotype when in homozygosity, exhibits an unusual and unexplained variability from mild PKU to classic PKU, with approximately 78% of the patients being responsive to BH₄^{15–17} (<http://www.biopku.org/>). The *R261Q* mutation has been predicted¹⁵ and indeed proven to result in unstable and misfolded PAH^{18,19}.

Hence, in the reported custom-made mouse model, the mutation c.782G > A was introduced in the *Pah* gene by CRISPR/Cas9 technology based on the use of programmable nucleases as a tool for targeted gene-editing, which is an efficacious and precise genome engineering method²⁰. In this work, we present the generation and metabolic, biochemical and biological characterization of this *Pah-R261Q* knock-in mouse line. The results obtained highlight (i) the robustness of this mouse model as a general archetype for mild HPA associated with PAH instability and misfolding, and (ii) the observation of large amyloid-like aggregates of mutant (p.R261Q-PAH) *in vivo*, which appears associated to the observed proteostasis dysregulation, oxidative stress and additional comorbidities. Overall, the *Pah-R261Q* mouse model paves the way for new exploratory avenues of research and treatment.

Results

Generation, genotyping, and breeding of *Pah-R261Q* mice.

There is a high PAH sequence homology (92.5% identity) between mouse and human PAHs, with Arg261 being in an evolutionarily conserved region (Supplementary Fig. 1a). Structurally, the residue Arg261 establishes several intra- and inter-subunit H-bonding and electrostatic contacts in the dimers that are crucial to maintaining the stability of the protein as well as proper oligomeric configuration^{21,22} (detailed in Supplementary Fig. 1b, c). The mutation p.R261Q is thus expected to trigger disruption of this interaction network and, as seen in expression analyses in different systems, elicit an unstable protein^{18,19,23} without substantially affecting the catalytic efficiency of the folded tetramer¹⁹.

The custom-made mouse model with the p.R261Q-PAH mutation was generated by CRISPR/Cas9 genome editing technology, as schematically represented in Supplementary Fig. 2a, and proven to have the correct genotype (Supplementary Fig. 2b, c). The designed primers for genotyping amplified a 537 bp polymerase chain reaction (PCR) product, which, after restriction fragment analysis with endonuclease BsmI, made it possible to discriminate electrophoretically between *Pah*^{WT/WT} (2 fragments: 294 and 243 bp), homozygous *Pah*^{R261Q/R261Q} (3 fragments: 243, 171, and 123 bp), and heterozygous *Pah*^{R261Q/WT} (4 fragments: 294, 243, 171, and 123 bp) mice (Supplementary Fig. 2c). There is evidence that BLAST hits with three or more total nucleotide mismatches have a low probability of off-target effects, specifically if two of these mismatches are situated in the

seed region²⁴. In any case, we evaluated all 16 candidate loci susceptible to being secondarily affected by the guide RNA sequence (Supplementary Table 1). These genes were subjected to heteroduplex analysis, all showing wild-type sequence, with no detection of off-target interactions.

A retrospective examination of the maternal genotype effect in the breeding revealed no abnormalities between homozygous *Pah^{R261Q/R261Q}* mice (referred to as *Pah-R261Q*) and *Pah^{WT/WT}* (*WT*) mice with respect to litters per mated female (3.7 ± 0.6 vs. 4.0) and progeny per litter (7.1 ± 0.4 vs. 7.0)²⁵. Furthermore, the compilation of historical data confirmed the expected offspring genotypic distribution as predicted by Mendelian laws.

***Pah-R261Q* mice exhibit mild HPA, higher body weight in the case of males, and reduced respiratory exchange ratio.** *Pah-R261Q* mice presented a small but significant increase in basal blood L-Phe levels, measured in dried blood spots in 3-month old mice ($108.0 \pm 36.6 \mu\text{M}$, $n = 23$ mice) compared to both *WT* ($59.9 \pm 7.7 \mu\text{M}$, $n = 9$; $p < 0.0001$) and heterozygous *Pah^{R261Q/WT}* ($71.22 \pm 21.86 \mu\text{M}$; $n = 6$; $p = 0.0201$), analyzed by Brown–Forsythe and Welch ANOVA test followed by Dunnett’s multiple comparisons tests. Source data are provided as a Source Data file. The blood L-Phe level in *Pah-R261Q* corresponds to very mild HPA in human subjects. In contrast to the *Enu2* PKU mouse model, which presents weight and length reduction, hypopigmentation, behavioral, and neurological problems²⁶, *Pah-R261Q* were no different from their heterozygote and *WT* counterparts in length, pigmentation, and behavior. Three-month-old male *Pah-R261Q* mice, however, were weightier than their *WT* counterparts (27.8 ± 0.4 vs. 25.1 ± 0.3 g, respectively) (Fig. 1a). *Pah-R261Q* females were as expected lighter than males and were not different in weight than their *WT* counterparts (22.1 ± 1.6 vs. 21.1 ± 1.4 g, respectively). Apart from the higher body weight in mutant males, we did not find gender-associated variations for any other parameter or metabolite measured in this work; thus, the mice groups for each experiment included evenly distributed males and females.

Various physiological murine parameters were controlled for the 48 h metabolic cage examinations for *WT* and *Pah-R261Q* (12 h acclimatization and 36 h of measured observations). The amount of food intake was equal (Fig. 1b), and no significant changes in activity and movement patterns were identified (Fig. 1c). However, the rates of O₂ consumption and CO₂ production normalized to body mass (VO₂ and VCO₂, respectively) were both decreased for *Pah-R261Q* compared with *WT* (Fig. 1d and Supplementary Fig. 3a, b), and the calculated respiratory exchange ratio ($\text{RER} = \text{VCO}_2/\text{VO}_2$) was also slightly lower for *Pah-R261Q* than for *WT* (0.988 ± 0.087 vs. 1.014 ± 0.093 ; the average for the total 36 h experimentation) (Fig. 1e, inset). RER values are approximately 1.0, 0.8, and 0.7 for carbohydrates, proteins, and fat, respectively, as sole metabolic fuel²⁷. Nevertheless, in heavy activity periods RER increases and reaches values >1.28 , and RER values reflect metabolic fuel utilization more accurately during periods of rest or mild exercise²⁹. During the 12 h resting period, RER was closer to 0.8 for *Pah-R261Q* and 1 for *WT* mice (Fig. 1e), indicating a higher utilization of fat and protein as a fuel source during this period among the mutant mice³⁰. The decreased RER at rest also contributed to lower energy expenditure in the same period compared with *WT* mice, even for non-weight-normalized values (Fig. 1f), although this difference did not translate into significantly lower energy expenditure for the mutant mice per day.

Metabolic characterization of *Pah-R261Q* mice show lipid metabolism alterations and oxidative stress. Detailed metabolic profiling of *Pah-R261Q* compared with *WT* mice was performed

by measuring 72 relevant metabolic biomarkers in extracted blood serum samples from the results obtained are presented in Supplementary Table 2. Table 1 summarizes the individual values for the 17 metabolites displaying differences at $p < 0.1$ level, with either higher or lower blood serum concentrations for *Pah-R261Q* compared to *WT*. This p value was selected to avoid type II error due to the limited sample size.

A blood serum L-Phe concentration in the mutant mice corresponding to very mild HPA ($113 \pm 22 \mu\text{M}$ vs. $71.9 \pm 10.3 \mu\text{M}$ for *WT*) was obtained in this study, similar to the values obtained from dried blood spots (see above). As seen in Table 1, the increased serum L-Phe was accompanied by decreased levels of L-Trp and L-Tyr, markers of the HPA phenotype, as well as decreased quinolinic acid and a trend for reduced kynurenine, both downstream metabolites of L-Trp. Interestingly, serum trimethyllysine, leucine, and isoleucine, which have been shown to increase in adiposity and altered lipid metabolism in humans³¹, were elevated in *Pah-R261Q* (Table 1). Moreover, increased β -hydroxybutyrate is also an established biomarker associated with impaired glucose homeostasis, diabetes, and defense against oxidative stress^{32,33}. Also, other serum metabolites observed in lower concentrations in *Pah-R261Q* have previously been linked to oxidative stress and immune function, such as α -ketoglutaric acid, glutamic acid, and quinolinic acid^{34–37}. These biomarkers are tightly associated metabolically to creatine and methylmalonic acid, and to the amino acids aspartic acid, alanine, glutamine, and proline, all with decreased trends (Table 1).

The incorporation of these metabolites to the Krebs cycle—a central hub of metabolism—through anaplerotic reactions is increased in situations of oxidative and cellular stress³⁸. Furthermore, the reduction in anaplerotic metabolites and increase in β -oxidation in *Pah-R261Q* are in agreement with increased utilization of proteins and fats as an energy source, as also inferred by the lower resting-state RER in these mice compared to *WT* (Fig. 1e). We acknowledge that the use of a high, explorative p value cutoff ($p < 0.1$) may have generated spurious hits among the metabolite biomarkers. However, we believe that the approach is justified by the overall coherence of the findings that support lipidic metabolic alterations and oxidative stress in the *Pah-R261Q* mice, in addition to the expected mild HPA.

***Pah-R261Q* mice show no apparent neurological alteration but a remarkable decrease of hepatic BH₄.** The elapsed time for a mouse to maintain its balance on a rotating rod is a good indicator of possible neurological deficits, as shown for the *Enu2* mouse³⁹. As illustrated in Supplementary Fig. 3c, *Pah-R261Q* had comparable performance to *WT* on the rotarod test, supporting that the *PAH* mutation has no impact in neuromuscular function or motor coordination, at least for young mice. We also corroborated no alterations in the levels of aromatic amino acids L-Phe, L-Tyr, and L-Trp (Supplementary Table 3) and monoamine neurotransmitters (Fig. 2a) in the brain. In addition, as seen in Fig. 2, we confirmed no significant difference in the total levels of BH₄ in the brain, where BH₄ acts as a cofactor of the other aromatic amino acid hydroxylases tyrosine hydroxylase (TH) and tryptophan hydroxylase 2 (TPH2) and of neuronal nitric oxide synthase (NOS)². However, the concentration of BH₄ in the liver, where it acts as the essential cofactor for the hydroxylating PAH reaction, showed a startling 50% reduction in *Pah-R261Q* (28.0 ± 1.7 pmol BH₄/mg protein) compared with *WT* mice (56.2 ± 3.2 pmol/mg) (Fig. 2b).

***Pah-R261Q* mice are sensitive to L-Phe challenge concomitant with BH₄ responsive hyperphenylalaninemia.** When we administered *Pah-R261Q* mice an L-Phe challenge—equivalent to the

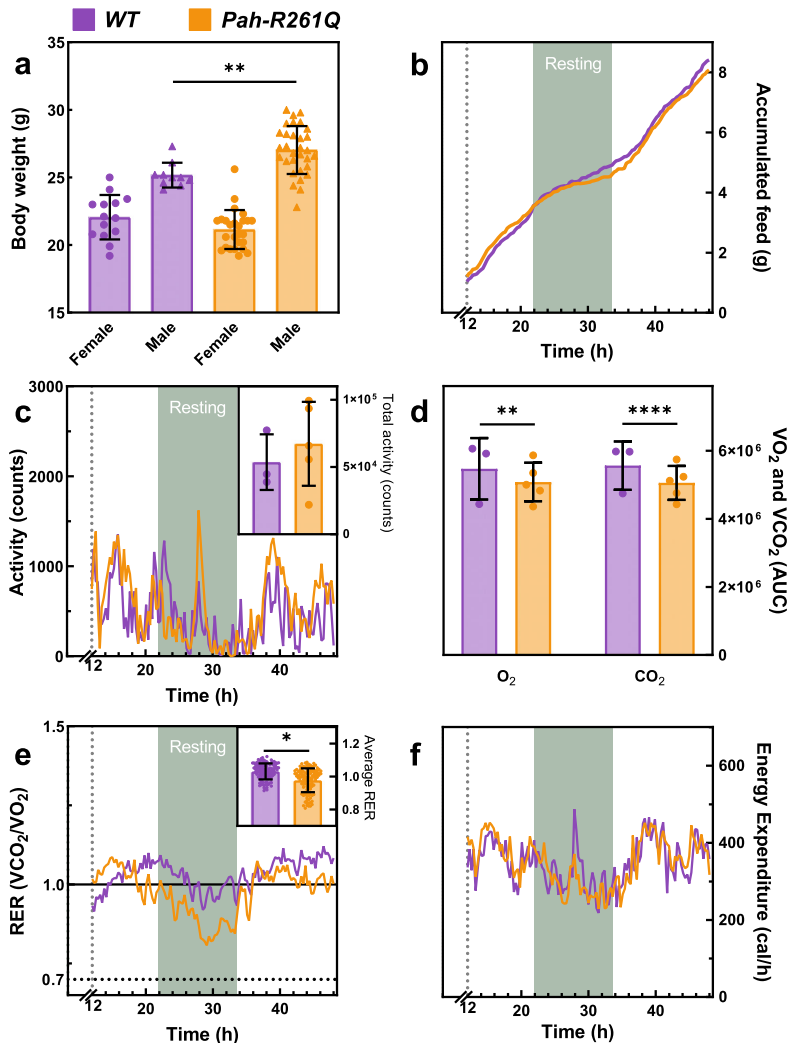


Fig. 1 Physiological and metabolic characterization of *Pah-R261Q* compared with WT mice. **a** Bodyweight distribution by sex and genotype. The weight of WT mice (controls) was in agreement with averaged registered data (<https://www.jax.org/strain/000664>). Data are presented as mean \pm SD, with individual values plotted as circles (females) and triangles (males) ($n = 10$ WT male, 14 WT female, 31 *Pah-R261Q* male, 26 *Pah-R261Q* female mice). Statistical significance for the weight difference for males in the two groups was calculated by two-tailed unpaired t test; $p = 0.0031$ (**). **b–f** Metabolic cage experiments, performed for 48 h, with 12 h of acclimation followed by 36 h of recordings. $n = 3$ WT and 5 *Pah-R261Q* mice in independent experiments, with one mouse per cage and 121 observations/animal. **b** Cumulative feed consumption (g). **c** Mice activity with continuous recording, expressed as mean \pm SD. Inset, total activity for each mouse group presented as mean \pm SD, individual values are plotted as circles. **d** Total Volume of O_2 consumed and volume of CO_2 produced for each mice type, obtained from the integration of the area under the curve (AUC) from data in Supplementary Fig. 3. Data are presented as the mean AUC \pm SD, with individual values plotted as circles. Statistical significance for the difference between both mice groups was calculated by two-tailed unpaired t test; $p = 0.0011$ (***) for O_2 and $p < 0.0001$ (****) for CO_2 . **e** Respiratory exchange ratio (RER) along the recording time. Inset: averaged RER presented as mean \pm SD; the circles represent mean for the group at each time point. Statistical significance for differences between both groups was calculated by two-tailed unpaired t test; $p < 0.0001$ (****). **f** Energy expenditure obtained by indirect calorimetry expressed as mean \pm SD. In all panels, the data for WT are depicted in purple and *Pah-R261Q* in ochre. Source data are provided as a Source Data file.

L-Phe loading test that is applied to HPA/PKU patients for their phenotypic classification⁴⁰—a transient but very prominent elevation of blood L-Phe values was observed. As shown in Supplementary Fig. 4, 40 min after i.p. injection with 200 μ g L-Phe/g body weight, *Pah-R261Q* mice presented a massive increase in

L-Phe concentrations ($990 \pm 220 \mu$ M), before returning to basal levels ca. 300 min later. A similar L-Phe challenge caused much lower increases of L-Phe concentrations in heterozygous and WT mice (Supplementary Fig. 4). The transient L-Phe-increase in *Pah-R261Q* mice allowed us to investigate the response to

Table 1 Blood serum concentrations of the metabolites whose levels were increased/decreased in *Pah-R261Q* mice in respect to the control *WT* group. Concentrations are expressed as arithmetic mean \pm SD; $n = 19$ *WT* and 19 *Pah-R261Q* mice.

Metabolite (name)	WT (μ M)	<i>Pah-R261Q</i> (μ M)	Difference	p Value (MW) ^a
Phenylalanine	71.9 (10.3)	113 (22)	41.1	0.000004
β -Hydroxybutyrate	150 (99)	282 (133)	132	0.029
Trimethyllysine	0.803 (0.165)	0.976 (0.213)	0.173	0.050
Leucine	143 (23)	164 (42)	21	0.075
Isoleucine	87.5 (12.8)	101 (24)	13.5	0.091
α -Ketoglutaric acid	38.6 (15.2)	26.3 (10.8)	-12.3	0.003
Glutamic acid	39.5 (20.7)	29.4 (10.2)	-10.1	0.008
Alanine	444 (71)	362 (80)	-82	0.010
Tryptophan	103 (24)	82.9 (30.9)	-20.1	0.013
Quinolinic acid	0.178 (0.090)	0.130 (0.041)	-0.48	0.023
Creatine	154 (40)	127 (30)	-27	0.026
Aspartic acid	27.4 (14.4)	22.7 (11.0)	-4.7	0.043
Glutamine	687 (76)	622 (112)	-65	0.043
Tyrosine	81.3 (25.3)	77.9 (14.0)	-3.4	0.050
Methylmalonic acid	0.701 (0.095)	0.585 (0.118)	-0.116	0.060
Kynurenine	0.740 (0.234)	0.573 (0.264)	-0.167	0.080
Proline	90.2 (25.4)	73.0 (17.2)	-17.2	0.085

^aTwo-tailed p values for differences between serum concentration in *WT* and *Pah-R261Q* mice were obtained from Mann Whitney (MW) U test. See also Supplementary Table 2.

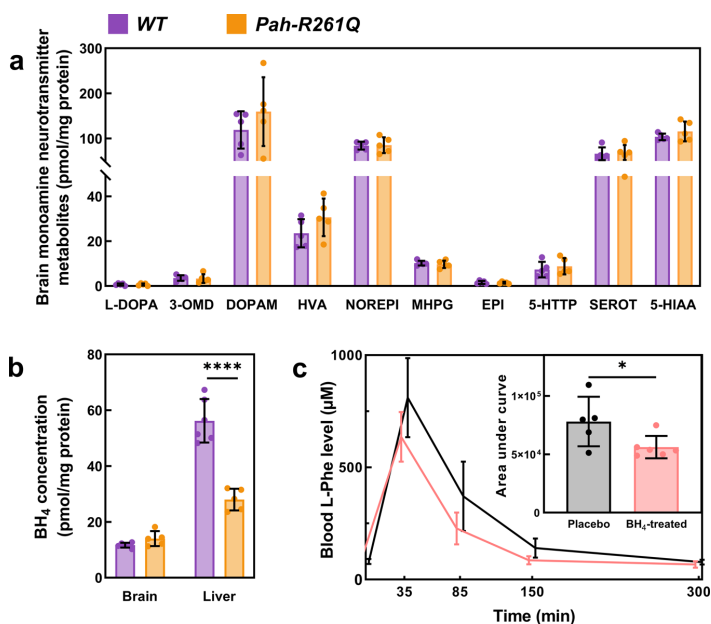


Fig. 2 Neurotransmitter and BH₄ content, and BH₄-responsiveness in the *Pah-R261Q* mouse model. **a** Monoamine neurotransmitter content in brain lysates; data are presented as mean \pm SD, individual values are plotted as circles ($n = 5$ *WT* and 5 *Pah-R261Q* mice). Abbreviations (from left to right): levodopa, 3-ortho-methylidopa, dopamine, homovanillic acid, norepinephrine, 3-methyl-4-hydroxyphenylglycol, epinephrine, 5-hydroxytryptophan, serotonin, and 5-hydroxyindoleacetic acid. **b** BH₄ determination in whole brain and liver lysates, presented as mean \pm SD, individual values are plotted as circles ($n = 6$ *WT* and 5 *Pah-R261Q*). Statistical significance for the difference in brain BH₄ content between both groups was calculated by two-tailed unpaired t test; $p < 0.0001$ (****). **c** Blood L-Phe concentration after L-Phe challenge in placebo-control (black) and BH₄-treated (pink) *Pah-R261Q* mice ($n = 5$ placebo and 6 treated mice). L-Phe (200 μ g L-Phe/g body weight) was administered by i.p. at time 0 and L-Phe concentration was monitored at 0, 35, 90, 150, and 300 min. The BH₄ treated mice received (by i.p.) 20 mg/kg BH₄ in 2% ascorbic acid and 10% DMSO, for 4 days, twice a day, previous to L-Phe administration, and the placebo control received the same solution without BH₄. Data are presented as mean \pm SD. Inset, area under the curve (AUC) for the time dependence of L-Phe concentration between 0 and 300 min for placebo and BH₄-treated groups. Individual values are represented by circles. Statistical significance for the difference between both groups was calculated by two-tailed unpaired t test; $p = 0.0299$ (*). In panels **a** and **b** the data for *WT* are depicted in purple and for *Pah-R261Q* in ochre. Source data are provided as a Source Data file.

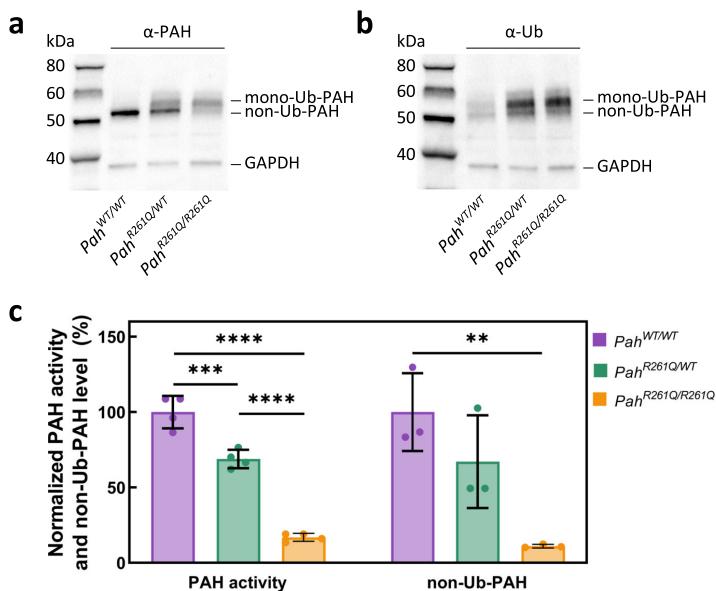


Fig. 3 PAH content in liver lysates of homozygous and heterozygous *Pah*-R261Q mice. **a** Western blots for immunodetection of PAH (α -PAH) (**a**) and ubiquitinated protein (α -Ub) (**b**) showing the decrease in non-ubiquitinated PAH (non-Ub-PAH; -51 kDa band) and increase of mono-ubiquitinated PAH (mono-Ub-PAH; -56 kDa) from genotype *Pah*^{WT/WT} to *Pah*^{R261Q/WT} to *Pah*^{R261Q/R261Q}. The blots are representative from $n = 3$ replicates for each mice group. GAPDH was used as loading control. **c** Overview of relative PAH specific activity normalized to activity in *Pah*^{WT/WT} liver lysates (23.2 ± 2.4 nmol L-Tyr/min/mg protein) ($n = 4$ mice for each genotype) and non-Ub-PAH protein (51 kDa) levels from densitometric analysis normalized to both *Pah*^{WT/WT} liver lysates as well as to GAPDH loading control ($n = 3$ mice for each genotype). Data are presented as mean \pm SD for *Pah*^{WT/WT} (purple), *Pah*^{R261Q/WT} (green), and *Pah*^{R261Q/R261Q} (ochre), individual values are represented as circles. Differences between genotypes were analyzed by one-way ANOVA followed by Tukey test; differences in PAH activity, $p = 0.0005$ (***) for *Pah*^{WT/WT} vs. *Pah*^{R261Q/WT}, $p < 0.0001$ (****) for both *Pah*^{WT/WT} vs. *Pah*^{R261Q/R261Q} and *Pah*^{R261Q/WT} vs. *Pah*^{R261Q/R261Q}; differences in PAH level, $p = 0.0080$ (**) for *Pah*^{WT/WT} vs. *Pah*^{R261Q/R261Q}. Source data are provided as a Source Data file.

BH₄-treatment. As seen in Fig. 2c, significantly lower blood L-Phe level was measured after an L-Phe challenge (200 μ g/kg body weight) was administered following a BH₄ treatment (20 mg/kg body weight for 4 days, twice a day⁴¹), compared with placebo. BH₄ treatment resulted in a 28% decrease in L-Phe content as calculated from the area under the curve (Fig. 2c, inset). Patients with the R261Q mutation in homozygosity present variable HPA phenotype but about 74% are positive responders to BH₄ treatment (<http://www.biopku.org/>), and the results with the mutant mice are consistent with the BH₄-responsive phenotype.

Hepatic p.PAH-R261Q protein presents increased ubiquitination and aggregation.

After the investigation of the metabolic status of *Pah*-R261Q mice, we also studied the effect of the mutation on the function and stability of PAH in the mouse liver. Immunodetection by Western blot of the PAH protein (p.R261-PAH and WT-PAH, for the mutant and WT proteins, respectively) in liver lysates showed the typical 51-kDa PAH band for WT mice, and two PAH bands at 51- and 56-kDa for the heterozygous *Pah*^{R261Q/WT} and homozygous *Pah*^{R261Q/R261Q} (*Pah*-R261Q) mutant mice (Fig. 3a). The 56-kDa PAH band, present in both mice with the mutant allele, was recognized by the anti-ubiquitin antibody (Fig. 3b). This band has been identified as mono-ubiquitinated PAH in previous studies with *Enu1* and *Enu1/2* HPA mouse models^{42,43}. The 51-kDa non-ubiquitinated PAH band was strongly reduced in *Pah*-R261Q, as best observed in the immunodetected PAH levels normalized to WT control

mice (Fig. 3c). We also measured PAH activity in the liver lysates, and for each genotype, the relative specific activity correlated well with the relative levels of non-ubiquitinated PAH protein in liver lysates (Fig. 3c). Nevertheless, the results with *Pah*-R261Q ($11.6 \pm 1.5\%$ non-ubiquitinated protein vs. $16.9 \pm 3.3\%$ specific activity, both relative to WT) support low level of PAH activity for the ubiquitinated enzyme.

The reduction of total p.R261Q-PAH protein levels and increased ubiquitination observed by Western blot in *Pah*-R261Q compared to WT mice, indicative of instability and misfolding of this PAH variant (Fig. 3a, b), was followed-up by immunofluorescence staining of hepatic tissue which confirmed a substantial reduction in PAH protein in *Pah*-R261Q (Fig. 4). The specificity of the PAH antibody was further proven by an antigen pre-adsorption test showing almost complete loss of PAH immunoreactivity in hepatic tissue of WT mice after incubation with PAH antibody preabsorbed with purified recombinant PAH (Supplementary Fig. 5). Moreover, the immunofluorescence images of *Pah*-R261Q revealed scattered PAH-immunoreactivity in discrete bright points, consistent with aggregation, as well as an increase in ubiquitination signal that presented substantial colocalization with mutant PAH (Fig. 4). To investigate the mutation dependent PAH misfolding and aggregation, we also performed immunofluorescence of hepatic tissue of the *Enu1* mouse model of mild HPA, which expresses the unstable p.V106A-PAH variant, also associated with PAH instability, leading to a considerable decrease of functional PAH in the liver (5% of WT)^{42,44,45}. *Enu1* liver also presented largely decreased

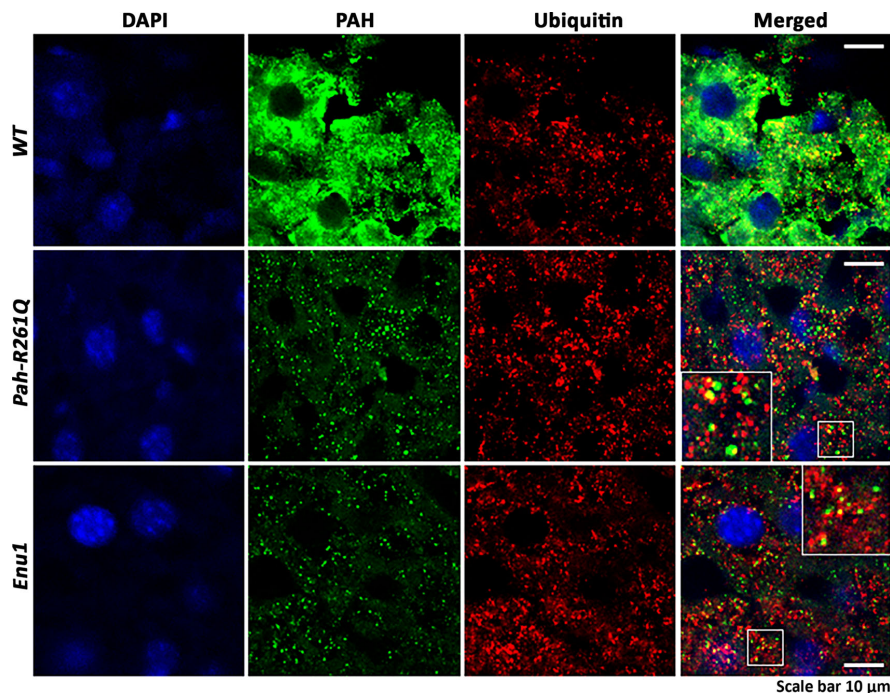


Fig. 4 Distribution of PAH in hepatic tissue of WT and mouse models *Pah-R261Q* and *Enu1*. Immunofluorescence of PAH and ubiquitin (Ub) detection in hepatic tissue of WT, *Pah-R261Q*, and *Enu1* mice, revealing the distribution pattern of PAH (green) and Ub (red). PAH was strongly reduced in both *Enu1* and *Pah-R261Q* when compared to WT, whereas Ub was highly expressed in both mutant mice. The micrographs are representative for $n = 3$ biological replicates in each mice group. The fluorescence intensity (mean \pm SD) calculated in 14 stacks of confocal images, relative to WT (=1), was 0.264 ± 0.105 (*Pah-R261Q*) and 0.154 ± 0.029 (*Enu1*) for PAH, and 1.315 ± 0.035 (*Pah-R261Q*) and 1.405 ± 0.103 (*Enu1*) for Ub. Colocalization of PAH and ubiquitin (yellow) was observed in both mutant mice, as highlighted in the inset. DAPI was used for nuclear staining (blue). Source data are provided as a Source Data file.

and particulate PAH-immunoreactivity and increased ubiquitination. There were, however, differences in the aggregation pattern of mutant PAH between both HPA-mouse models (Fig. 4) as well as in the size of the PAH aggregates, larger in *Pah-R261Q* than in *Enu1*.

We further studied the distribution of PAH aggregates between the nucleus and the cytoplasm in hepatic cells. The use of the nuclear pore marker Nup98 and 3D-rendering of the stacks of confocal images revealed that the smaller aggregates of mutant PAH in *Enu1* appeared more ubiquitously distributed in hepatocytes, where they are also present in the nucleus (Fig. 5a). On the other hand, the PAH aggregates in *Pah-R261Q* did not show nuclear localization and appear distributed at the cytoplasmic side of the nuclear membrane (Fig. 5a). As fluorescence detection may alter the shape and size of macromolecules and complexes, we also performed immunohistochemistry (IHC) with optical detection by DAB staining in order to assess the size of the mutant PAH aggregates in hepatic tissue (Fig. 5b, c). The averaged area of DAB-stained particles was 0.18 ± 0.06 and 0.11 ± 0.03 (SD) μm^2 for *Pah-R261Q* and *Enu1*, respectively (Fig. 5c).

Amyloid-like aggregation of p.PAH-R261Q. The different size and nucleocytoplasmic distribution of the aggregates of p.R261Q and p.V106A PAH variants in *Pah-R261Q* and *Enu1* livers, respectively, suggests different misfolding and aggregation mechanisms for these two mutants. As larger aggregates,

especially those with amyloid aggregation, can be cytotoxic⁴⁶, we investigated if the mutant protein p.R261Q-PAH could aggregate through cross- β -sheet prone motives around the mutation site. Positively, in silico evaluation with the program TANGO⁴⁷ predicted a high (>50%) propensity to form intermolecular cross- β (amyloid-like) aggregates in region 254–263 in the mutant (FLGGLAFQVF), while the same region in the WT sequence (FLGGLAFRVF) was not predicted to be prone to amyloid-like aggregation (Supplementary Fig. 1), for both the human and mouse PAH sequences. We tested the propensity of all PAH missense variants registered at BIOPKU (<http://www.biopku.org>), and also included p.V106A-PAH (*Enu1*), which is very rare in human⁴⁸. The calculations supported a high susceptibility to undergo this type of aggregation for a few variants, i.e., p.E78V, p.N167Y, p.P211L, p.R261G, and p.E390G, all rare, but not for p.V106A (*Enu1*).

To confirm the formation of amyloid-like aggregates by the mutant p.R261Q-PAH we used the Amytracker[®] 680 fluorescence assay with purified recombinant mutant protein. An accelerated formation of amyloid-like aggregates was observed for p.R261Q-PAH compared to WT-PAH (Supplementary Fig. 6a). After 5 h incubation, parallel samples of p.R261Q-PAH without Amytracker were visualized by transmission electron microscopy (TEM). Imaging revealed larger amorphous aggregates of a diameter up to >100 nm, together with small aggregates of about 20 nm diameter, whereas fibrillary structures were not observed (Supplementary Fig. 6b).

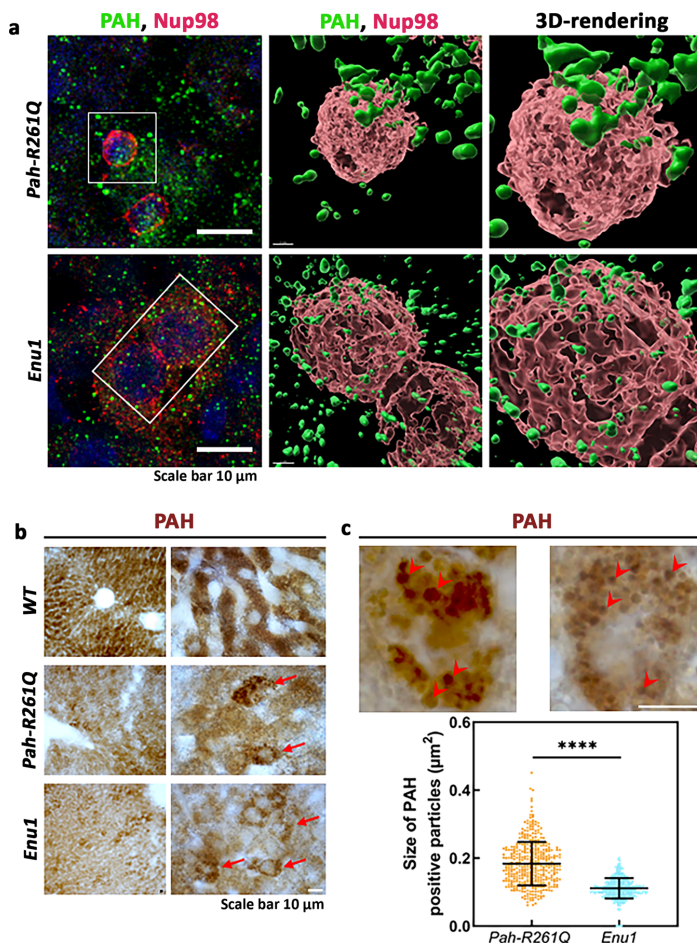


Fig. 5 Nuclear distribution of mutant PAH protein in *Pah-R261Q* and *Enu1* mice liver. **a** Immunofluorescence of PAH (green) and the nuclear pore marker Nup98 (red) in hepatic tissue of *Enu1* and *Pah-R261Q* mice (left panels), and 3D-rendering of stacks of confocal images using the surface tool in Imaparis software at two different magnifications (middle and right panels). The images reveal the subcellular distribution of PAH in the nucleus and cytoplasm of *Enu1* mice, whereas in *Pah-R261Q* mice PAH is distributed in the cytoplasm. Hoechst was used for nuclear staining (blue). **b** Immunohistochemically DAB-stained hepatocytes from *WT*, *Pah-R261Q*, and *Enu1* mice at low (left panels) and high (right panels) magnification. Arrows indicate PAH immunoreactive hepatocytes in *Pah-R261Q* and *Enu1* mice. **a, b** The micrographs are representative of $n = 3$ biological replicates in each mice group. **c** Two representative PAH immunoreactive hepatocytes at higher magnification in *Pah-R261Q* (left) and *Enu1* (right) mice are shown, where arrowheads point to PAH-positive particle-like structures. Measurement of PAH particle size was performed in 30 μm -thick liver sections ($n = 10$) for each mice. At least 400 single PAH-positive particles in randomly selected regions of liver sections from each mice group were analyzed, and the size distribution of PAH-positive particles in *Pah-R261Q* and *Enu1* hepatocytes is shown (lowest panel). Data are presented as mean \pm SD and each dot represents a PAH-positive particle. The difference in size is statistically significant, as calculated by the two-tailed unpaired *t* test; P value < 0.0001 (****). Source data are provided as a Source Data file.

PAH aggregates in *Pah-R261Q* mice colocalize with autophagy markers and are associated with oxidative stress. Larger aggregates are commonly processed by autophagy rather than by the ubiquitin-dependent proteasome system (UPS)⁴⁹. We thus performed immunofluorescence microscopy of liver samples of *WT*, *Pah-R261Q*, and *Enu1* mice with autophagy markers Ser403-phosphorylated p62 protein (p62/SQSTM1 (sequestosome-1)), a selective receptor and marker for autophagic clearance^{50,51}. The level of phosphorylated p62 (P-p62) was indeed much higher in *Pah-R261Q* than in *Enu1* mice, which presented similar immunodetected levels as in *WT* mice (Fig. 6a). Immunofluorescence

staining with the standard marker for autophagosomes LC3 was also increased in *Pah-R261Q*, but not in *Enu1*, compared with *WT* (Fig. 6b). Both autophagy markers P-p62 and LC3 presented colocalization with mutant PAH in *Pah-R261Q* mice (Fig. 6a, b). These results suggest that the larger PAH aggregates in *Pah-R261Q*, but not the smaller aggregates in *Enu1*, engage the autophagic system. Moreover, we also performed TEM imaging of hepatic tissue, which showed hepatocytes with normal cell and organelle morphology in *Pah-R261Q* and no abnormality in nuclei or the nuclear membrane (Supplementary Fig. 7a). We noticed an increased number of lysosomes and of autophagic structures,

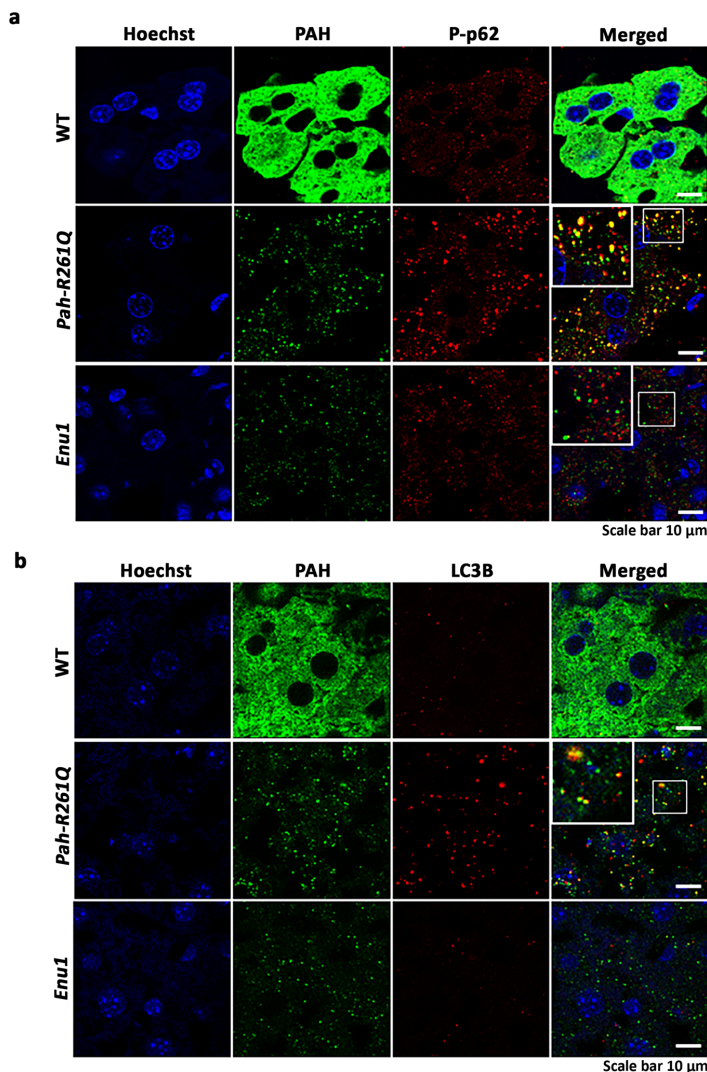


Fig. 6 Colocalization of mutant PAH in *Pah-R261Q* mice with autophagic markers. Immunofluorescence micrographs showing the codistribution of PAH (green) with autophagy markers p62 phosphorylated at Ser403 (P-p62, red) in **(a)** or LC3 (red) in **(b)** in hepatic tissue from WT, *Pah-R261Q* and *Enu1* mice. Both markers were increased in *Pah-R261Q* when compared to both WT and *Enu1*. The fluorescence intensity (mean \pm SD) calculated in 14 stacks of confocal images, relative to WT (=1), was 1.326 ± 0.121 (*Pah-R261Q*) and 0.778 ± 0.158 (*Enu1*) for P-p62 **(a)**, and 2.277 ± 0.174 (*Pah-R261Q*) and 1.535 ± 0.175 (*Enu1*) for LC3 **(b)**. *Pah-R261Q* but not WT or *Enu1* showed clear colocalization (yellow) of PAH with both P-p62 **(a)** and LC3 **(b)**, as highlighted in the insets. Hoechst was used for nuclear staining (blue). All micrographs are representative for $n = 3$ biological replicates in each mice group. Source data are provided as a Source Data file.

i.e., double-membrane autophagosomes and autolysosomes (Supplementary Fig. 7b) and exhaustive counting of these structures confirmed that they were increased in *Pah-R261Q* compared to WT mice whereas no difference in the number of peroxisomes and lipid drops was found (Supplementary Fig. 7c).

The nuclear quality control system customarily collaborates on the degradation of misfolded cytoplasmic proteins and small aggregates⁵². However, larger aggregates may hinder nuclear uptake⁴⁶, leading to toxic accumulation of the aggregates in the cytoplasm, saturation of the autophagy system, and increased oxidative stress^{49,53}. For some aggregation disorders associated

with the formation of amyloid fibrils by Tau, such as polyglutamine diseases, AD and Tau-dementia, invaginations or indentations of the nuclear membrane, filled by fibrillary rods, as well as nuclear pore pathology are observed^{54,55}. These alterations are also observed in ALS/FTD caused by aggregation of TDP-43 in non-fibrillary oligomeric amyloid-like aggregates⁵⁶ and seem related with the interference of the proteins with the nucleocytoplasmic system, e.g., microtubules in the case of Tau⁵⁴ or the nuclear transport machinery in the case of TDP-43⁵⁶, resulting in the invaginations. The lack of nuclear invaginations in *Pah-R261Q* is in accordance with the non-fibrillary nature of the PAH

aggregates and with PAH being a cytoplasmic enzyme with no known functional association with the nucleocytoplasmic system.

Despite a lack of significant disturbances in nuclear morphology in *Pah-R261Q*, it appears that the aggregates of p.R261Q-PAH do not enter the nucleus (Fig. 5a), which can be associated with overload of the cytoplasmic quality control system and oxidative stress. We measured the total equivalent antioxidant capacity (TEAC) in liver lysates of both HPA models (*Enu1* and *Pah-R261Q*) and *WT* mice by the Trolox assay. *Pah-R261Q* but not *Enu1* presented elevated TEAC values compared with *WT* (Supplementary Fig. 8), indicating a specific upregulation of the antioxidant response in *Pah-R261Q* mice in agreement with the metabolic changes associated with oxidative stress (see above and Table 1).

Gene (mRNA) expression assays. Finally, ten genes related to the PAH system, protein quality control, and oxidative stress pathways were selected and subjected to analysis by quantitative TaqMan mRNA expression in liver extracts (RT-qPCR; results overview in Table 2). In absolute terms, *Pah* and *Hsc70* showed the highest levels of gene expression. Comparatively, for *Pah-R261Q* vs. *WT* mice, we found the following: (i) *Pah* expression was not altered; (ii) expression of the *GCH1-feedback regulatory (Gchfr)* gene was upregulated; (iii) the PAH specific Hsp40 co-chaperone *Dnajc12* exhibited increased expression levels while two heat shock family members, namely the transcription factor *Hsf1* and the molecular chaperone *Hsp70* were downregulated, and the expression of the constitutive *Hsc70* was unmodified; (iv) no significant changes in expression levels were identified for targets associated with protein degradation, *Stub1* (coding for the co-chaperone CHIP, with ubiquitin ligase activity) and the autophagy marker *Sqstm1* (coding for p62/SQSTM1), and for the oxidative stress-responsive transcription factor *Ap-1*. The implication of these results together with the other findings in this work are discussed below.

Discussion

Mouse models of genetic diseases do not always entirely recapitulate the main phenotypic characteristics found in patients⁹. The

Pah-R261Q knock-in mouse that carries a frequent mutation in HPA/PKU patients exhibits reduced total hepatic PAH activity and presents phenotypic traits characteristic of homozygous patients with the *R261Q:R261Q* genotype, such as increased L-Phe and decreased L-Trp and L-Tyr in blood compared to *WT*, sensitivity to L-Phe challenge, and responsiveness to BH₄ supplementation (<http://www.biopku.org>)^{8,16}. Moreover, there is similar PAH residual activity (~15% of *WT*) in both *Pah-R261Q* mice and homozygous humans¹⁶, however, we encountered a remarkable difference between absolute blood L-Phe-levels in mice and patients. While patients present metabolic phenotypes from mild PKU to classic PKU (off-diet blood L-Phe values > 600 μmol/L) (247 records in <http://www.biopku.org>; see also refs. ^{16,17}), our mouse model exhibited very mild HPA (~110 μmol L-Phe/L). Thus, for the same PAH genotype with similar remaining activity, the blood L-Phe concentration (metabolic phenotype) is higher in humans, which might be explained by a lower steady-state level of hepatic PAH in humans compared with mice. There is a high similarity in sequence, structure, specific activity and regulatory properties of human and mouse PAH, and thus different PAH amounts between rodents and humans have been associated with differences in the rate of transcription, translation, and/or protein homeostasis⁵⁷. Nevertheless, based on the similar propensity to aggregate through a cross-β-sheet formation for human and mouse PAH around the mutation area (Supplementary Fig. 1), it is very probable that similar amyloid-like soluble aggregates are formed in the liver of patients with the Arg261 → Gln mutation.

The *Pah-R261Q* mouse appears to offer considerable potential for mechanistic and therapeutic investigations as it presents with a tunable blood L-Phe concentration. By applying an L-Phe challenge, we could transiently attain L-Phe concentrations characteristic of PKU, and by adjusting the L-Phe concentration and length of supplementation, it might be possible to modulate the metabolic phenotype and fully develop the capacity of this mouse model as a prototype to study a range of mild to severe forms of HPA. Furthermore, upon L-Phe challenge, the resulting transient HPA in *Pah-R261Q* is responsive to treatment with BH₄ (Kuvan®). Consequently, this mouse model can contribute to evaluate protocols and understand the multifactorial mechanisms

Table 2 Relative mRNA quantification for selected genes in liver of *WT* and *Pah-R261Q* mice.

Gene (name)	<i>Pah</i> genotype	Expression level (relative to <i>WT</i> mice, defined as 1)	Fold change ^a	p Value ^b
<i>Pah</i>	<i>WT</i>	1.0000 (0.7878 ± 1.2693)	1.15	0.2273
	<i>R261Q</i>	1.1524 (1.0967 ± 1.2110)		
<i>Gch1</i>	<i>WT</i>	0.2512 (0.2146 ± 0.2939)	1.08	0.5440
	<i>R261Q</i>	0.2714 (0.2115 ± 0.3483)		
<i>Gchfr</i>	<i>WT</i>	0.0163 (0.0131 ± 0.0203)	1.70	0.0024
	<i>R261Q</i>	0.0277 (0.0228 ± 0.0336)		
<i>Dnajc12</i>	<i>WT</i>	0.0040 (0.0030 ± 0.0053)	1.78	0.0048
	<i>R261Q</i>	0.0071 (0.0057 ± 0.0088)		
<i>Hsp70</i>	<i>WT</i>	0.0010 (0.0007 ± 0.0015)	0.31	0.0012
	<i>R261Q</i>	0.0003 (0.0002 ± 0.0005)		
<i>Hsc70</i>	<i>WT</i>	0.9704 (0.7478 ± 1.2592)	1.34	0.0855
	<i>R261Q</i>	1.2983 (1.0279 ± 1.6399)		
<i>Hsf1</i>	<i>WT</i>	0.0280 (0.0251 ± 0.0313)	0.65	0.0054
	<i>R261Q</i>	0.0183 (0.0140 ± 0.0238)		
<i>Stub1</i>	<i>WT</i>	0.0156 (0.0126 ± 0.0193)	1.22	0.0808
	<i>R261Q</i>	0.0191 (0.0175 ± 0.0208)		
<i>Sqstm1</i>	<i>WT</i>	0.2483 (0.2203 ± 0.2799)	1.04	0.6389
	<i>R261Q</i>	0.2571 (0.2287 ± 0.2892)		
<i>Ap-1</i>	<i>WT</i>	0.0163 (0.0140 ± 0.0189)	1.0	0.9815
	<i>R261Q</i>	0.0163 (0.0149 ± 0.0179)		

^aFold change in *Pah-R261Q* mice relative to *WT* mice.

^bTwo-tailed p values for differences between both mice groups, obtained from the Mann Whitney U test.

Genes upregulated or downregulated in *Pah-R261Q* (*n* = 5 mice) compared to *WT* (*n* = 6 mice) (*p* < 0.05) are highlighted in bold text.

for BH₄ responsiveness in mice, including the increase of total PAH enzyme activity by PAH variant stabilization through protection against oxidative damage and proteolytic degradation, thus prolonging the half-life of PAH as seen in vitro¹⁹.

The large variability and spectrum of metabolic phenotypes presented by homozygous *PAH-R261Q* patients^{15–17} are thus far not observed in the mouse model. *Pah-R261Q* mice, in fact, present low variation in the basal concentration of blood L-Phe and other parameters measured in this work. The proteostasis network that maintains the synthesis, folding, localization, and degradation of proteins, and counteracts the effect of aggregates, involves a large number of protein components that are regulated at the cellular, tissue, and organismal level⁵³. This complex proteostasis network provides additional polymorphic modifier variants that contribute to the broader phenotypic spectrum in patients with unstable PAH variants, but not necessarily in the mouse model where a uniform genetic background has been achieved by careful backcrossing.

In PKU, the neurological defects include monoamine neurotransmitter deficiencies, which are fully manifested in the classical PKU (*Enu2*) mouse that is almost devoid of PAH activity²⁶. The *Enu1/2* mouse, which presents 2.5% of regular PAH activity and blood L-Phe levels just slightly higher (~150 μmol/L) than in *Pah-R261Q*, also shows a decrease in brain serotonin and 5HIAA⁵⁸. However, the remaining 16% PAH activity in *Pah-R261Q* mice appears high enough to result in apparently normal L-Phe catabolism and monoamine neurotransmitter synthesis, as well as in absence of detectable neurological deficiencies. Nevertheless, despite their mild HPA, *Pah-R261Q* mice manifested several biomarkers and indicators of adiposity and altered lipid metabolism, and oxidative stress. These traits have been previously observed in patients and animal models of PKU where they have been related to neurotoxic HPA levels and (micro)nutritional deficiencies of the L-Phe-free diet^{59,60}, factors that are absent in this case. Further evidence suggests that the increased weight in *Pah-R261Q* males is not a direct consequence of elevated L-Phe levels; the classical PKU model *Enu2* is underweight, despite its tenfold higher blood L-Phe levels than in *Pah-R261Q*²⁶. The molecular basis behind the observed mild overweight and oxidative stress in *Pah-R261Q* mice appears to be related to a toxic aggregation of mutant PAH and contributes to the identification of a gain-of-function contribution to the HPA/PKU pathology.

The misfolding defect of the p.R261Q-PAH protein variant is manifested both in biochemical characterizations as a reduced conformational stability and accelerated degradation^{18,19,23} and in computational predictions by FoldX¹⁵. The Arg to Gln residue change is expected to disrupt the interdimer interactions in p.R261Q-PAH (Supplementary Fig. 1), and the area around the mutation would then become available for unspecific intersubunit interactions. Among the few HPA/PKU-associated PAH variants with a high predicted propensity for β-cross amyloid-like aggregation by in silico TANGO calculations⁴⁷, p.R261Q-PAH is the variant with the highest allele frequency among patients.

The *Pah-R261Q* mice presented a reduction in steady-state hepatic PAH levels and PAH-specific activity, as well as increased ubiquitination of the protein in the liver. The current understanding of the loss-of-function of misfolding PAH variants is an accelerated degradation carried out preferentially by the ubiquitination-dependent proteasome system (UPS), as recently proven for a large number of PAH variants in cellular studies⁶¹. Our results with *Pah-R261Q* show that selective autophagy may be involved in the degradation of a PAH variant, as strongly indicated by the colocalization of markers of autophagy Ser403-phosphorylated p62 and LC3 with mutant PAH. In the case of the lightly aggregating *Enu1* variant p.V106A-PAH there is no colocalization of these markers with PAH, and the aggregates

seem to enter the nucleus where they may also be degraded by the nuclear UPS. There is an intricate cross-talk between the UPS and autophagy^{62,63}, and it is thus likely that PAH amyloid-like aggregates in *Pah-R261Q* that are not effectively processed by the UPS can be co-aggregated with phosphorylated p62 for autophagic processing^{51,64}.

Although insoluble deposits may protect from oxidative stress⁶⁵, amyloid-like aggregation-prone conformers—e.g., resulting from mutations—perturb cellular homeostasis and induce oxidative stress, increasing the production of reactive oxygen species (ROS) at the cellular and tissue levels⁵³. Toxic aggregation in the cytoplasm overwhelms the protein quality control system, resulting in increased ROS, further exacerbation of protein aggregation³³, and activation of p62/SQTM1 by phosphorylation⁵¹. Together, our results point to an oxidative and cellular stress condition in *Pah-R261Q* mice associated with a toxic aggregation of the PAH variant. The reduction of BH₄ levels manifested in the liver of *Pah-R261Q* has also been observed in other disorders associated with oxidative stress². In hepatocytes, BH₄ also acts as the cofactor of alkylglycerol monooxygenase², an enzyme involved in the degradation of ether lipids. Alteration of BH₄ synthesis mainly affects the entire cellular lipidome⁶⁶, providing a link between oxidative stress and alterations of lipid metabolism, the two main comorbidities postulated from the metabolic characterization of *Pah-R261Q* mice (Table 1). As part of the physiological and metabolic characterization of *Pah-R261Q*, we noted three related findings: slightly increased body weight of males (26.8 ± 0.4 vs. 25.1 ± 0.3 g (WT)), lower RER in the resting period, and higher serum levels of some metabolites that have been associated with adiposity and altered lipid metabolism, namely trimethyllysine, leucine, and isoleucine³¹. Although no gender-associated changes were found for any parameter or metabolite measured in this work for *Pah-R261Q* compared to WT, including RER and relevant metabolites, a priori indicates a similar propensity for altered metabolism in both genders, only males were heavier than their WT counterparts. A male-specific body weight increase due to altered lipid metabolism and adiposity has been detected in other mice and human studies, which has been associated with a different genetic architecture and potential sex chromosome effects on metabolism (reviewed in ref. 67).

A recent study has also reported the reduction of soluble BH₄ in the liver lysates of *Enu1* and *Enu1/2* mice and the decrease has been linked to the entrapment of the cofactor in aggregates of the p.V106A-PAH variant⁴⁵, resulting in a secondary BH₄-deficiency. Here, we measured total BH₄ in non-centrifuged homogenates, showing a net reduction in *Pah-R261Q* mice, which is also supported by the upregulation of *Gchfr*-mRNA (Table 2). Furthermore, no decrease of hepatic BH₄ was measured by the same method in liver *Enu1/2* mice⁴³, supporting that the BH₄ reduction in *Pah-R261Q* is PAH mutation-specific and associated with the formation of large amyloid-like aggregates and oxidative stress.

Oxidative stress in *Pah-R261Q* mice elicits the activation of the antioxidant response, as seen by increased serum levels of β-hydroxybutyrate³³, as well as an increase in total antioxidant capacity measured by the Trolox assay. Likewise, the reduction of quinolinic acid could also be linked to an increased synthesis of NAD⁺, which polymerizes to poly ADP-ribose for the protection of DNA in case of oxidative stress^{36,37}. Conversely, increased β-oxidation (demonstrated by lower RER and elevated β-hydroxybutyrate) and the concomitant increase in anaplerosis, supported by the observed reduction in α-ketoglutaric acid and other anaplerotic amino acids and metabolites (Table 1) has also been shown to cause an increase in oxidative stress and inflammation³⁸. Another sign of oxidative stress in *Pah-R261Q* is the upregulation of *Dnajc12*, the specific co-chaperone of the aromatic amino acid hydroxylases, which was not altered in

*Enu1*⁴². Interestingly, overexpression of *Dnajc12* has been associated with oxidative stress^{68,69}. On the other hand, the downregulation of both the transcription factor *Hsf1* and the chaperone *Hsp70* appears somehow counterintuitive in this context since *Hsf1* in mammals is the primary regulator of the heat shock response, which is activated by cellular stress and elicits transcriptional upregulation of major HSPs, notably *Hsp70*⁷⁰. In contrast, downregulation of *Hsf1* and consequent reduction in expression of HSF1 target genes is observed in neurodegenerative diseases such as Parkinson's, Alzheimer's, and Huntington's diseases, characterized by toxic amyloid deposits⁷¹, and a similar downregulation of *Hsf1* and *Hsp70* is also observed in this case.

In conclusion, the observation of amyloid-like PAH aggregates in the liver of the *Pah-R261Q* mouse introduces the concept of toxic gain-of-function for specific PKU-associated mutations. Overall, our results suggest that the lipid profile alterations and oxidative stress found in these mice are linked to intracellular toxic aggregation of the p.R261Q-PAH variant rather than to the severity of the HPA and/or the diet. The *Pah-R261Q* mouse model thus represents a unique research tool to support the evaluation and discovery of additional biomarkers in PKU and to investigate mutation-specific comorbidities, of benefit to the large number of PKU patients harboring the *R261Q* mutation. Interestingly, recent studies aiming to assess the prevalence of comorbid associations among large groups of adult PKU patients are starting to reveal several conditions in addition to the known neuropsychiatric disorders, including overweight and renal and cardiovascular dysfunctions^{5,6,72}. A proper patient stratification that takes into account the predisposition of the coded PAH variants to amyloid-like aggregation is expected to result in a better association of the comorbidities and improved patient-tailored treatment, encouraging follow-up investigations of the PAH aggregates. Lastly, this mouse model might contribute to investigations on pharmacological chaperone-based therapies targeting unstable PAH variants.

Methods

Materials. All chemicals in this section were acquired from Sigma-Aldrich unless otherwise indicated. Animals evenly matched for sex were distributed in each group for the different experiments presented. Recombinant human WT-PAH and p.R261Q-PAH proteins were expressed and purified using the pMAL expression vectors^{18,19} coding for the fusion protein maltose-binding protein (MBP)-(pep)xa-PAH), where (pep)xa is the cleavage site for the restriction protease Factor Xa. The fusion proteins were expressed in *Escherichia coli* TBI cells at 28 °C for 16–18 h with 1 mM IPTG and purified by affinity chromatography with amylose resin (New England Biolabs) with elution with 10 mM maltose. The fusion proteins were cleaved for 3 h with Factor Xa (New England Biolabs) at a protease:PAH ratio of 1:300. The tetrameric purified WT-PAH and p.R261Q-PAH proteins were isolated by size exclusion chromatography on a Superdex HiLoad 16/600 200 column (GE Healthcare) in 20 mM Hepes pH 7, 200 mM NaCl.

Generation of *Pah-R261Q* knock-in mouse. The constitutive knock-in mouse model was generated by Taconic Biosciences GmbH (Köln, Germany) via CRISPR/Cas9-mediated gene editing. The guide RNA target sequence + protospacer adjacent motif (PAM) sequence 5'-AGTGGAAAGCTCGGAAGGCC_AGG-3' (non-seed sequence_seed sequence_PAM) was designed and guide RNA was prepared as a hybrid of CRISPR-RNA (crRNA; 6 ng/μl) (Dharmacon, Lafayette, USA) and trans-activating crRNA (tracrRNA; 10.5 ng/μl) (Dharmacon, Lafayette, USA). The guide RNA was co-injected into C57BL/6N zygotes – essentially as described²⁰ – along with Cas9 protein (55 ng/μl; New England Biolabs, Ipswich, USA) and homology-directed repair (HDR) oligonucleotide (5'-GCTTAGATCCATGCCTAA TGACTGTGTGTCAGTGGAAAGACTTGGAAATGCCAGGCCACCCCAAGAAATC TCGAGACAGACATGAGCCG-3') (100 ng/μl) from Integrated DNA Technologies, Coralville, USA. This HDR oligonucleotide harbored the point mutation c.782 G > A (p.Arg261Gln) to be introduced in exon 7 of the *Pah* gene on murine chromosome 10 (point mutation and exon annotation according to NCBI transcript NM_008777.3) as well as a silent mutation (c.777C > A) to create an additional restriction site (*BsmI*) for analytical purposes (Supplementary Fig. 2). These CRISPR reagents were microinjected (until the pronucleus swells up, typically ~1

pl) into 304 mouse embryos resulting in a total of 51 pups born, and three animals (5.9%) displayed positive detection of the *R261Q* knock-in allele.

Confirmation of the on-target mutation was completed as detailed^{73,74} whereas verification of the absence of undesired potential off-target modifications was achieved by heteroduplex mobility assays conducted on the top 16 hits originated from BLAST analysis of the guide RNA onto *M. musculus* genome assembly (GRCm38/mm10) (Supplementary Table 1).

Animal husbandry and colony expansion. The animal studies were approved by the Norwegian Food Safety Authority and performed at the Laboratory Animal Facility, University of Bergen, according to the guidelines and standards from the Regulation on the use of animals in the research of this institution. Mice were housed in a temperature-controlled (21 °C and 50% air humidity) environment with 12 h light/dark cycles. Food (standard chow pellets) and water were available ad libitum.

The colony was continuously backcrossed to avoid genomic drift. Every 6 months wild-type mice (C57BL/6J, males and females every second time) were bought from an approved vendor (Charles River) and bred with heterozygous *Pah^{R261Q}/WT* mice. Six to eight weeks old heterozygous *Pah^{R261Q}/WT* siblings from this backcrossing and breeding were used to produce homozygous *Pah^{R261Q}/R261Q* mice. The resultant *Pah^{R261Q}/WT* and *Pah^{WT}/WT* mice (siblings) from the breeding were utilized as control counterparts. This method of breeding is recommended to maintain the strain genetic integrity. We make sure to avoid going beyond three generations of inbreeding (F3) before we reset the generation by using new breeding animals from the backcrossing. The strain has been backcrossed eight times (N8) and the latest mice that have been used in the experiments presented in this work are from generation N8F3.

Genotyping. In order to determine the mouse genotype, ear biopsies were collected and DNA was extracted and purified from these tissue samples using the DNeasy Blood and Tissue kit (QIAGEN) following the manufacturer's instructions. After that, DNA was amplified by standard PCR (See primers in Table S4), initial denaturation at 95 °C/5 min followed by 35 cycles of denaturation-annealing-extension, 95 °C/30 s, 60 °C/30 s and 72 °C/1 min, with a final extension at 72 °C for 10 min) using Taq Polymerase (New England Biolabs). The PCR product was then incubated with the endonuclease *BsmI* (New England Biolabs) for 15 min at 65 °C. Finally, the digestion fragments were resolved in 2.5% agarose gel electrophoresis (1× TAE buffer/90 min/90 v) and bands visualized in a ChemiDoc XRS (Bio-Rad Laboratories) imaging system.

Metabolic cage. The physiological parameters: rate of O₂ and CO₂ consumption, food intake and activity of *Pah-R261Q* and control WT mice (4–5-month old; n = 3–5 mice per group, 121 observations/animal) were directly determined using the Oxymax-Comprehensive lab animal system (CLAMS, Columbus Instruments), with data being recorded for 36 h after an acclimatization period of 12 h. Other valuable calorimetric properties such as respiratory exchange rate (RER) and energy expenditure were indirectly calculated using Lusk classical equations provided in the Oxymax processing software.

Rotarod performance test. The assessment of motor function was conducted on a rotarod instrument (Harvard Apparatus) consisting of a 5 cm plastic grooved rod and a platform situated approximately 25 cm below equipped with a lever to trigger the recording for the time of fall. *Pah-R261Q* and control WT mice (3 months old; n = 10–11 mice per group) were, initially, habituated to the setting and trained to stay on the rod for 1 min at a constant speed of 5 rpm. Trained mice were then placed again on the rod with a gradual acceleration from an initial 4 rpm to a final 40 rpm speed over a 5 min testing period. The latency of fall as well as rod revolutions at fall was logged, and trials were repeated three times, separated by a 15 min break.

L-Phe challenge and BH₄-responsiveness. Adult mice (3–4-month-old) were employed in all the animal experiments of this section. For the effect of L-Phe challenge, intraperitoneal injection of an L-Phe solution (200 μg/g body weight) to *Pah^{R261Q}/R261Q*, *Pah^{R261Q}/WT*, and *Pah^{WT}/WT* mice (n = 23, 6 and 4 mice per group, respectively) was followed by whole blood sampling from the saphenous vein at time points: 1 day before injection (baseline level) and 35, 85, 150, and 300 min after injection. For BH₄-responsiveness, a treatment solution of BH₄ (Schircks Laboratories) (12.73 mM BH₄, 2% ascorbic acid, and 10% DMSO; in a dosage of 20 mg BH₄/kg body weight) or placebo solution (2% ascorbic acid and 10% DMSO), were injected into *Pah-R261Q* mice (n = 5–6 mice per group, per experiment) intraperitoneally twice a day⁴¹ for 4 days, before conducting the L-Phe challenge protocol as indicated above. The obtained blood samples were collected onto filter paper cards (PerkinElmer) according to the vendor's guidelines wherein L-Phe was measured by tandem mass spectrometry in, at minimum, 3 h fasted mice.

Metabolic markers analysis. In order to obtain serum specimens, whole blood was collected by cardiac puncture and 1 mL was transferred to a microcentrifuge

tube. Subsequently, blood samples were left for 45 min at room temperature to facilitate coagulation, preceding two consecutive centrifugation steps (2,100 rcf, 10 min, and 4 °C) where the respective supernatants were pipetted out to a clean tube. The isolated serum fractions were stored at -80 °C until examination. The extracted serum samples from *Pah-R261Q* and *WT* mice (4–5 months old; $n = 19$ mice per group) were subjected to an exhaustive analysis to determine the concentration of 72 relevant metabolic biomarkers. Analyses were performed at Bevilat (<http://bevilat.no/>) across four different platforms supporting high-throughput multi-analyte assays. A combination of chromatographic techniques with mass spectrometry detection (GC-MS/MS and LC-MS/MS) was applied (See references for individual experimental protocols in Supplementary Table 2).

Preparation of liver and brain lysates. Mice (age and numbers indicated in the specific studies) were sacrificed in a carbon dioxide euthanize chamber. Immediately after, the brain and liver were surgically excised and snap-frozen in liquid nitrogen, and tissue was manually ground into a fine powder and stored in aliquots at -80 °C. Liver homogenates from the ground aliquots (~200 mg powder) were prepared by adding 800 μ l of a lysis buffer solution containing 1 \times PBS and protease inhibitor cocktail (Roche), a 5 mm diameter stainless steel bead (Qiagen), and a mechanical disruption step in a Tissue Lysor II (Qiagen) instrument (2 \times 1 min 30 s, 20 Hz). Cellular debris was then removed through centrifugation (20,000 rcf, 20 min) to obtain a clear supernatant. The total protein concentration of the liver lysates was determined in a Direct Detect infrared spectrometer (Millipore). For the Trolox equivalent antioxidant capacity assay, 600 μ l of identical lysis buffer, a mechanical homogenization with a pellet pestle sitting on ice, and a modified centrifugation step (18,000 rcf, 10 min) was preferred.

Brain extracts were prepared by powder homogenization in 10 \times volume of 50 mM Tris-HCl, pH 7.5, 100 mM KCl, 1 mM EDTA, 1 mM DTT, 1 μ M leupeptin, 1 μ M pepstatin, and 200 μ M PMSF, at otherwise identical experimental conditions as standard liver extracts (see above).

Neurotransmitters, BH₄, and amino acid determination in tissues. The relative levels of BH₄ in liver and brain and of monoamine neurotransmitter metabolites in the brain of *Pah-R261Q* and *WT* ($n = 5–6$ mice per group) were measured in liver and brain lysates of 3–4-month-old mice as reported⁵⁸. Briefly, tissue lysates were oxidized for 60 min in the dark by 0.5 g/L iodine and 0.1 g/L potassium iodide in 0.1 M HCl. The oxidation was stopped by adding 2 g/L ascorbic acid and adjusting the pH to 8.5 with NaOH before incubation with calf intestine alkaline phosphatase (Roche Applied Science) at 37 °C for 1 h. The lysates were then adjusted to pH 2 with HCl and deproteinized (Ultrafree-MC filters, Millipore) before BH₄ and neurotransmitters were measured by HPLC⁷⁵.

The relative levels of the amino acids L-Phe, L-Tyr, and L-Trp of *Pah-R261Q* and *WT* ($n = 5–6$ mice per group) were measured in liver and brain lysates of 3–4-month-old mice as reported⁷⁶. Samples were prepared according to the Phenomenex EZ:faast kit's manual, with the following modifications: prior to amino acid extraction and derivatization, 20 μ l of each internal standard solution containing 100 μ mol/L Phe-d5 and 20 μ mol/L Tyr-d4 (in 50 mmol/L HCl) were added to 20 μ l of sample lysate. Using the kit's reagents, the amino acids were derivatized with propyl chloroformate resulting in the addition of propyl formate at the amine moiety and a propyl group at the carboxylic end of the amino acids, respectively. The hydroxy group of Tyr was also derivatized by the addition of a propyl formate group, and the amino acids were then measured by LC-ESI-MS/MS⁷⁶.

PAH enzymatic activity assay. Liver lysates were first loaded into 0.5 mL Zeba-Spin desalting columns (7,000 Da cutoff; ThermoFisher Scientific), previously equilibrated with 20 mM HEPES, pH 7.0, 200 mM NaCl, and protease inhibitor cocktail solution, and centrifuged (1,700 rcf) for 2 min. PAH activity in the homogenates was measured at 25 °C using 5–20 μ g of total protein in each assay, with 1 mM L-Phe in 20 mM Na-Hepes, 0.2 M NaCl, pH 7.0, containing catalase (0.04 mg/ml). After 4 min preincubation at 25 °C, ferrous ammonium sulfate (100 μ M) was added, and the reaction triggered after 1 min by adding 200 μ M BH₄ and 5 mM DTT (final concentrations in the assay). The reactions were allowed to run for 2 min and stopped with 2% acetic acid in ethanol. Under these conditions, PAH activity was linear to the amount of protein in the extracts. L-Tyr formed was quantified by HPLC with fluorimetric detection.

Immunoblotting. Protein immunodetection was performed by Western blot. Total protein (2.5 μ g/well) was separated using 10% polyacrylamide gel and immunodetected by using primary antibodies, 1:5000 for primary antibody α -PAH (1:5000; Millipore-MAB5278), α -ubiquitin (1:500; Thermo Fisher Scientific-131600); α -glyceraldehyde 3-phosphate dehydrogenase (GAPDH) (1:1000; Abcam-ab9485), and 1:2500 for secondary antibodies goat anti-mouse (GAM) (Bio-Rad Laboratories) and goat anti-rabbit (GAR) (Bio-Rad Laboratories), conjugated to horseradish peroxidase. Quantification of non-ubiquitinated and mono-ubiquitinated PAH and GAPDH proteins was performed by gel band densitometry.

Immunofluorescence and IHC. Mice (4–5-month-old) were anesthetized with pentobarbital (20 mg/kg, IP), and transcardially perfused with 50 ml of warm saline (0.9%, 37 °C), followed by 50 ml of warm paraformaldehyde (4%, 37 °C) in 0.16 M phosphate buffer (PBS; pH 7.2). The hepatic tissue was dissected out and postfixed in the same fixative for 3 h at 4 °C and subsequently stored in 20% sucrose diluted with PBS containing 0.01% sodium azide (Sigma) and 0.02% Bacitracin (Sigma) at 4 °C overnight. Tissues were embedded with Optimal cutting temperature (OCT) compound (Tissue Tek, Miles Laboratories, Elkhart, Ind., USA), frozen and cut in a cryostat (Microm, Heidelberg, Germany) at 20 or 50 μ m thickness, collected and stored free-floating in PBS at 4 °C or mounted onto SuperFrost Plus microscope slides (ThermoFisher Scientific), dried at room temperature for 30 min and stored at -80 °C until use.

For immunofluorescence, Triton-X 100 (0.5%) was used to permeabilize the tissues followed by blocking with 5% FBS in PBS for 1 h prior to the primary antibody incubation. Tissues were then incubated overnight at 4 °C in a humidity chamber with the corresponding primary antibody, α -PAH (1:100; Abcam-ab178430), α -Ubiquitin N-terminal (1:200; ABIN350072), anti-NUP98 (1:100; Abcam-ab50610), α -phospho-p62 (S403) (1:200; MBL-D343-3), and goat anti-LC3B (1:100; Signalway antibody-C48312), in 10% (w/v) NGS, 1 \times PBS, pH 7.4 solution. Then, a 30 min incubation in a humidity chamber at 37 °C was carried out with the corresponding secondary antibody, donkey anti-rabbit IgG H&L (1:200; Alexafluor 488, Invitrogen-A21206), donkey anti-goat IgG H&L (1:400; Alexafluor 555, Abcam-ab150130), donkey anti-goat IgG (1:200; Cy3 conjugate, Millipore-AP180C), goat anti-rat IgG H&L (1:100; TRITC, Jackson immunoresearch-112-025-143), goat anti-rabbit IgG H&L (1:200; Alexafluor 647, Invitrogen-A21245), donkey anti-rat IgG H&L (1:200; Alexafluor 488, ThermoFisher Scientific-A21208), in the same blocking solution. A washing step of 15 min with 1 \times PBS, pH 7.4 was included prior to and after each incubation period. Hoechst or DAPI, as indicated, were used to counterstain the nucleus for 30 min at RT followed by washing in PBS and mounted with DABCO mounting media. Images were acquired by using Leica TCS SP5 confocal microscope (Leica Microsystems GmbH) using a pinhole airy 1 and a 63 \times , 1.4 numeric aperture oil immersion objective. Acquired images were processed using the LAS AF Lite software (Leica Microsystems). For each sample, a stack of images ($n = 14$) with a step-size of either 290 or 170 nm was taken. Fluorescence intensity measurements were performed using Fiji freeware using the stacks of confocal images. Integrated density values of each stack were used to compare the relative fluorescence intensity of the samples. 3D rendering of the confocal images (z-stacks) was performed by using image analysis software Imapris (Bitplane Inc.). The nuclei marked with Nup98 (red) and PAH (green) were reconstructed by using the surface tool.

For immunohistochemistry (IHC), the stored free-floating sections were employed. Sections were first rinsed in 0.3% H₂O₂ in PBS for 10 min at RT for quenching endogenous peroxidase activity, and then incubated with blocking buffer containing Blocking Serum (VECTOR Laboratories), 0.5% Triton X-100 (Sigma), and 5% bovine serum albumin (Sigma-Aldrich) in PBS for 1 h at RT. Sections were incubated for 45 min with primary antibody α -PAH (1:800; Abcam-ab191415) and 30 min with goat anti-rabbit IgG H + L (1:200; HRP, BioRad-1706515) secondary antibody, and followed by a 30-min incubation with prepared VECTASTAIN Elite ABC (VECTOR Laboratories). The sections were immersed in a peroxidase substrate solution (DAB, Sigma) for 7–8 min and washed with water, mounted on Super Frost slides, and coverslipped with glycerol/PBS (9:1) containing 0.1% para-phenylenediamine. Finally, the sections were analyzed and images were captured using a Leica microscope equipped with a Leica camera. The average size and size distribution of PAH-positive “particles” in the cytoplasm of hepatic cells was quantified using ImageJ software. As the PAH staining pattern in the light microscope (objective 100 \times) was evenly distributed in *WT* mouse liver, the quantification was performed on liver sections of *Pah-R261Q* and *Emu1*. Ten liver sections (30 μ m thickness) were randomly selected from each animal. PAH-positive particles were analyzed in randomly selected regions of the sections. Only single PAH-positive particles were analyzed and at least 400 particles from each group, from at least 10–12 hepatic cells, were counted.

Amyloid-like aggregation assay (Amytracker). Amyloid detection was carried out by recording the fluorescence emission of amyloid ligand heptamer formyl thiophene acetic acid (Amytracker[®] 680; Ebbia Biotech) at 680 nm in a 96-well plate, black F-bottom (Griener Bio-one), for 24 h at 37 °C in a multimode microplate reader (Tecan spark), with excitation at 540 nm. The time course of the fluorescence intensity for purified WT-PAH and p.R261Q-PAH (20 μ M subunit) with Amytracker[®] 680 (1:1000) was acquired in 20 mM HEPES, 150 mM NaCl, pH 6.0. Samples lacking protein were used as controls and normalized. Three measurements were carried out for each protein.

Transmission electron microscopy (TEM). For TEM of hepatic tissue, 5-month-old mice (*WT* and *Pah-R261Q*) were anesthetized with isoflurane and transcardially perfused with 50 ml of warm saline (0.9%, 37 °C), followed by 50 ml of 2.5% glutaraldehyde (diluted in a 0.1 M sodium cacodylate buffer) at RT. The hepatic tissue was dissected out and postfixed in the same fixative for 24 h at 4 °C. The tissues were then transferred to 0.1 M sodium cacodylate buffer and kept at 4 °C. Postfixation was performed for 1 h (on ice) in 1% osmium tetroxide (EMS # 19134)

diluted in 0.1 M sodium cacodylate buffer, followed by two washing steps. The samples were then dehydrated using a graded ethanol series (30%, 50%, 70%, 96%, and 3 × 100%) before transferred to a 1:1 solution of 100% ethanol:propylene oxide (15 min). Samples were then transferred to 100% propylene oxide (15 min) before gradually introducing agar 100 resin (AgarScientific R1031) drop by drop over the next hours. Samples were then transferred to a small drop of 100% resin and excess propylene oxide was allowed to evaporate (1 h). Samples were then transferred to 100% resin and placed in molds and left at RT overnight. The molds were then placed at 60 °C for 48 h to polymerize. Ultrasections of approximately 60 nm were placed on 100 mesh Copper grids (EMS #G100H-Cu) and stained with 2% uranyl acetate (EMS # 22400) and lead citrate (VWR #1.07398). Grids were imaged using a Jeol JEM-1230 transmission electron microscope at 80 kV. Different organelles were counted in images acquired at 20,000× magnification from the cytoplasm in hepatocytes, in liver samples of both WT and *Pah-R261Q* mice (40 TEM micrographs for each mouse).

For protein TEM with negative staining, 5 µl samples of protein solutions (20 µg/ml) in the indicated buffer were allowed to be absorbed (1 min) on a glow discharged, 300 mesh (EMS # G300H-Cu), carbon-coated grid. The grids were then stained for 1 min in 2% uranyl acetate. Grids were allowed to dry for 30 min before imaging. The incorporation of two consecutive washing steps with double distilled water after absorption of the protein improved the background, but we observed loss of aggregates.

Oxidative stress assay (Trolox). The antioxidant capacity of small molecules (such as ascorbate, glutathione, and vitamin E) in *Pah-R261Q* and WT liver homogenates was determined by the Trolox equivalent antioxidant capacity assay using the colorimetric Total Antioxidant Capacity Assay kit (Abcam). Samples were diluted 1:1 with the included reagent Protein Mask to avoid the potential contribution of other biological species. Otherwise, the standard protocol indicated in the product manual was followed. Results were obtained by interpolation to a Trolox (reference antioxidant) standard curve and expressed as Trolox equivalent antioxidant capacity.

Gene (mRNA) expression. Total RNA was extracted from powdered livers of *Pah-R261Q* and WT mice (3-months-old; $n = 5-6$ per group) with the QIAamp RNA Blood Mini Kit (QIAGEN) and translated into cDNA using the Reverse Transcription System (Promega). Quantitative PCR was performed in standard triplicate assays for each mouse sample with 50 ng of cDNA using TaqMan technology, an ABI Prism 7700 sequence detector, and the TaqMan Universal PCR Master Mix from ABI. Detailed information about the specific transcript detection cannot be given, as we used ABI TaqMan Gene Expression Assays, which are under a proprietary license, and the exact primer and probe sequence are not disclosed. The ABI assay numbers for the indicated murine mRNA and NCBI nucleotide sequence numbers are summarized in Supplementary Table 4. Murine *Gapdh*-mRNA was included as a control for normalization and the analyses of the relative gene expression were performed based on the $2^{-\Delta\Delta Ct}$ method⁷⁷.

Software. The computer algorithm TANGO⁴⁷ was used for the prediction of aggregating regions in the relevant mutants and WT PAH sequences. Calculations were performed online (<http://tango.crg.es/>) with default parameters. PAH particles were analyzed and measured using Fiji ImageJ.

Statistics and reproducibility. Quantitative data are presented as mean ± standard deviation (SD). Individual values are plotted as circles in both scatter dot plots and bar graphs, except in the inset of Fig. 1e where the circles represent the mean for the group for each time point. Statistical significant differences were determined by unpaired two-tailed *t* test for pairs of groups, except when indicated, i.e., two-tailed Mann Whitney *U* tests were used for the analysis of data in Table 1 and Supplementary Table 2. For comparisons of more than two groups one-way ANOVA followed by post hoc Tukey test was used, except for data in the inset of Supplementary Fig. 4 where due to unequal variance and sample size Brown-Forsythe and Welch ANOVA test was used followed by Dunnett's multiple comparisons test, as indicated. Note that despite the fact that mean ± SD is presented in this figure, the analysis is run on mean AUC ± SEM data, which is also the case for the *t* test applied on the AUC data in the inset of Fig. 1d and inset of Fig. 2c. We considered $p < 0.05$ as statistically significant and *p* values are provided with accurate numbers down to <0.0001. Statistical analyses were performed using GraphPad Prism[™] (version 8.3.0, San Diego) software and the applied analysis in each case is included in the corresponding Table and Figure legend only for the results for which statistical significance was obtained.

For representations of quantitative data, *n* customarily refers to the number of independent biological samples (mice) examined in each analysis, except when explicitly referring to the number of independent enzyme purifications. When required, i.e., Figure 5c and Supplementary Fig. 7, the number of sections and/or particles analyzed is also provided in the corresponding figure legend.

The representative Western blots (Fig. 3a, b) have been repeated at least three times in independent experiments, using different mice in each experiment ($n \geq 3$ for each genotype). Densitometric results obtained with the Western blots are represented in Fig. 3c. The agarose gel in Supplementary Fig. 2c represents the

procedure used for genotyping after breeding and similar results have been obtained at least 20 times in independent experiments including in total $n \geq 40$ mice of each genotype. Representative micrographs showing results from immunofluorescence and IHC (Figs. 4, 5a,b and 6a,b) have been successfully repeated with $n \geq 3$ for each genotype in independent experiments. The results in the representative micrograph from TEM with purified p.R261Q-PAH (Supplementary Fig. 6b) have been observed with $n = 3$ protein preparations. For the TEM of hepatic tissue, representative micrographs with the relevant organelles are shown and have been observed in liver samples from $n = 3$ mice in each genotypic group.

Ethical compliance. We have complied with all relevant ethical regulations for mice breeding, testing and research. The animal experiments in this study have received the appropriate approval from the Norwegian Food Safety Authority (Brumunddal, Norway) (approved application 20168698) and performed at the Laboratory Animal Facility, University of Bergen, according to the guidelines and standards from the Regulation on the use of animals in the research of this institution.

Reporting summary. Further information on research design is available in the Nature Research Reporting Summary linked to this article.

Data availability

Source data underlying Figs. 1–6, Supplementary Figs. 2c and 3–6, Tables 1 and 2 and Supplementary Tables 2 and 3 are provided with this paper as a Source Data file. The rest of the data that support Supplementary Figs. 7 and 8 within this paper, other findings and the mouse and derived materials will be made available upon reasonable request to the correspondence author. Web-links for NCBI nucleotide sequences: *Pah*-mRNA NM_008777.3 https://www.ncbi.nlm.nih.gov/nucore/NM_008777.3, *Hsc70*-mRNA NM_031165.4 https://www.ncbi.nlm.nih.gov/nucore/NM_031165.4, *Gch1*-mRNA NM_008102.3 https://www.ncbi.nlm.nih.gov/nucore/NM_008102.3, *Hsp1*-mRNA NM_008296.2 https://www.ncbi.nlm.nih.gov/nucore/NM_008296.2, *stb1*-mRNA NM_019719.3 https://www.ncbi.nlm.nih.gov/nucore/NM_019719.3, *Gchfr*-mRNA NM_177157.4 https://www.ncbi.nlm.nih.gov/nucore/NM_177157.4, *Dnajc12*-mRNA NM_001253685.1 https://www.ncbi.nlm.nih.gov/nucore/NM_001253685.1, *p62*-mRNA NM_001290769.1 https://www.ncbi.nlm.nih.gov/nucore/NM_001290769.1, *Hsp70*-mRNA NM_001163434.1 https://www.ncbi.nlm.nih.gov/nucore/NM_001163434.1, *Ap-1*-mRNA NM_001243043.1 https://www.ncbi.nlm.nih.gov/nucore/NM_001243043.1, *Gapdh*-mRNA NM_008084.3 https://www.ncbi.nlm.nih.gov/nucore/NM_008084.3 Web-link for PAH structure in complex with BH₄ PDB 6HYC (<https://www.rcsb.org/structure/6HYC>) Web-link for data on C57BL/6J mouse strain (<https://www.jax.org/strain/000664>). Source data are provided with this paper.

Received: 15 November 2019; Accepted: 25 February 2021;

Published online: 06 April 2021

References

- Fitzpatrick, P. F. Tetrahydropterin-dependent amino acid hydroxylases. *Annu. Rev. Biochem.* **68**, 355–381 (1999).
- Werner, E. R., Blau, N. & Thony, B. Tetrahydrobiopterin: biochemistry and pathophysiology. *Biochem. J.* **438**, 397–414 (2011).
- Blau, N., van Spronsen, F. J. & Levy, H. L. Phenylketonuria. *Lancet* **376**, 1417–1427 (2010).
- Bone, A., Kuehl, A. K. & Angelino, A. F. A neuropsychiatric perspective of phenylketonuria I: overview of phenylketonuria and its neuropsychiatric sequelae. *Psychosomatics* **53**, 517–523 (2012).
- Burton, B. K. et al. Prevalence of comorbid conditions among adult patients diagnosed with phenylketonuria. *Mol. Genet. Metab.* **125**, 228–234 (2018).
- Trefz, K. F. et al. Clinical burden of illness in patients with phenylketonuria (PKU) and associated comorbidities – a retrospective study of German health insurance claims data. *Orphanet J. Rare Dis.* **14**, 181 (2019).
- Blau, N. & Longo, N. Alternative therapies to address the unmet medical needs of patients with phenylketonuria. *Expert Opin. Pharmacother.* **16**, 791–800 (2015).
- Levy, H. L. et al. Efficacy of sapropterin dihydrochloride (tetrahydrobiopterin, 6R-BH₄) for reduction of phenylalanine concentration in patients with phenylketonuria: a phase III randomised placebo-controlled study. *Lancet* **370**, 504–510 (2007).
- Perlman, R. L. Mouse models of human disease: an evolutionary perspective. *Evol. Med. Public Health* **2016**, 170–176 (2016).
- McDonald, J. D. & Charlton, C. K. Characterization of mutations at the mouse phenylalanine hydroxylase locus. *Genomics* **39**, 402–405 (1997).
- Haefele, M. J., White, G. & McDonald, J. D. Characterization of the mouse phenylalanine hydroxylase mutation Pahenu3. *Mol. Genet. Metab.* **72**, 27–30 (2001).

12. Sarkissian, C. N., Boulais, D. M., McDonald, J. D. & Scriver, C. R. A heteroallelic mutant mouse model: a new orthologue for human hyperphenylalaninemia. *Mol. Genet. Metab.* **69**, 188–194 (2000).
13. Sarkissian, C. N. et al. Preclinical evaluation of multiple species of PEGylated recombinant phenylalanine ammonia lyase for the treatment of phenylketonuria. *Proc. Natl Acad. Sci. USA* **105**, 20894–20899 (2008).
14. Villiger, L. et al. Treatment of a metabolic liver disease by in vivo genome base editing in adult mice. *Nat. Med.* **24**, 1519–1525 (2018).
15. Wettstein, S. et al. Linking genotypes database with locus-specific database and genotype-phenotype correlation in phenylketonuria. *Eur. J. Hum. Genet.* **23**, 302–309 (2015).
16. Danecka, M. K. et al. Mapping the functional landscape of frequent phenylalanine hydroxylase (PAH) genotypes promotes personalised medicine in phenylketonuria. *J. Med. Genet.* **52**, 175–185 (2015).
17. Guldberg, P. et al. A European multicenter study of phenylalanine hydroxylase deficiency: classification of 105 mutations and a general system for genotype-based prediction of metabolic phenotype. *Am. J. Hum. Genet.* **63**, 71–79 (1998).
18. Pey, A. L. et al. Mechanisms underlying responsiveness to tetrahydrobiopterin in mild phenylketonuria mutations. *Hum. Mutat.* **24**, 388–399 (2004).
19. Erlandsen, H. et al. Correction of kinetic and stability defects by tetrahydrobiopterin in phenylketonuria patients with certain phenylalanine hydroxylase mutations. *Proc. Natl Acad. Sci. USA* **101**, 16903–16908 (2004).
20. Wang, H. et al. One-step generation of mice carrying mutations in multiple genes by CRISPR/Cas-mediated genome engineering. *Cell* **153**, 910–918 (2013).
21. Arturo, E. C. et al. First structure of full-length mammalian phenylalanine hydroxylase reveals the architecture of an autoinhibited tetramer. *Proc. Natl Acad. Sci. USA* **113**, 2394–2399 (2016).
22. Flydal, M. I. et al. Structure of full-length human phenylalanine hydroxylase in complex with tetrahydrobiopterin. *Proc. Natl Acad. Sci. USA* **116**, 11229–11234 (2019).
23. Gjetting, T., Petersen, M., Guldberg, P. & Guttler, F. In vitro expression of 34 naturally occurring mutant variants of phenylalanine hydroxylase: correlation with metabolic phenotypes and susceptibility toward protein aggregation. *Mol. Genet. Metab.* **72**, 132–143 (2001).
24. Hsu, P. D. et al. DNA targeting specificity of RNA-guided Cas9 nucleases. *Nat. Biotechnol.* **31**, 827–832 (2013).
25. Flurkey K., Curren J. M., Leiter E. H., Wither B. *The Jackson Laboratory Handbook on Genetically Standardized Mice*. (The Jackson Laboratory, 2009).
26. Fiori, E. et al. Early-onset behavioral and neurochemical deficits in the genetic mouse model of phenylketonuria. *PLoS ONE* **12**, e0183430 (2017).
27. Prentice, R. L. et al. An exploratory study of respiratory quotient calibration and association with postmenopausal breast cancer. *Cancer Epidemiol. Biomark. Prev.* **22**, 2374–2383 (2013).
28. Farinatti, P., Castinheiras Neto, A. G. & Amorim, P. R. Oxygen consumption and substrate utilization during and after resistance exercises performed with different muscle mass. *Int. J. Exerc. Sci.* **9**, 77–88 (2016).
29. Speakman, J. R. Measuring energy metabolism in the mouse—theoretical, practical, and analytical considerations. *Front. Physiol.* **4**, 34 (2013).
30. Westbrook, R., Bonkowski, M. S., Strader, A. D. & Bartke, A. Alterations in oxygen consumption, respiratory quotient, and heat production in long-lived GHRKO and Ames dwarf mice, and short-lived bGH transgenic mice. *J. Gerontol. A Biol. Sci. Med. Sci.* **64**, 443–451 (2009).
31. Strand, E. et al. Serum carnitine metabolites and incident type 2 diabetes mellitus in patients with suspected stable angina pectoris. *J. Clin. Endocrinol. Metab.* **103**, 1033–1041 (2018).
32. Mahendran, Y. et al. Association of ketone body levels with hyperglycemia and type 2 diabetes in 3,998 Finnish men. *Diabetes* **62**, 3618–3626 (2013).
33. Puchalska, P. & Crawford, P. A. Multi-dimensional roles of ketone bodies in fuel metabolism, signaling, and therapeutics. *Cell Metab.* **25**, 262–284 (2017).
34. Zdzisinska, B., Zurek, A. & Kandfer-Szerszen, M. Alpha-ketoglutarate as a molecule with pleiotropic activity: well-known and novel possibilities of therapeutic use. *Arch. Immunol. Ther. Exp.* **65**, 21–36 (2017).
35. Liu, S., He, L. & Yao, K. The antioxidative function of alpha-ketoglutarate and its applications. *Biomed. Res. Int.* **2018**, 3408467 (2018).
36. Kubicova, L., Hadacek, F. & Chobot, V. Quinolinic acid: neurotoxin or oxidative stress modulator? *Int. J. Mol. Sci.* **14**, 21328–21338 (2013).
37. Moffett, J. R. & Namboodiri, M. A. Tryptophan and the immune response. *Immunol. Cell Biol.* **81**, 247–265 (2003).
38. Satapati, S. et al. Mitochondrial metabolism mediates oxidative stress and inflammation in fatty liver. *J. Clin. Investig.* **125**, 4447–4462 (2015).
39. Mazzola, P. N. et al. Voluntary exercise prevents oxidative stress in the brain of phenylketonuria mice. *JIMD Rep.* **27**, 69–77 (2016).
40. Blaskovics, M. E., Schaeffler, G. E., & Hack, S. Phenylalaninaemia. Differential diagnosis. *Arch. Dis. Child* **49**, 835–843 (1974).
41. Kor, D., Yilmaz, B. S., Bulut, F. D., Ceylaner, S. & Mungan, N. O. Improved metabolic control in tetrahydrobiopterin (BH4), responsive phenylketonuria with sapropterin administered in two divided doses vs. a single daily dose. *J. Pediatr. Endocrinol. Metab.* **30**, 713–718 (2017).
42. Jung-Kc, K. et al. Phenylalanine hydroxylase variants interact with the co-chaperone DNAJC12. *Hum. Mutat.* **40**, 483–494 (2019).
43. Sarkissian, C. N., Ying, M., Scherer, T., Thony, B. & Martinez, A. The mechanism of BH4-responsive hyperphenylalaninemia—as it occurs in the ENU1/2 genetic mouse model. *Hum. Mutat.* **33**, 1464–1473 (2012).
44. Gersting, S. W. et al. Pahenu1 is a mouse model for tetrahydrobiopterin-responsive phenylalanine hydroxylase deficiency and promotes analysis of the pharmacological chaperone mechanism in vivo. *Hum. Mol. Genet.* **19**, 2039–2049 (2010).
45. Eichinger, A. et al. Secondary BH4 deficiency links protein homeostasis to regulation of phenylalanine metabolism. *Hum. Mol. Genet.* **27**, 1732–1742 (2018).
46. Woerner, A. C. et al. Cytoplasmic protein aggregates interfere with nucleocytoplasmic transport of protein and RNA. *Science* **351**, 173–176 (2016).
47. Fernandez-Escamilla, A. M., Rousseau, F., Schymkowitz, J. & Serrano, L. Prediction of sequence-dependent and mutational effects on the aggregation of peptides and proteins. *Nat. Biotechnol.* **22**, 1302–1306 (2004).
48. Okano, Y., Kudo, S., Nishi, Y., Sakaguchi, T. & Aso, K. Molecular characterization of phenylketonuria and tetrahydrobiopterin-responsive phenylalanine hydroxylase deficiency in Japan. *J. Hum. Genet.* **56**, 306–312 (2011).
49. Levine, B. & Kroemer, G. Autophagy in the pathogenesis of disease. *Cell* **132**, 27–42 (2008).
50. Matsumoto, G., Wada, K., Okuno, M., Kurosawa, M. & Nukina, N. Serine 403 phosphorylation of p62/SQSTM1 regulates selective autophagic clearance of ubiquitinated proteins. *Mol. Cell* **44**, 279–289 (2011).
51. Lamark, T., Svenning, S. & Johansen, T. Regulation of selective autophagy: the p62/SQSTM1 paradigm. *Essays Biochem.* **61**, 609–624 (2017).
52. Prasad, R., Xu, C. & Ng, D. T. W. Hsp40/70/110 chaperones adapt nuclear protein quality control to serve cytosolic clients. *J. Cell Biol.* **217**, 2019–2032 (2018).
53. Sala, A. J., Bott, L. C. & Morimoto, R. I. Shaping proteostasis at the cellular, tissue, and organismal level. *J. Cell Biol.* **216**, 1231–1241 (2017).
54. Paonessa, F. et al. Microtubules deform the nuclear membrane and disrupt nucleocytoplasmic transport in tau-mediated frontotemporal dementia. *Cell Rep.* **26**, 582–593 e585 (2019).
55. Fernández-Nogales, M. et al. Huntington’s disease is a four-repeat tauopathy with tau nuclear rods. *Nat. Med.* **20**, 881–885 (2014).
56. Chou, C.-C. et al. TDP-43 pathology disrupts nuclear pore complexes and nucleocytoplasmic transport in ALS/FTD. *Nat. Neurosci.* **21**, 228–239 (2018).
57. Ledley, F. D., Grenett, H. E., Dunbar, B. S. & Woo, S. L. Mouse phenylalanine hydroxylase. Homology and divergence from human phenylalanine hydroxylase. *Biochem. J.* **267**, 399–405 (1990).
58. Scherer, T. et al. Tetrahydrobiopterin treatment reduces brain L-Phe but only partially improves serotonin in hyperphenylalaninemic ENU1/2 mice. *J. Inher. Metab. Dis.* **41**, 709–718 (2018).
59. Sirtori, L. R. et al. Oxidative stress in patients with phenylketonuria. *Biochim. Biophys. Acta* **1740**, 68–73 (2005).
60. Rocha, J. C. et al. Dietary treatment in phenylketonuria does not lead to increased risk of obesity or metabolic syndrome. *Mol. Genet. Metab.* **107**, 659–663 (2012).
61. Scheller, R. et al. Toward mechanistic models for genotype-phenotype correlations in phenylketonuria using protein stability calculations. *Hum. Mutat.* **40**, 444–457 (2019).
62. Lamark, T. & Johansen, T. Autophagy: links with the proteasome. *Curr. Opin. Cell Biol.* **22**, 192–198 (2010).
63. Kocaturk, N. M. & Gozuacik, D. Crosstalk between mammalian autophagy and the ubiquitin-proteasome system. *Front. Cell Dev. Biol.* **6**, 128 (2018).
64. Bjørkøy, G. et al. p62/SQSTM1 forms protein aggregates degraded by autophagy and has a protective effect on huntingtin-induced cell death. *J. Cell Biol.* **171**, 603–614 (2005).
65. Carija, A., Navarro, S., de Groot, N. S. & Ventura, S. Protein aggregation into insoluble deposits protects from oxidative stress. *Redox Biol.* **12**, 699–711 (2017).
66. Watschinger, K. et al. Tetrahydrobiopterin and alkylglycerol monoxygenase substantially alter the murine macrophage lipidome. *Proc. Natl Acad. Sci. USA* **112**, 2431–2436 (2015).
67. Zore, T., Palafox, M. & Reue, K. Sex differences in obesity, lipid metabolism, and inflammation—a role for the sex chromosomes? *Mol. Metab.* **15**, 35–44 (2018).
68. Choi, J., Djebbar, S., Fournier, A. & Labrie, C. The co-chaperone DNAJC12 binds to Hsc70 and is upregulated by endoplasmic reticulum stress. *Cell Stress Chaperones* **19**, 439–446 (2014).
69. Jagannathan, L., Cuddapah, S. & Costa, M. Oxidative stress under ambient and physiological oxygen tension in tissue culture. *Curr. Pharm. Rep.* **2**, 64–72 (2016).
70. Morimoto, R. I. Regulation of the heat shock transcriptional response: cross talk between a family of heat shock factors, molecular chaperones, and negative regulators. *Genes Dev.* **12**, 3788–3796 (1998).

71. Gomez-Pastor, R., Burchfiel, E. T. & Thiele, D. J. Regulation of heat shock transcription factors and their roles in physiology and disease. *Nat. Rev. Mol. Cell Biol.* **19**, 4–19 (2018).
72. Rocha, J. C. & MacDonald, A. Dietary intervention in the management of phenylketonuria: current perspectives. *Pediatr. Health Med. Ther.* **7**, 155–163 (2016).
73. Zischewski, J., Fischer, R. & Bortesi, L. Detection of on-target and off-target mutations generated by CRISPR/Cas9 and other sequence-specific nucleases. *Biotechnol. Adv.* **35**, 95–104 (2017).
74. Zhu, X. et al. An efficient genotyping method for genome-modified animals and human cells generated with CRISPR/Cas9 system. *Sci. Rep.* **4**, 6420 (2014).
75. Blau, N. et al. Variant of dihydropteridine reductase deficiency without hyperphenylalaninaemia: effect of oral phenylalanine loading. *J. Inherit. Metab. Dis.* **22**, 216–220 (1999).
76. Heintz, C., Troxler, H., Martinez, A., Thony, B. & Blau, N. Quantification of phenylalanine hydroxylase activity by isotope-dilution liquid chromatography-electrospray ionization tandem mass spectrometry. *Mol. Genet. Metab.* **105**, 559–565 (2012).
77. Livak, K. J. & Schmittgen, T. D. Analysis of relative gene expression data using real-time quantitative PCR and the 2(-Delta Delta C(T)) method. *Methods* **25**, 402–408 (2001).

Acknowledgements

We are very grateful to Altanchimeg Altankhuyag for skilled technical help with genotyping of mice, Trond-André Kråkenes for the TANGO calculations with PAH variants in the BIOPKU database, Dr. Marte Flydal and Dr. Helene Bustad Johannessen for expert help with purification of p.R261Q-PAH and consequent protein electron microscopy. We thank Dr. Øyvind Midttun and Professor Per M. Ueland for useful discussions on analyses and results on metabolic markers. This work was supported by Research Council of Norway grants FRIMEDBIO 261826/F20 and FORNY 248889/O30, the K.G. Jebsen Centre for Neuropsychiatric Disorders, and the Western Norway Regional Health Authorities (project 912246) (to A.M.). We acknowledge the Molecular Imaging Center and the BiSS core facility, both at the Department of Biomedicine, University of Bergen.

Author contributions

O.A., K.S.P., K.J.-K.C., M.Y., T.J.S.S., A.K.G., T.S., A.U., A.McC., and E.S. performed the experiments and analyzed the data. B.T. contributed to analyses and tools. K.S.P. was

responsible for breeding, genotyping and selection of mice, as well as specific mice studies. A.M. conceived and managed the project and analyzed the data. O.A. and A.M. wrote the paper with the contribution from all authors.

Competing interests

The authors declare no competing interests.

Additional information

Supplementary information The online version contains supplementary material available at <https://doi.org/10.1038/s41467-021-22107-1>.

Correspondence and requests for materials should be addressed to A.M.

Peer review information *Nature Communications* thanks Masato Ohtsuka, Eddy Van der Zee and the other, anonymous, reviewer(s) for their contribution to the peer review of this work.

Reprints and permission information is available at <http://www.nature.com/reprints>

Publisher's note Springer Nature remains neutral with regard to jurisdictional claims in published maps and institutional affiliations.



Open Access This article is licensed under a Creative Commons Attribution 4.0 International License, which permits use, sharing, adaptation, distribution and reproduction in any medium or format, as long as you give appropriate credit to the original author(s) and the source, provide a link to the Creative Commons license, and indicate if changes were made. The images or other third party material in this article are included in the article's Creative Commons license, unless indicated otherwise in a credit line to the material. If material is not included in the article's Creative Commons license and your intended use is not permitted by statutory regulation or exceeds the permitted use, you will need to obtain permission directly from the copyright holder. To view a copy of this license, visit <http://creativecommons.org/licenses/by/4.0/>.

© The Author(s) 2021



Graphic design: Communication Division, UIB / Print: Skjipes Kommunikasjon AS



uib.no

ISBN: 9788230858530 (print)
9788230869635 (PDF)